

Lecture Book

Drive Systems

D. T. McGuiness, Ph.D

Version: 2025.SS

(2025, D. T. McGuines, Ph.D)

Current version is 2025.SS.

This document includes the contents of Drive Systems, official name being *Antriebssysteme*, taught at MCI in the Mechatronik Smart Technologies. This document is the part of the module MECH-M-2-ATS-ATS-VO taught in the M.Sc degree.

All relevant code of the document is done using *SageMath* where stated using v10.3 and Python v3.13.1.

This document was compiled with *LuaT_EX* v1.18.0, and all editing were done using *GNU Emacs* v29.4 using *AUCT_EX* and *org-mode* package.

This document is based on the books and resources: *Advanced electric drives: analysis control and modeling using MATLAB/Simulink* by Mohan Ned. , John Wiley & Sons 2014. *Analysis of electric machinery and drive systems* by Krause Paul C. et. al. , Vol. 2 IEEE Press 2002. *Design of rotating electrical machines* by Pyrhonen Juha et. al , John Wiley & Sons 2013. *Electric Machinery Fundamentals (5th Edition)* by Stephen J. Chapman. , (2012). *Electric Machinery*. by Fitzgerald A. E. et. al. , McGraw Hill (2003). *Electric Motors and Drives: Fundamentals Types and Applications* by Hughes A. et. al. , Newnes 2019. *Electrical Machines and Drives: Fundamentals and Advanced Modelling* by Melkebeek A. , Springer 2018. *Electrical machines, drives, and power systems* by Wildi T. , Pearson Education 2006. *Fundamentals of Electrical Drives* by Veltman A. et. al. , Springer 2007.

The current maintainer of this work along with the primary lecturer
is D. T. McGuines, Ph.D. (dtk@mci4me.at).

Contents

I. DC Machines	3
1. Modelling DC Machines	5
1.1. Introduction	5
1.2. Operation Principle	6
1.3. Induced EMF	7
1.4. Equivalent Circuit and Electromagnetic Torque	9
1.5. Electromechanical Modelling	10
1.6. State-Space Modelling	10
1.7. Block Diagrams and Transfer Functions	11
1.8. Field Excitation	12
1.8.1. Separately Excited	12
1.8.2. Shunt Excited	14
1.8.3. Series Excited	14
1.8.4. Compound	15
1.8.5. Permanent-Magnets	16
1.9. Measuring the Motor Constants	16
1.9.1. Armature Resistance	16
1.9.2. Armature Inductance	16
1.9.3. EMF Constant	17
1.10. Simulation	17
1.10.1. Separately-Excited	17
2. Phase Controlled DC Machines	21
2.1. Introduction	21
2.2. Principles of DC Machine Speed Control	22
2.2.1. Important Relationships	22
2.2.2. Field Control	23
2.2.3. Armature Control	23
2.2.4. Armature and Field Control	24
2.2.5. Four Quadrant Operation	26
2.3. Phase Controlled Converters	29
2.3.1. Single-Phase Controlled Converter	29
2.3.2. Three-Phase Controlled Converter	33
2.3.3. Control Circuit	35
2.3.4. Control Modelling of the Three-Phase Converter	36

2.3.5. Half-Controlled Converter	37
2.4. Steady State Analysis of 3-Phase Converter Drive	39
2.4.1. Average Analysis	39
2.5. Two Quadrant 3-Phase Converter Control	41
2.6. Transfer Functions of the Subsystems	42
2.6.1. DC Motor with Load	42
2.6.2. Converter	43
2.6.3. Current and Speed Controllers	43
2.6.4. Current Feedback	43
2.6.5. Speed Feedback	43
2.7. Designing Controllers	43
2.7.1. Current Controller	44
II. Induction Machines	47
3. Induction Motor Dynamics and Control	49
3.1. Introduction	49
3.2. Steady-State Analysis	50
3.2.1. Speed of Operation	50
3.2.2. Normal Operation	52
3.3. Construction	53
3.4. Dynamic Modelling	59
3.4.1. Real Time Model of a Two-Phase Induction Machine	60
3.4.2. Transformations for Constant Matrices	62
3.4.3. Three-Phase to Two-Phase Transformation	65
3.4.4. Power Equivalence	68
3.4.5. Generalised Model in Arbitrary Reference Frame	68
3.4.6. Electromagnetic Torque	70
3.4.7. Derivation of Commonly Used Induction-Machine Models	72
3.4.8. Equations in Flux Linkages	75
3.5. Dynamic Simulation Equations	76
3.5.1. Simulation Example	78
3.5.2. No-load Startup	79
3.5.3. Application of a Step Torque Load	81
4. Vector Controlled Induction Machines	85
4.1. Introduction	85
4.2. Principles of Vector Control	87
4.3. Direct Vector Control	90
4.3.1. Description	90
4.3.2. Calculating the Torque and Flux	91
4.3.3. Case II: Induced Electro-motive Force (EMF) from Flux-Sensing Coils of Hall Sensors	93

III. Permanent Magnet Synchronous Machines	97
5. Permanent Magnet Machine Dynamics and Control	99
5.1. Introduction	99
5.2. Properties of Permanent Magnets	100
5.3. Permanent Magnet Synchronous Machines	106
5.3.1. Machine Configurations	106
5.3.2. Flux Density Distribution	108
5.3.3. Line-Start PMSM	108
5.3.4. Types of PM Synchronous Machines	109
5.4. Vector Control	111
5.4.1. Mathematical Model	111
5.4.2. Vector Control	113
5.4.3. Drive System Schematic	114
5.5. Control Strategies	114
5.6. Flux Weakening Operation	116
5.6.1. Maximum Speed	117
5.6.2. Direct Flux Weakening	117
5.7. Speed-Controller Design	120
5.7.1. Deriving the Block Diagram	121
5.8. Sensorless Control	122
5.9. Brushless DC Motor	123
5.9.1. Mathematical Model	124
5.9.2. Commutation-Torque Ripple	125
5.9.3. Sensorless Control	127
Bibliography	133

List of Figures

1.2. A close-up view of the Direct Current (DC) machine. Please observe the commutator part of the motor (left size and the brushes which are a signature feature of these kind of machines [8].	6
1.1. A pair of carbon brushes used in DC drives which allow commutation. While solid-state commutation has become popular in the last decades, their cost effective nature still makes them the prevalent choice in industry [7].	6
1.3. A Schematic representation of a DC machine during operation with the path of the flux lines shown.	7
1.4. Equivalent circuit of a DC machine.	9
1.5. Block diagram of a DC motor.	11
1.6. Circuit diagram of a separately-excited DC machine.	12
1.7. Circuit diagram of a shunt-excited DC machine.	14
1.8. Circuit diagram of a series-excited DC machine.	14
1.9. Circuit diagram of a separately-excited DC machine.	15
1.10. A standard out-runner rotor Brushless DC (BLDC) motor. Here the rotor which contains Permanent Magnet (PM) is spinning outside whereas the stator is inside [13].	16
1.11. Induced EMF v. rotor speed characteristics at rated field current.	17
1.12. The simulation diagram of a separately excited DC machine.	18
1.13. Simulation Results of the separately-excited DC motor.	19
 2.1. Mechanical commutation is done via physical contact points being interfaced by brushes. During changing of contact, the brushes create a short-circuit creating arcs [15].	23
2.2. Normalised characteristics of a variable-speed DC motor.	24
2.3. Four-quadrant Torque-speed characteristics.	27
2.4. Thyristors are diodes which their conduction could be controlled.	28
2.5. The Simulink implementation of a single phase rectifier circuit. The parameters are: firing angle (α) = 30° , resistance (R) is	29
2.6. The generated waveforms of the SIMULINK implementation of a single phase rectifier circuit.	30
2.7. The Simulink implementation of a single phase rectifier circuit. The parameters are: firing angle (α) = 30° , resistance (R) is	31
2.8. The characteristic behaviours of a thyristor in different conduction modes.	32
2.9. The Simulink implementation of a single phase rectifier circuit. The parameters are: firing angle (α) = 30° , resistance (R) is	32

3.1. Cross-sectional view of Induction Machine (IM) [17].	49
3.2. A wound-rotor IM [24].	50
3.3. Steady-state torque behaviour of an IM. Here important parameters and concepts can be observed. An important aspect is to mention is the stability of an IM only occurs between %2 to %8 slip during normal operation.	52
3.4. Lamination on a stator is done to reduce eddy currents [17].	53
3.5. Form winding.	56
3.6. The materials used in the construction of an IM.	59
3.7. Stator and rotor winding of a two-phase IM. The model shows the stator inductances as L_{qs} and L_{ds} , and the rotor as L_α and L_β . as the rotor spins these inductances will interact with one another and produce mutual inductance.	60
3.8. Transformation on actual to fictitious rotor variables.	63
3.9. A Simulink Model of an Induction Machine.	79
3.10. The parametric plot of rotor speed v. torque when the motor starts from standstill without an external load.	80
3.11. The parametric plot of rotor speed v. torque when an instantenous load is applied to the motor at 0.4 s.	80
3.12. Simulation results for starting IM from standstill.	82
3.13. Simulation of the IM when an instantenous load is applied to the motor at 0.4 s.	83
4.1. Block diagram from Blaschke's 1971 US patent application [44].	86
4.2. Phasor diagram of the vector controller. Observe that regardless of the reference frame, the magnitude stays the same.	88
4.3. An example of a flux sensing coil [45].	93
5.1. The second quadrant $\vec{B} - \vec{H}$ curve characteristics of PM.	100
5.2. A stack of ferrite magnets, with stuck metal pieces [48].	101
5.3. A collection of AlNiCo magnets [52].	102
5.4. A collection of SmCo magnets [55].	102
5.5. A collection of NdFeB magnets [57].	103
5.6. The operating point of a magnet during operation.	104
5.7. Types of Permanent Magnet Synchronous Motor (PMSM)s.	106
5.8. Finite element simulation results of a PMSM with 8-poles (Simulation was done with getDP).	108
5.9. The waveforms of a BLDC motor during operation.	110
5.10. Vector controlled PMSM drive.	115
5.11. A Schematic Example of a PMSM-drive control strategy.	120
5.12. Block diagram of the speed-controlled PMSM drive.	121
5.13. Placement of the hall sensors on the stator [61].	123

List of Tables

1.1.	Simulation parameters for the separately-excited DC motor.	18
3.1.	Simulation parameters for the IM example.	78
5.1.	A quick view on different types of PMs used/produced in industry.	101
5.2.	Useful properties of PMs [47] (Here Sin. stands for sintered)	101

Part I.

DC Machines

Chapter 1

Modelling DC Machines

Table of Contents

1.1. Introduction	5
1.2. Operation Principle	6
1.3. Induced EMF	7
1.4. Equivalent Circuit and Electromagnetic Torque	9
1.5. Electromechanical Modelling	10
1.6. State-Space Modelling	10
1.7. Block Diagrams and Transfer Functions	11
1.8. Field Excitation	12
1.9. Measuring the Motor Constants	16
1.10. Simulation	17

1.1. Introduction

DC machines have been in service for more than a century [1]. Their structure has changed a great deal since the introduction of the IM¹. DC machines have seen a resurgence of use with the advent and cost effective nature of the Silicon Controlled Rectifier (SCR) [2], facilitating a wide-range speed control of these motors and are still used in a wide range of industries such as mining [3], automotive industries [4], and public transportation [5].

¹Due to historical reasons, IM is also called Alternating Current (AC) shunt motor by people who refuse to keep up with the times.

A great benefit of DC machines over any type is its simple control mechanisms.

This chapter contains a brief description of the theory of operation of separately-excited² and PM DC brush motors and of their modeling and transfer functions, an evaluation of steady state and transient responses. A representation of the motor can be seen in **Fig. 1.2**.

²One of the more industrially relevant DC motor connection.

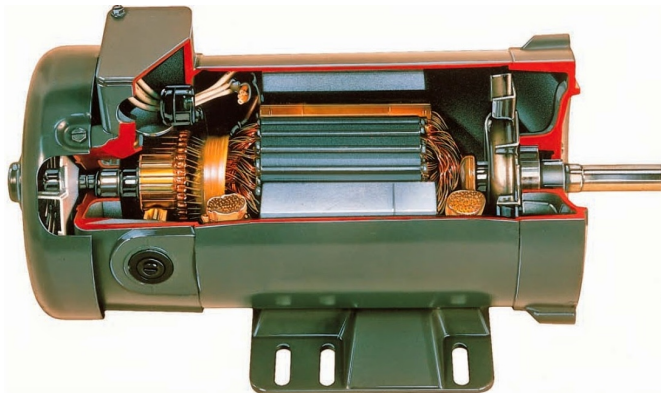


Figure 1.2.: A close-up view of the DC machine. Please observe the commutator part of the motor (left side) and the brushes which are a signature feature of these kind of machines [8].

1.2. Operation Principle

³Recall that a wire in an external field experiences maximum torque when the field passes the wire perpendicularly.

It is well known that maximum torque is produced when two (2)fluxes are in quadrature³ [6]. The fluxes are created with two (2)current-carrying conductors. The flux path is of low reluctance with steel. **Fig. 1.2** shows such a schematic representation.

Coil 1: Field Winding wound on the pole produces a flux (ϕ_f) with an input current i_f .

Coil 2: Armature Winding called the armature winding on a rotating surface produces a flux ϕ_a with a current i_a .

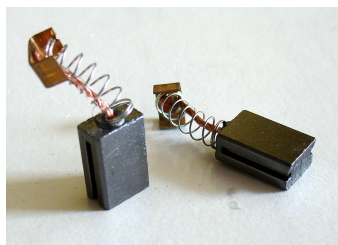


Figure 1.1.: A pair of carbon brushes used in DC drives which allow commutation. While solid-state commutation has become popular in the last decades, their cost effective nature still makes them the prevalent choice in industry [7].

⁴i.e., unidirectional torque.

For the given position, the two (2)fluxes are mutually perpendicular ($\phi_f \perp \phi_a$) and will in turn exert a maximum torque on the rotor. This in turn will move the rotor in clockwise direction. If we assume the rotor has moved by 180°, coils which were under the influence of south pole will be under the south pole and will be carrying negative current.

The generated torque will be such as to move the rotor in the counterclockwise direction, keeping the rotor in oscillation. To have a uniform torque⁴ and a clockwise (or counterclockwise) direction of rotation, the armature winding needs to carry a current of the same polarity underneath a field pole. That is arranged by separating the armature coils and connecting them to separate copper bars, called a **commutator**, mounted on the same shaft as the armature and field from tubes.

The brushes are stationary and supplied with currents of fixed polarity. This means the commutator segments under a brush will continue to receive a current of fixed polarity. [9]

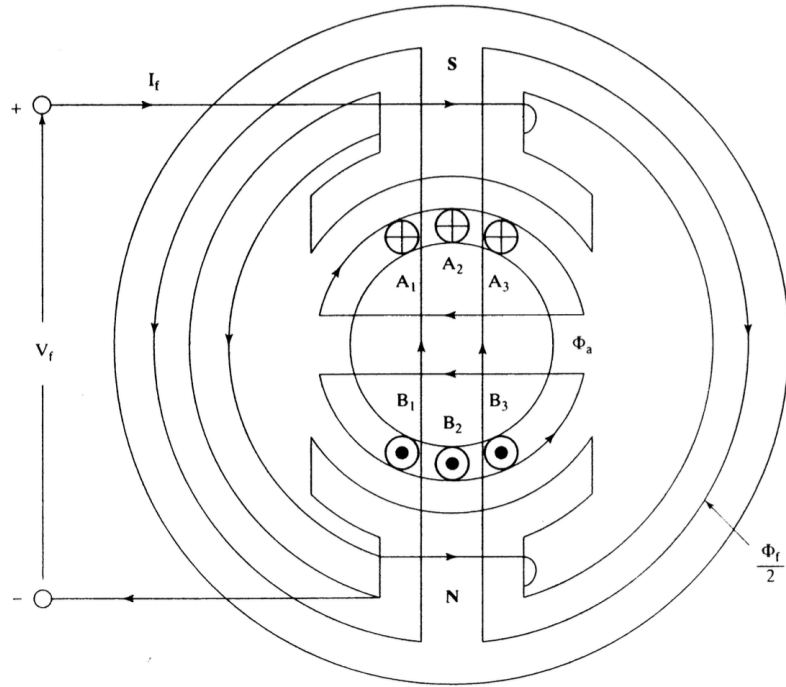


Figure 1.3.: A Schematic representation of a DC machine during operation with the path of the flux lines shown.

1.3. Induced EMF

The mathematical expression for induced emf (e) and torque is derived for a machine with P poles, Z armature conductors in a field with a flux per pole of ϕ_f and its rotor rotating at n_r rpm.

According to Faraday's law⁵, the induced EMF (neglecting the sign) is:

$$e = Z \frac{d\phi_f}{dt} = Z \frac{\phi_f}{t} \quad (1.1)$$

⁵ For a brief refreshment, please look at the lecture materials for M.Sc Electrodynamics

where t is the time taken by the conductors to cut ϕ_f flux lines. Therefore:

$$t = \frac{1}{2 \times \text{frequency}} = \frac{1}{2 \left(\frac{P}{2} \right) \left(\frac{n_r}{60} \right)} \quad (1.2)$$

The flux change occurs for each pole pair. By substituting Eq. (1.1) in Eq. (1.2):

$$e = \frac{Z\phi_f P n_r}{60}$$

If the armature conductors are divided into a parallel paths⁶, then:

$$e = \frac{Z\phi_f P n_r}{60a} \quad (1.3)$$

⁶ How a motor is wound is paramount during design as some windings can improve efficiency, decrease torque pulsations or determine parameters such as speed. However this topic is too detailed for this margin to contain and beyond the scope of this lecture.

There are two (2)possible arrangements of conductors in the armature, wave windings and lap windings. The values of a for these two (2)types of windings are:

$$a = \begin{cases} 2 & \text{for wave winding} \\ P & \text{for lap winding} \end{cases}$$

It is usual to write the expression Eq. (1.3) in a **compact** form as:

$$e = K\phi_f\omega_m,$$

where $\omega_m = 2\pi n_r/60$ rad s⁻¹, and

$$K = \left(\frac{P}{a}\right) Z \left(\frac{1}{2\pi}\right).$$

In literature K is defined as a **machine constant**. The name comes from the fact all parameters making up the constant are defined during the construction of the machine and therefore are fixed values during operation. If the field flux is assumed to be **constant**, then the **induced emf** is **proportional to the rotor speed** and the constant of proportionality is known as the **induced emf**⁷

⁷also known as back emf

or constant. Then the induced emf is represented as:

$$e = K_b\omega_m, \quad (1.4)$$

where K_b is the induced emf constant, given by the relation:

$$K_b = K\phi_f \text{ V rad}^{-1} \text{ s}^{-1}$$

The field flux (ϕ_f) is written as the ratio between the field Magneto-motive Force (MMF) and mutual reluctance \mathcal{R}_m ,

$$\phi_f = \frac{N_f i_f}{\mathcal{R}_m}, \quad (1.5)$$

where N_f is the number of turns in the field winding, i_f is the field current, and \mathcal{R}_m is the reluctance of the mutual flux path⁸.

The mutual flux is the resultant of the armature and field fluxes.

By substituting Eq. (1.5) into Eq. (1.4), the emf constant is obtained as:

$$K_b = \frac{KN_f i_f}{\mathcal{R}_m} = Mi_f \quad (1.6)$$

where M is the **fictitious mutual inductance** between armature and field windings given by:

$$M = \frac{KN_f}{\mathcal{R}_m} = \left(\frac{P}{\pi}\right) \frac{Z}{2a} \frac{N_f}{\mathcal{R}_m}$$

Here $Z/(2a)$ is the number of turns in the armature per parallel path and together in product with the field winding turns N_f gives the familiar mutual inductance definition.

The factor P/π makes it a **fictitious inductance**.

By substituting Eq. (1.6) to Eq. (1.4), the induced emf is obtained as:

$$e = M i_f \omega_m \quad (1.7)$$

The mutual inductance is a function of the field current and must be taken note of to account for saturation of the magnetic material⁹. For operation within the linear range, mutual inductance is assumed to be a constant in the machine.

⁹i.e., effects caused by stator laminations.

1.4. Equivalent Circuit and Electromagnetic Torque

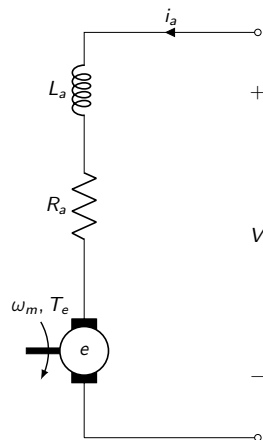


Figure 1.4.: Equivalent circuit of a DC machine.

The equivalent circuit of a DC motor armature¹⁰ is based on the fact that the armature winding has a resistance R_a , a self-inductance L_a , and an induced emf.

This is shown in **Fig. 1.4.** In the case of a motor operation, the input is electrical energy and the output is the mechanical energy, with an air gap torque of T_e at a rotational speed of ω_m . The terminal relationship is written as

$$v = e + R_a i_a + L_a \frac{di_a}{dt} \quad (1.8)$$

In steady state, the armature current is constant and hence the rate of change of the armature current is zero. Hence the armature voltage equation reduces to

$$v = e + R_a i_a \quad (\text{Steady-state}) \quad (1.9)$$

The power balance is obtained by multiplying Eq. (1.9) by i_a :

$$vi_a = ei_a + R_a i_a^2$$

The term $R_a i_a^2$ denotes the **armature copper losses** and vi_a is the total input power. Therefore, ei_a denotes the effective power that has been transformed from electrical to mechanical form, which we will call the air-gap power (P_{ag}).

The air-gap power¹¹ is expressed in terms of the electromagnetic torque (T_e) and rotor speed (ω_m) as:

$$P_{ag} = \omega_m T_e = ei_a$$

¹¹Air gap power can be defined as the transferred power from the stator to the rotor.

This allows us to represent the electromagnetic torque or air gap torque as:

$$T_e = \frac{ei_a}{\omega_m} \quad (1.10)$$

By substituting for the induced EMF from Eq. (1.4) into Eq. (1.10), it is further simplified to be:

$$T_e = K_b i_a \quad (1.11)$$

The torque constant (K_b) is equal to the EMF constant if it is expressed in volt-sec/rad for a constant-flux machine.

1.5. Electromechanical Modelling

To keep things simple, the load is modeled as a moment of inertia (J) in $\text{kg m}^2 \text{s}^{-2}$, with a viscous friction coefficient¹² B_l in N. Then the acceleration torque (T_a) given in Nm drives the load and is given by:

$$J \frac{d\omega_m}{dt} = B_l \omega_m = T_e - T_l = T_a \quad (1.12)$$

where T_l is the load torque. Eq. (1.8) and Eq. (1.12) constitute the dynamic model of the DC motor with load.

1.6. State-Space Modelling

The dynamic equations can be written in state-space form and are given by:

$$\begin{bmatrix} p_t i_a \\ p_t \omega_m \end{bmatrix} = \begin{bmatrix} -\frac{R_a}{L_a} & -\frac{K_b}{L_a} \\ -\frac{K_b}{J} & -\frac{B_l}{J} \end{bmatrix} \begin{bmatrix} i_a \\ \omega_m \end{bmatrix} + \begin{bmatrix} \frac{1}{L_a} & 0 \\ 0 & -\frac{1}{J} \end{bmatrix} \begin{bmatrix} V \\ T_l \end{bmatrix} \quad (1.13)$$

where p_t is the differential operator with respect to time. Eq. (1.12) is expressed compactly in the form given by

$$\dot{\vec{X}} = \vec{A}\vec{X} + \vec{B}\vec{U}$$

where:

$$\vec{X} = [i_a \ \omega_m]^T, \quad \text{and} \quad \vec{U} = [V \ T_l]^T.$$

Here \vec{X} is the state variable vector, and \vec{U} is the input vector. Even though the load torque is a disturbance, for sake of a compact representation it is included in the input vector in this text.

$$\vec{A} = \begin{bmatrix} -\frac{R_a}{L_a} & -\frac{K_b}{L_a} \\ -\frac{K_b}{J} & -\frac{B_l}{J} \end{bmatrix}, \quad \vec{B} = \begin{bmatrix} \frac{1}{L_a} & 0 \\ 0 & -\frac{1}{J} \end{bmatrix}$$

The roots of the system are evaluated from the A matrix, which are:

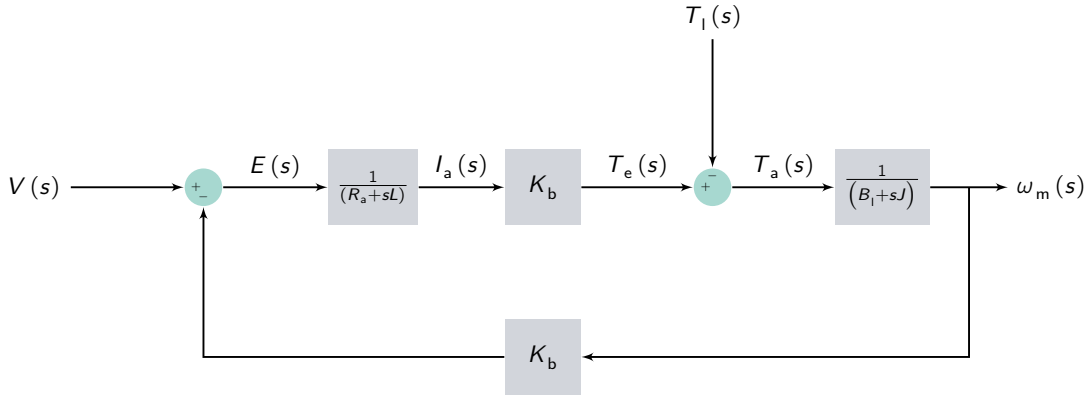


Figure 1.5.: Block diagram of a DC motor.

$$\lambda_{1,2} = \frac{-\left(\frac{R_a}{L_a} + \frac{B_1}{J}\right) \pm \sqrt{\left(\frac{R_a}{L_a} + \frac{B_1}{J}\right)^2 - 4\left(\frac{R_a B_1}{J L_a} + \frac{K_b^2}{J L_a}\right)}}{2} \quad (1.14)$$

It is interesting to observe that these eigenvalues will **always have a negative real part**.

This indicates the the motor is stable on open-loop operation.

1.7. Block Diagrams and Transfer Functions

Taking Laplace transforms of Eq. (1.8), Eq. (1.12) and neglecting initial conditions, we get

$$I_a(s) = \frac{V(s) - K_b \omega_m(s)}{R_a + sL_a} \quad \text{and} \quad \omega_m(s) = \frac{K_b I_a(s) - T_l(s)}{B_1 + sJ} \quad (1.15)$$

The relationship is represented in **Fig. 1.5**. We derive the transfer functions as follows:

$$G_{\omega V}(s) = \frac{\omega_m(s)}{V(s)} = \frac{K_b}{s^2(JL_a) + s(B_1L_a + JR_a) + (B_1R_a + K_b^2)} \quad (1.16)$$

$$G_{\omega I}(s) = \frac{\omega_m(s)}{T_l(s)} = \frac{-(R_a + sL_a)}{s^2(JL_a) + s(B_1L_a + JR_a) + (B_1R_a + K_b^2)} \quad (1.17)$$

The separately-excited DC motor is a **linear system**, and therefore the speed response due to the simultaneous voltage input and load torque disturbance can be written as a **sum of their individual responses**:

$$\omega_m(s) = G_{\omega V}(s)V(s) + G_{\omega I}(s)T_f(s) \quad (1.18)$$

Laplace inverse of $\omega_m(s)$ in Eq. (2.21) gives the time response of the speed for a simultaneous change in the input voltage and load torque. The treatment so far is based on a DC motor obtaining

its excitation separately. There are various forms of field excitation, discussed in the following section.

Exercise 1.1: DC Motor Starting Speed Response

A DC motor whose parameters are given in example 2.3 is started directly from a 220-V DC supply with **no load**. Find its starting speed response and the time taken to reach 100 rad s^{-1}

Solution

$$\frac{\omega(s)}{V(s)} = G_{\omega V}(s) = \frac{K_b}{s^2(JL_a) + s(B_a L_a + JR_a) + (B_a R_a + K_b^2)} = \frac{15,968}{s^2 + 167s + 12874}$$

$$V(s) = \frac{220}{s}$$

$$\omega(s) = \frac{3.512 \times 10^6}{s(s^2 + 167s + 12874)}$$

$$\omega(t) = 272.8 [1 - 1.47e^{-83.5t} \sin(76.02t + 0.744)]$$

The time to reach 100 rad/sec is evaluated by equating the left-hand side of the above equation to 100 and solving for t, giving an approximate value of 10 rad/ms. ■

1.8. Field Excitation

The excitation to the field is **dependent on the connections of the field winding relative to the armature winding**. Based on how these connections are made, there are different configurations used in industry.

1.8.1. Separately Excited

If the field winding is physically and electrically separate from the armature winding, then it is known as a separately-excited DC machine, whose equivalent circuit is shown in **Fig. 1.6**.

The independent control of field current and armature current allows it to have simple but high performance control on this machine, as the torque and flux can be independently and precisely controlled.

The field flux (ϕ_f) is controlled **only** by the control of the field current (i_f).

For simplicity, assume that the field is constant. Then the torque is proportional only to the armature current,

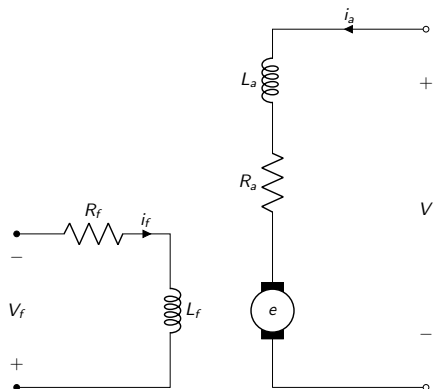


Figure 1.6.: Circuit diagram of a separately-excited DC machine.

and, therefore, by controlling only this variable, the dynamics of the motor drive system can be controlled. With the independence of the torque and flux-production channels in this machine, it is easy to generate varying torques for a given speed, making torque generation independent of the operating speed.

This is an important operating feature in a machine: the speed regulation can be zero¹³. This can be done via a feedback control and via open-loop operation.

¹³This basically means the motor can sustain the same level of torque with varying speed and this is achieved by controlling the field current.

Exercise 1.2: Separately Excited DC - I

A separately-excited DC motor is delivering rated torque at rated speed. Find the motor efficiency at this operating point. The details of the machine are as follows:

$$1500 \text{ kW}, \quad \text{Brush voltage drop} = 2 \text{ V}, \quad \text{rated current} = 2650 \text{ A}, \quad 600 \text{ rpm}, \\ 600 \text{ V}, \quad \text{Field power input} = 50 \text{ kW}, \quad R_a = 0.00364552 \Omega, \quad L_a = 0.1 \text{ mH},$$

and the machine frictional torque coefficient = 51 N m rad⁻¹ s
Field current is constant and the armature voltage is variable.

Solution

To find the input power, the applied voltage to the armature to support a rated torque and rated speed has to be determined. In steady state, the armature voltage is given by

$$V_a = R_a I_{ar} + K_b \omega_{mr} + V_r,$$

where I_{ar} is the rated armature current, given as 2650A, ω_{mr} is the rated speed in rad s⁻¹, and V_r is the voltage drop across the brushes in the armature circuit and is equal to 2 V as given by the problem. To solve this equation, the EMF constant has to be solved for from the available data. Recalling the torque and EMF constants being equal, the torque constant can be calculated from the rated electromagnetic torque and the rated current as

$$K_I = \frac{T_{er}}{I_{ar}} = \frac{T_s + T_f}{I_{ar}}$$

where the rated electromagnetic torque generated in the machine (T_{er}) is the sum of the rated shaft torque (T_s), and friction torque (T_f). The rated shaft or output torque is obtained from the output power and rated speed as follows:

$$\begin{aligned} \text{Rated speed } \omega_{mr} &= \frac{2\pi}{60} 600 = 62.83 \text{ rad s}^{-1} \\ \text{Rated shaft torque } T_s &= \frac{P_m}{\omega_{mr}} = \frac{1500 \times 10^3}{62.83} = 23,873 \text{ N m} \\ \text{Friction torque } T_f &= B_f \omega_{mr} = 15 \times 62.83 = 942.45 \text{ N m} \\ \text{Electromagnetic torque } T_{er} &= T_s + T_f = 23,873 + 942.45 = 24,815.45 \text{ N m} \end{aligned}$$

Therefore, the torque constant is:

$$\begin{aligned} K_f &= \frac{T_{er}}{I_{ar}} = \frac{24,815.45}{2650} = 9.364 \text{ N m A}^{-1} \\ K_b &= 9.364 \text{ V rad}^{-1} \text{ s} \end{aligned}$$

We can now calculate the input armature voltage as:

$$V_a = 0.003645 \times 2650 + 9.364 \times 62.83 + 2 = 600 \text{ V}$$

Armature and field power inputs:

$$V_a I_{ar} + \text{Field power input} = 600 \times 2650 + 50,000 = 1640 \text{ kW}$$

Therefore it's efficiency is:

$$\text{Efficiency} = \eta = \frac{P_m}{P_i} = \frac{1500}{1640} = 91.46\% \blacksquare$$

1.8.2. Shunt Excited

If the field winding is connected in **parallel** to the armature winding, it is called **shunt-excited DC machine** or **DC shunt machine**. The equivalent circuit of the machine is shown in **Fig. 1.7.**

The field winding does not need a separate power supply, as it does in the case of the separately-excited DC machine.

For a constant input voltage, the field current and hence the field flux are **constant**. While it is good for a constant-input-voltage, unfortunately this cannot be said for variable speed operation. In variable-input voltage operation, an independent control of armature and field currents is lost, leading to a **coupling** of the flux and torque production channels in the machine. This is in contrast to the control simplicity of the separately-excited DC machine.

As torque is increased, the armature current increases, and hence the armature voltage drop also increases, while at the same time, the induced EMF is decreased. The reduction in the induced EMF is reflected in a lower speed, since the field current is constant in the machine.

The drop in speed from its no-load speed is relatively small, and because of this, the DC shunt machine is considered a **constant-speed machine**.

Such a feature makes it unsuitable for variable-speed application.

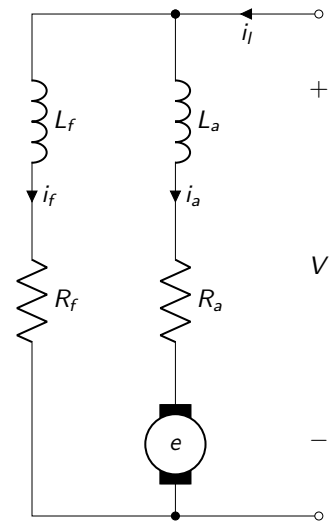


Figure 1.7.: Circuit diagram of a shunt-excited DC machine.

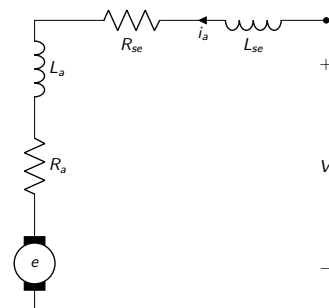


Figure 1.8.: Circuit diagram of a series-excited DC machine.

1.8.3. Series Excited

If the field winding is connected in series with the armature winding, then it is known as the **series-excited DC machine** or **dc series machine**, and its equivalent circuit is shown in **Fig. 1.8.**

It has similar disadvantages as the shunt machine, as there is **no independence** between the control of the field and the armature currents. The electromagnetic torque of the machine is proportional to the square of the armature current, as the field strength is equal to the armature current.

At low speeds, a high armature current is possible, with a large difference between a fixed applied voltage and a small induced EMF. This results in high torque at starting and low speeds, making it

an ideal choice for applications requiring high starting torques.¹⁴ With the dependence of the torque on the square of the armature current and the fact that the armature current availability goes down with increasing speed, torque-vs-speed characteristic resembles a hyperbola.

¹⁴ Generally this has seen good usage in public transportation project, such as trams or trains.

At zero speed and low speeds, the torque is large but somewhat curtailed from the square current law because of the saturation of the flux path with high currents. However when the machine starts with **NO** load, then there will be zero (**0**) load current which means zero field current. For zero field current there will be zero flux. Based on the equation governing the speed of a DC motor:

$$n_r = \frac{(V - I_a R_a - I_f R_f)}{K\phi_f}$$

As can be seen as $\lim_{\phi_f \rightarrow \infty}$, and if you don't have the proper safety measures in place, you gonna have a bad time.

1.8.4. Compound

Combining the best features of the series and shunt DC machines by having **both a series and shunt field** in a machine leads to the **dc compound machine** [10], shown in **Fig. 1.9**. The manner in which the shunt-field winding is connected in relation to the armature and series field provides two (**2**) kinds of compound DC machine [11].

- If the shunt field encompasses the series field and armature windings, then that configuration is known as **long-shunt** compound DC machine.
- If the shunt field encompasses only the armature winding it is called **short-shunt** compound DC machine.

Whether the field fluxes of the shunt and series field are opposing or strengthening each other gives two (**2**) other configurations, known as [12]:

- differential compound,
- cumulatively compound.

respectively, for each of the long and short shunt connections.

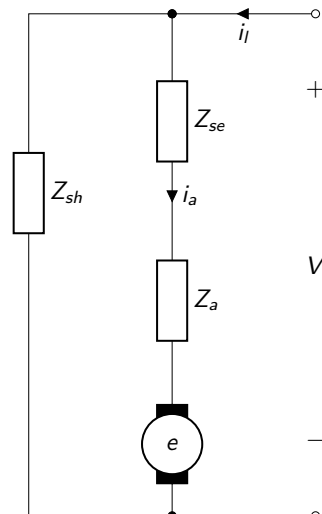


Figure 1.9.: Circuit diagram of a separately-excited DC machine.

1.8.5. Permanent-Magnets

Instead of an electromagnet with an external DC supply, the excitation can be provided by PMs such as ceramic, AlNiCo, and others¹⁵. The advantage of such an excitation consists in the compactness of the field structure and elimination of resistive losses in the field winding. These features contribute to a compact and, temperature-wise¹⁶, cooler machine, desirable features for a high-performance motor. For a sneak peek, you can see a structure of BLDC in **Fig. 1.10.**



Figure 1.10.: A standard out-runner rotor BLDC motor. Here the rotor which contains PM is spinning **outside** whereas the stator is inside [13].

the armature is similar to other DC motors in construction and performance.

1.9. Measuring the Motor Constants

To analyse a DC motor, the constants R_a , L_a and K_b and the resistance and inductance of field windings are required. Some of them are given in the manufacturers' data sheets. In case of non-availability of the data, it is helpful to have knowledge of procedures to measure these constants.

In this short digression we will have a look at the test methods to a separately excited dc motor¹⁷.

1.9.1. Armature Resistance

Armature, if you recall is the part where AC current flows, in which case for DC motor is the **rotor**. The DC value of the armature resistance is measured between the armature terminals by applying a DC voltage to circulate rated armature current.

It is important to subtract the brush and contact resistance from the measurement and to correct for the temperature at which the motor is expected to operate at steady state.

1.9.2. Armature Inductance

By applying a low AC voltage through a variac¹⁸ to the armature terminals, the current is measured. The motor has to be at a standstill, keeping the induced EMF at zero.

Permeability, the residual voltage in the machine is wiped out by repetitive application of positive and negative DC voltage to the armature terminals.

¹⁵These will be covered in Chapter 5 in significant detail.

¹⁶Cooling is an age old problem when designing machines and expect to use %5-%6 of the generated energy to cool the machine itself.

¹⁷The reason as why this motor was chosen instead of other types is that it is the most widely used motor for variable-speed applications.

The inductance is

$$L_a = \frac{\sqrt{(V_a^2/I_a) - R_a^2}}{2\pi f_s}$$

where f_s is the frequency in Hz and the armature resistance has to be the AC resistance of the armature winding.

This is different from the DC resistance, because skin effect¹⁹ produced by the alternating current.

¹⁹The tendency of AC to become distributed within a conductor such that the current density is largest near the surface of the conductor and decreases exponentially with greater depths in the conductor.

1.9.3. EMF Constant

Rated voltage²⁰ is applied and kept constant, and the shaft is rotated by a prime mover (another DC motor) up to the speed given in the name plate (called rated speed or base speed).

The armature is open-circuited, with a voltmeter connected across the terminals. The voltmeter reads the induced EMF, and its readings are noted for various speeds and are plotted as shown in **Fig. 1.11**. The slope of this curve at a specific speed gives the EMF constant in volt-sec/rad as seen from Eq. (1.3). The relationship shown in **Fig. 1.11** is known as the open-circuit characteristic of the DC machine²¹.

²⁰Also known by some engineering wizards as specific field voltage [14].

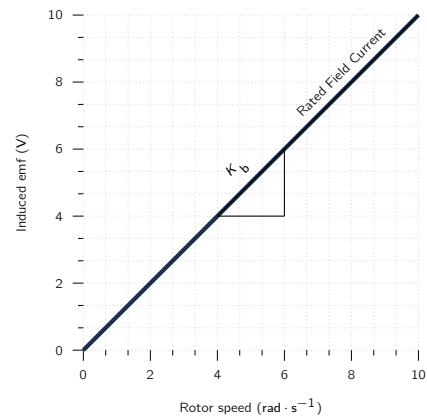


Figure 1.11.: Induced EMF v. rotor speed characteristics at rated field current.

²¹for a permanent-magnet machine, this procedure is not applicable.

1.10. Simulation

Based on previous knowledge, let's do a simulation of a separately-excited DC machine. For this we will use OpenModelica.

1.10.1. Separately-Excited

The model for the simulation is given in **Fig. 1.12**. As can be seen there are a few things which are worth discussing. First is we need to turn on the motor, for that we employ a ramp function which increases the armature voltage in a linear fashion²².

Second aspect is the introduction of a load. While it is true that the motor has inherent inertial load, as it is spinning the rotor, an additional load is introduced to study its dynamics when sudden change in load occurs.

²²Think of this as someone slowly turning down a potentiometer to slowly start a machine.

Parameter	Value	Symbol	Parameter	Value	Symbol
Field Voltage	100	V	Armature Voltage	100	V
Field Resistance	100Ω	R_f	Armature Resistance	0.05Ω	R_a
Field Inductance	1 H	L_f	Armature Inductance	0.0015 H	L_a
Nominal Armature Voltage	100 V	$V_{a(nom)}$	Nominal Armature Current	100 A	$I_{a(nom)}$
Nominal Rotor Speed	1425 rpm	$\omega_{r(nom)}$	Rotor Inertial Load	0.15 kg m^{-2}	J_r
Torque Step	-66.93 N m	T_{step}	Torque Step start-time	1 s	t_{torque}
Ramp duration	0.8 s	$t_{ramp(dur)}$	Ramp start time	0.2 s	$t_{ramp(start)}$

Table 1.1.: Simulation parameters for the separately-excited DC motor.

The results are shown in the following section.

Let's have a look at the results. As we can see the field current has an almost instant but a delayed response. This is caused by the field inductance having a delayed response to the current²³. The current does not change with regards to the load as the field is **independent** from the load of the rotor.

Some of you who may be observant may ask about the effect of the armature reaction on the field current. While the effect can be noticeable the complexity of mathematical modelling is not justified for the accuracy one would get from implementing it.

Another important factor to mention is the **proportional relationship** between the generated electromagnetic torque and the armature current. As can be seen one is just a direct proportion of another. The machine with its internal load (J_r) stabilises at around 60 N m but once the new load is introduced, the machine has increased the torque production and with it, it is drawing even higher current from the grid.

Final thing to consider is the rotational speed (ω_r). Here without the load the motor is reaching around 1500 rpm, which is higher than its defined nominal operational speed²⁴. Once the significant load is introduced, the rotor speed stabilises to its nominal value.

²³While in steady-state the entire system can be analysed as a DC, in transient behaviour the AC properties **must** be taken into account.

²⁴This is due to the fact that the machine, when designed, assumes a load to be operated upon and its nominal speed is calculated based on that.

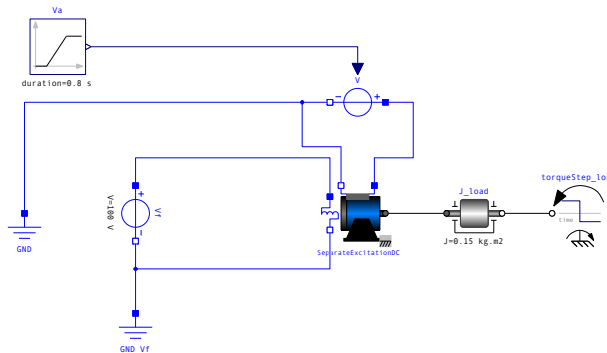


Figure 1.12.: The simulation diagram of a separately excited DC machine.

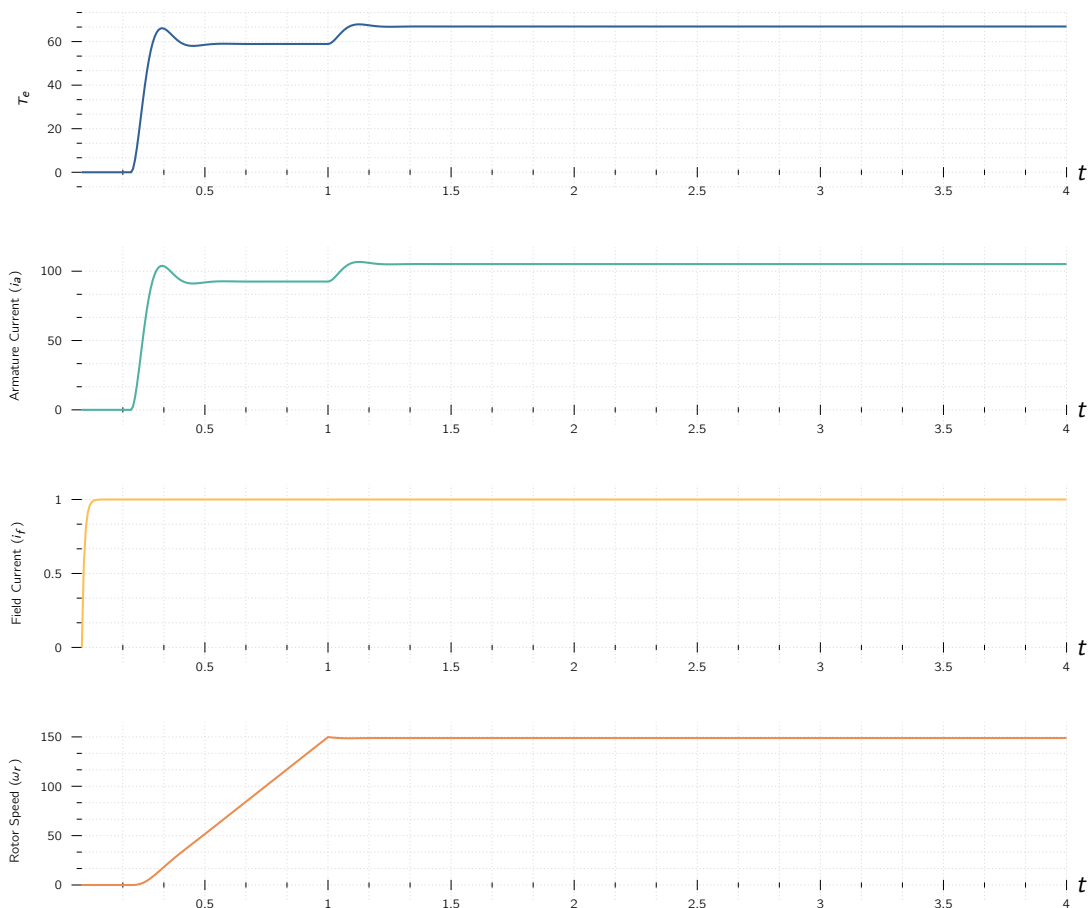


Figure 1.13.: Simulation Results of the separately-excited DC motor.

Chapter 2

Phase Controlled DC Machines

Table of Contents

2.1. Introduction	21
2.2. Principles of DC Machine Speed Control	22
2.3. Phase Controlled Converters	29
2.4. Steady State Analysis of 3-Phase Converter Drive	39
2.5. Two Quadrant 3-Phase Converter Control	41
2.6. Transfer Functions of the Subsystems	42
2.7. Designing Controllers	43

2.1. Introduction

The principle of speed control for DC motors is developed from the basic DC equation of the motor given in Chapter 1. Torque, flux, current, induced EMF, and speed are then **normalised** to present the motor characteristics.

There are two (2) types of control available:

1. armature control,
2. field control.

These methods are then combined to give a wide range of speed control to the DC motor.

An important aspect to consider, which will be discussed here is the torque-speed characteristics **for both directions of rotation** and delivering both motoring and regenerating torques in any direction of rotation. Such an operation, known as **four-quadrant** operation, has a unique set of requirements

on the input voltage and current to the motor armature and field.

Modern power converters constitute the power stage for variable-speed DC drives. These power converters are chosen for a particular application depending on a number of factors such as:

cost, input power source, harmonics, power factor, noise, and speed of response.

Here we will focus on controlled-bridge rectifiers fed from single-phase and three-phase AC. The theory, operation and control of the three-phase controlled-bridge rectifier is considered in detail, because of its widespread use.

2.2. Principles of DC Machine Speed Control

2.2.1. Important Relationships

Recalling Chapter 1, the dependence of induced voltage on the field flux and speed has been derived and shown to be:

$$e = K\phi_f \omega_m, \quad (2.1)$$

where e is the EMF, K is the machine constant, ϕ_f is the field flux, and ω_m is the rotor speed. The field flux is proportional¹ to the field current if the iron is NOT saturated and is represented as:

$$\phi_f \propto i_f, \quad (2.2)$$

By substituting Eq. (2.2) into Eq. (2.1) the rotor speed (ω_m) is expressed as:

$$\omega_m \propto \frac{e}{\phi_f} \propto \frac{e}{i_f} \propto \frac{(v - i_a R_a)}{i_f}, \quad (2.3)$$

where v and i_a are the applied voltage and armature current, respectively.

From Eq. (2.3), we can see the rotor speed is dependent on the applied voltage and field current. As resistive armature voltage drop is very small compared to the rated applied voltage, the armature current has only a secondary effect.

To make its effect dominant, an external resistor in series with armature can be connected. In that case, the speed can be controlled by varying stepwise the value of the external resistor as a function of operational speed. As power dissipation in the external resistor leads to lower efficiency we will not consider this as a useful approach in this lecture.

Only two (2)other forms of control, using armature voltage and field current will be discussed as practically applicable.

2.2.2. Field Control

In **field control**, the applied armature voltage (v_a) is **maintained constant**. Then the speed is represented by Eq. (2.3) as:

$$\omega_m \propto \frac{1}{i_f} \quad (2.4)$$

As we can see, the **rotor speed is inversely proportional to the field current**.

By varying the field current, the rotor speed is changed.

Reversing the field current changes the rotational direction. By weakening the field flux, the speed can be increased. The upper speed is limited by the commutator and brushes and the time required to turn off the armature current from one commutator segment to another.

It is **NOT** possible to strengthen the field flux current (total nominal) value, on account of saturation of the steel limitations. Therefore, field control for speed variation is **NOT** suitable below the rated (nominal) speed.

At rated speed, the field current by design is at rated value, and, therefore, the flux density is chosen to be near the knee of the magnetisation curve of the steel lamination used in construction of the machine.



2.2.3. Armature Control

In this control method, the field current is maintained **constant**.

Then the speed is derived from Eq. (2.3) as:

$$\omega_m \propto (v - i_a R_a)$$

We can see here, varying the applied voltage changes speed and reversing the applied voltage changes the direction of rotation of the motor.

Armature control has the advantage of controlling the armature current **swiftly**, by adjusting the applied voltage.

The response is determined by the armature time constant, which has a very low value, contrast to the field time constant, which is at least 10 to 100 times greater than the armature time constant². The large time constant of the field causes the response of a field-controlled DC motor drive to be slow and sluggish.

Armature control is limited in speed by the limited magnitude of the available DC supply voltage and armature winding insulation. If the supply DC voltage is varied from zero to its nominal value, then the speed can be controlled from zero to nominal or rated value.

Figure 2.1.: Mechanical commutation is done via physical contact points being interfaced by brushes. During changing of contact, the brushes create a short-circuit creating arcs [15].

²This is due to field winding having a significant inductance compared to armature winding.

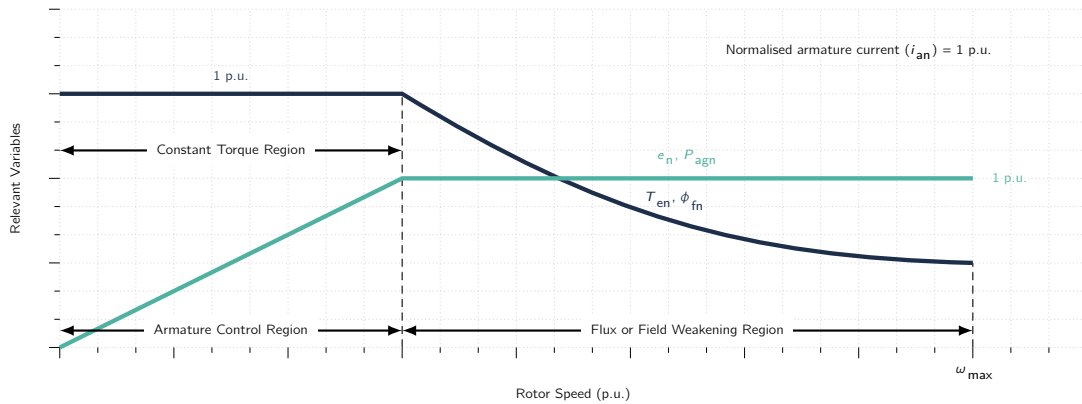


Figure 2.2.: Normalised characteristics of a variable-speed DC motor.

Armature control is ideal for speeds **lower than rated speed** and field control is suitable for speeds higher than the rated speed.

2.2.4. Armature and Field Control

By combining both armature and field control for speeds below and above the rated speed, respectively, a wide range of speed control is possible. For speeds lower than rated speed, applied armature voltage is varied while the field current is kept at its rated value and to obtain speeds above the rated speed, field current is decreased while keeping the applied armature voltage constant. The induced EMF, power, electromagnetic torque, and field-current v. speed characteristics are shown in **Fig. 2.2.**

The armature current is assumed to be equal to the rated value for now. The power and torque curves need some derivation. The following equation:

$$T_e = K\phi_f i_a \quad (2.5)$$

Eq. (2.5) can be normalised if it is divided by rated torque, which is expressed as

$$T_{er} = K\phi_{fr} i_{ar}$$

where the additional subscript *r* denotes the rated or nominal values of the corresponding variables. Therefore, the normalised version of Eq. (2.5) is

$$T_{en} = \frac{T_e}{T_{er}} = \frac{K\phi_f i_a}{K\phi_{fr} i_{ar}} = \left(\frac{\phi_f}{\phi_{fr}} \right) \left(\frac{i_a}{i_{ar}} \right) = \phi_{fn} i_{an} \quad \text{p.u.} \quad (2.6)$$

where the additional subscript *n* expresses the variables in **normalised** terms, commonly known as per unit (p.u.) variables.

a per-unit system is the expression of system quantities as fractions of a defined base unit quantity. Calculations are simplified because quantities expressed as per-unit do **NOT** change when they are referred from one side of a transformer to the other.

Normalisation **eliminates** machine constants, simplifies the performance equations, and enables the visualisation of performance characteristics **regardless of machine size** on the same scale³. The normalised torque, flux, and armature current are:

$$T_{\text{en}} = \frac{T_e}{T_{\text{er}}}, \quad \phi_{\text{fn}} = \frac{\phi_f}{\phi_{\text{fr}}}, \quad i_{\text{an}} = \frac{i_a}{i_{\text{ar}}} \quad \text{per unit} \quad (2.7)$$

As the armature current is maintained at 1 p.u. in **Fig. 2.2**, the normalised torque becomes:

$$T_{\text{en}} = \phi_{\text{fn}} \quad (2.8)$$

Therefore, the normalised electromagnetic torque characteristic coincides with the normalised field flux, as shown in **Fig. 2.2**. Similarly, the air gap power is:

$$P_{\text{agn}} = e_n i_{\text{an}} \quad (2.9)$$

where e_n is the normalised induced EMF. As i_{an} is set to 1 p.u., the normalised air gap power becomes

$$P_{\text{agn}} = e_n \quad (2.10)$$

The normalised power output characteristic is similar to the induced EMF of the DC motor in the field-weakening and constant-torque regions. The normalised induced EMF is the product of the normalised flux and speed. Flux is at 1 p.u. in the armature control region, so the normalised induced EMF is equal to the normalised speed.

The flux is hyperbolic in the field-wakening region with an inverse relationship with the speed.

Field weakening needs to be discussed in detail here.

At rated speed, the motor is delivering rated power with e_n and i_a at their rated values. Beyond the rated speed, the field current is decreased to reduce the field flux. This will affect the load-mode power output of the hence the power output.

It is very important that the steady-state power output of the machine be kept from exceeding its rated design value, which is 1 p.u..

The implication of the air gap power constraint is that the induced EMF and field flux are to be coordinated to achieve this objective. The coordination gives the value of field flux as:

$$P_{\text{agn}} = 1 \text{ p.u.} = e_n i_{\text{an}} = \phi_{\text{fn}} \omega_{\text{mn}} i_{\text{an}} \quad (2.11)$$

If i_{an} is equal to 1 p.u., then:

$$\phi_{\text{fn}} \omega_{\text{mn}} = 1 \quad \phi_{\text{fn}} = \frac{1}{\omega_{\text{mn}}}$$

Therefore, the normalised induced EMF is given as.

³Designers and seasonal analysts prefer the p.u. representation because of all these features

$$e_n = \phi_{fn} \omega_{mn} = \frac{1}{\omega_{mn}} \times \omega_{mn} = 1 \text{ p.u.} \quad (2.12)$$

The power output and induced EMF are maintained at their rated values in the field-weakening region by programming the field flux to be inversely proportional to the rotor speed. They are shown in **Fig. 2.2**.

2.2.5. Four Quadrant Operation

⁴such as in robotic actuation.

Many applications require controlled starts and stops of the DC motor⁴. Consider a DC machine is operating at a steady speed of ω_m , and it is desired to bring the speed to zero. There are two (2)ways to achieve it:

- Cut off the armature supply to the machine and let the rotor come to zero speed.
- The machine can be made to work as a DC generator, thereby the stored kinetic energy can be effectively transferred to the source. This saves energy and brings the machine rapidly to zero speed.

Cutting off supply produces a **haphazard speed response** whereas the second method provides a controlled braking of the DC machine. To make the machine operating in the 2nd mode go to the generation mode, all that needs to be done is to reverse the armature current flow in the DC machine. First, the armature current drawn from the source has to be brought to zero. Then, a current in the opposite direction has to be built. Zeroing the current is achieved by making the source DC voltage zero or, better, by making it negative. After this, the armature current is built in the opposite direction by making the source voltage smaller than the induced EMF.

As the speed reduces, note that the induced EMF decreases, necessitating a continued corresponding reduction in the source voltage to keep the armature current constant.

The power flows from the machine armature to the DC source. This mode of operation is termed **regenerative machine**. The braking is accomplished by regeneration which implies a negative torque is generated in the machine as opposed to the positive motoring torque. Therefore a mirror reflection of the speed-torque characteristics, shown in **Fig. 2.2**, is required on the IV quadrant of the regeneration.

Quadrants I and IV are for on direction of rotation.

Some applications, such as a feed drive in machine tools, require operation in both directions of rotation. In that case, the III quadrant signifies the reverse motoring and II quadrant, the reverse regeneration mode.

A motor drive capable of operating in both directions of rotation and of producing both motoring and

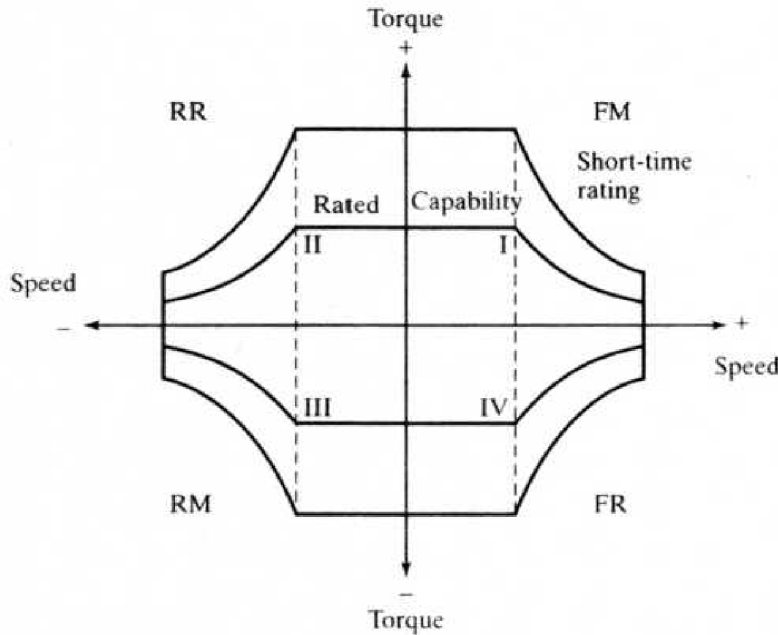


Figure 2.3.: Four-quadrant Torque-speed characteristics.

regeneration is referred to as a **four-quadrant variable-speed drive**. The torque-speed characteristics of such a motor drive is shown in **Fig. 2.3**. This contains two (2) characteristics:

- For rated operating conditions,
- Short time (intermittent) operation.

The short-time characteristic is used for acceleration and deceleration of the machine⁵

Figure 3.5 illustrates the speed and torque variation from a point P_1 to Q_1 and Q_1 to P_2 for the machine. On receiving the command to go from P_1 to Q_1 , the torque is changed to negative by regenerating the machine, as shown to be a trajectory P_1M_1 . This regeneration torque, along with the load torque, produces a trajectory torque. The torque is maintained at the permitted maximum levels both in the field-weakening and the constant-flux regions. As the machine decreases, as shown by the trajectory M_1M_2 , it will reach zero speed, and keeping the torque at a negative maximum will drive the motor in the reverse direction along the trajectory M_2M_1 . Once the desired speed ω_{m2} is reached, the torque is adjusted to equal the specified value, $-T_{c2}$; along the trajectory M_2Q_2 . Similarly, to change the operating point from Q_2 to P_2 , the trajectory shown along $Q_2M_2M_1P_2$ is followed.

⁵it normally encompasses 50 to 100% greater than the rated torque for DC machines

From this illustration, it is seen that the use of all quadrants of operation leads to a very responsive motor drive. Contrast this to the supply cut-off technique. In such a case, only the load torque contributes to the deceleration, as opposed to the combined machine and load torques in a four-quadrant motor drive.

Converter Requirements

The voltage and current requirements for four-quadrant operation of the DC machine are derived as follows. Assuming the field flux is constant, the speed is proportional to the induced EMF and hence approximately proportional to the applied voltage to the armature. Also, the electromagnetic torque is proportional to the armature current. Then the speed axis becomes the armature voltage axis and the torque axis is equivalent to the armature current axis. From this observation, the armature voltage and armature current requirements for four-quadrant operation are given in Table 3.2.

These requirements in turn, set the specifications for the electronic converter. For a pump application as an example, the motor needs only unidirectional operation with no regenerative braking. Therefore, only first is required, thereby limiting the converter specification to only positive voltage and current variations. Therefore, the power flow is **unidirectional** from source to load. For a golf cart electric-vehicle propulsion-drive application, a four-quadrant operation is required, with the attendant converter capability to handle power in both directions with bipolar voltage and current requirements. This, in turn, makes the converter more complex than that required for a one-quadrant drive.

From a fixed utility AC source, a variable-voltage and variable-current DC output is obtained through two (2) basic methods by using static power converters. The first method uses a controllable rectifier to convert the AC source voltage directly into a variable DC voltage in one single stage of power conversion, using phase-controlled converters. The second method converts the AC source voltage to a fixed DC voltage by a diode bridge rectifier and then converts the fixed DC variable DC voltage with electronic choppers. The first method is considered in this chapter.



Figure 2.4.: Thyristors are diodes which their conduction could be controlled.

Thyristor Converter

The realisation of an AC/DC variable-voltage converter by means of the SCR known as thyristors will be our current focus and we will look into the distinct features of the thyristor are given here, without going into the device physics. Thyristors are four-element (PNPN), three-junction devices with the terminals of:

- Anode (A),
- Cathode (K)
- Gate (G)

A gate current is injected by applying a positive voltage between gate (G) and cathode (C) for turning **ON** the device.

The device turns **ON** only if the anode is positive compared to cathode at least by 1 V.

Once turned-on, the device drop is around 1 V for most devices⁶ and will act like a diode. To turn off the thyristor, the device has to be **reverse biased** by making the anode **negative with respect to the cathode**. This is easily achieved with ac input voltage during its negative full-cycle.

This control of this electronic device is known as *device commutation*.

Unlike a diode, SCR can hold of conduction even when anode is positive compared to anode, without triggering the angle.

These features mentioned previously make the thyristors ideal devices for AC/DC conversion. Instead of diodes in the diode bridge rectifier, thyristors can be substituted, and by delaying the condition from their zero crossings, a **part** of the AC voltage is rectified for feeding to a load. The DC load is reduced from the maximum available in the half-cycle AC voltage waveform, which in turn varies the average load voltage. The line voltage commutes the devices when it reverses polarity with each half cycle and applies a negative voltage across the cathode and anode⁷.

⁶This is analogous to the voltage drop caused by diodes. Of course this drop is directly determined by the materials. For example, the reason why it is silicon and NOT germanium is for exactly to minimise the voltage drop.

⁷This method is known as line (natural) commutation and the inverters are also known as **line-commutated** converters.

2.3. Phase Controlled Converters

2.3.1. Single-Phase Controlled Converter

A simulation of a single-phase-controlled rectifier is shown in **Fig. 2.5** with its input and output voltage and current waveform shown in **Fig. 2.6**.

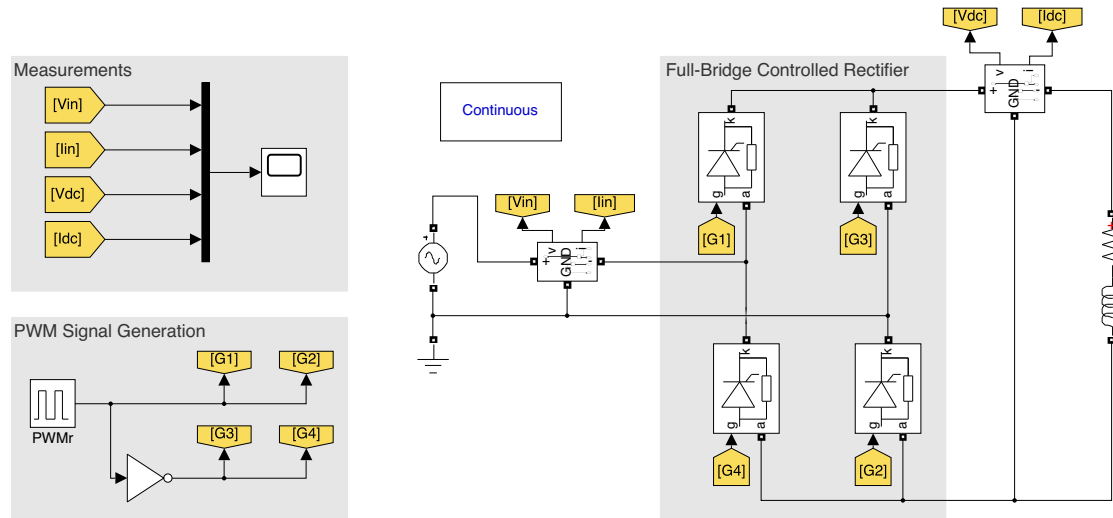


Figure 2.5.: The Simulink implementation of a single phase rectifier circuit. The parameters are: firing angle (α) = 30° , resistance (R) is

In this circuit, the load consists of a resistance (R) and an inductance (L), and the current is assumed to be **continuous and constant**.

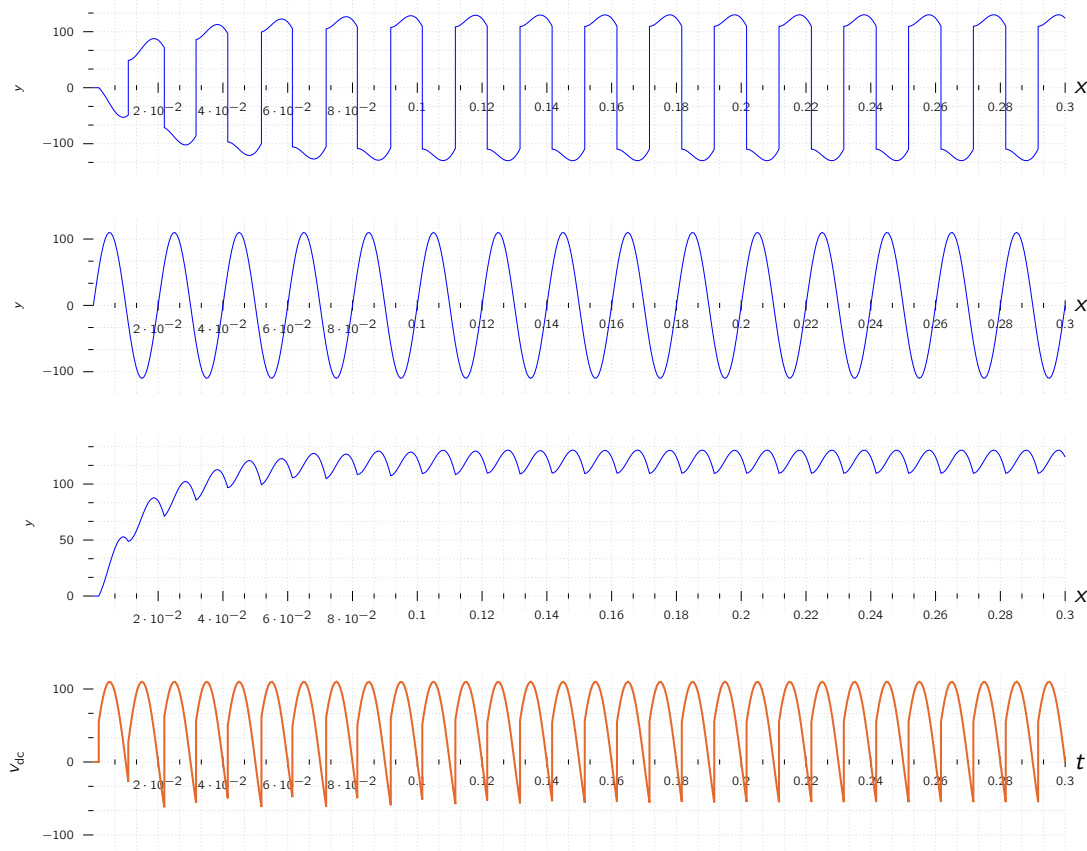


Figure 2.6.: The generated waveforms of the SIMULINK implementation of a single phase rectifier circuit.

The difference between the diode and this thyristor (i.e., SCR) version is that conduction can be delayed in the latter **beyond positive zero crossing**.

The delay is introduced in the form of triggering signals to the gates of the thyristors. The delay angle is measured from the zero crossing of the voltage waveform and is generally termed α^8

⁸usually measured in radians.

. Although the load voltage has both positive and negative V , its average is a **net positive** and indicated by the horizontal dashed lines denoted as V_{dc} . Assuming continuous load current, this voltage is quantified as

$$V_{dc} = \frac{1}{\pi} \int_{\alpha}^{\alpha+\pi} V_m \sin(\omega_s t) d(\omega_s t) = \frac{2V_m}{\pi} \cos \alpha \quad (2.13)$$

where V_m is the maximum value of the input AC voltage. Increasing the delay angle (α) to greater than 90° produces a **negative voltage** on average, as is shown in **Fig. 2.8**.

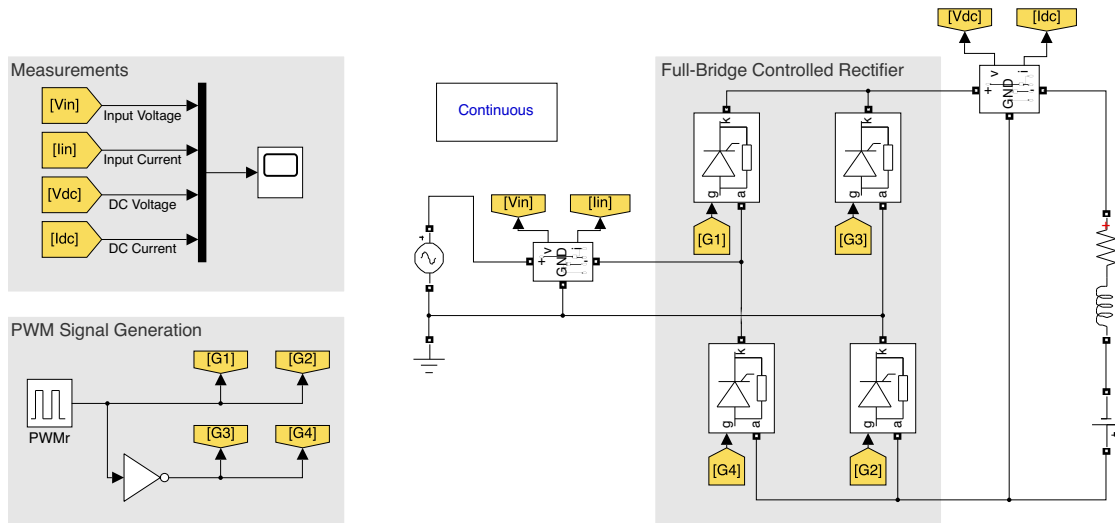


Figure 2.7.: The Simulink implementation of a single phase rectifier circuit. The parameters are: firing angle (α) = 30° , resistance (R) is

when $\alpha > 90^\circ$ The current is in the same direction, thus contributing to a negative power input, known as inversion.

It is assumed here that there is an EMF source⁹ in the load contributing to the power transfer from the load to source. Such a load is known as an **active load**. Because the load is active, the load current can be **discontinuous**. In that case, the average output voltage is derived to be:

$$V_{dc} = \frac{1}{\pi} \int_{\alpha}^{\alpha+\gamma} V_m \sin(\omega_s t) d(\omega_s t) = \frac{V_m}{\pi} [\cos(\alpha) - \cos(\alpha + \gamma)] \quad (2.14)$$

where γ is the **current conduction angle**. Comparing Eq. (2.13) and Eq. (2.14), we can see, for certain values of γ , the output voltage for discontinuous conduction can be greater than that for continuous conduction. For example, let:

$$\alpha + \gamma = \pi \quad \text{and} \quad \alpha = 30^\circ.$$

Which in turn gives the average output voltage for discontinuous current conduction as:

$$V_{dc(dcm)} = \frac{V_m}{\pi} \left(\cos \frac{\pi}{6} - \cos \pi \right) = \frac{V_m}{\pi} (1.866), \quad (2.15)$$

and, for the same triggering angle, the average output voltage for continuous-current conduction is given by:

$$V_{dc(ccm)} = \frac{2V_m}{\pi} \times \cos \frac{\pi}{6} = \frac{2V_m}{\pi} \times 0.866 = \frac{V_m}{\pi} 1.732 \quad (2.16)$$

The transfer characteristics for continuous conduction for an active load and discontinuous conduction for a resistive load are shown in **Fig. 2.8**.

The source¹⁰ inductance delays the current transfer from one pair of conducting thyristors to another set. During this time, the source is short-circuited through the source impedance, invariably reducing the load voltage to zero (0).

⁹As we are studying here DC machines, one could consider the combination of R-L-E as the motor with R-L being the stator impedance.

¹⁰Remember the grid is a massive infrastructure and there is some electrical elements between the plug and the circuit.

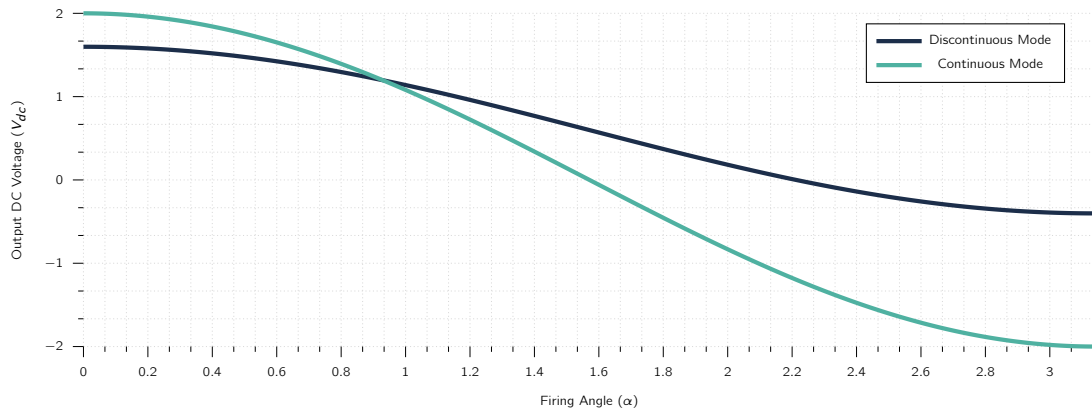
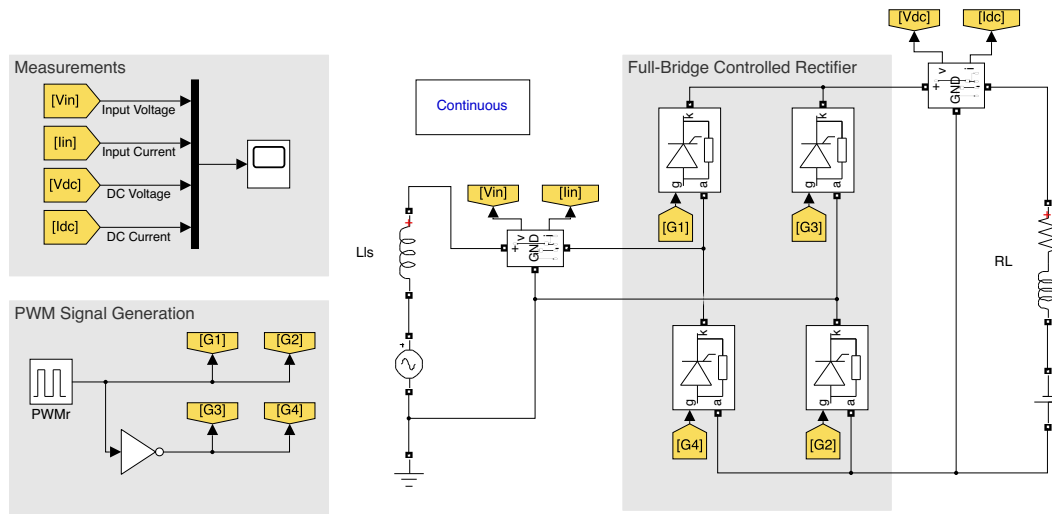


Figure 2.8.: The characteristic behaviours of a thyristor in different conduction modes.

Figure 2.9.: The Simulink implementation of a single phase rectifier circuit. The parameters are: firing angle (α) = 30°, resistance (R) is

Therefore, the overall effect of source inductance is to reduce the available DC output voltage.

Figure 3.9 contains the operational waveforms with source inductance.

The source inductance can be introduced by the isolation transformer or by intentionally placed reactors, to reduce the rate of rise of currents in the thyristors.

If the source inductance is defined as L_{ls} , the voltage lost due to it is:

$$V_{dc} = \frac{1}{\pi} \int_{\alpha}^{\alpha+\mu} V_m \sin(\omega_s t) d(\omega_s t) = \frac{V_m}{\pi} [\cos(\alpha) - \cos(\alpha + \mu)] \quad (2.17)$$

where μ is the overlap conduction period. By equating this voltage to the voltage drop in the source reactance, we can calculate the overlap angle μ as:

$$\mu = \cos^{-1} \left[\cos \alpha = \frac{\pi \omega_s L_{ls} I_{dc}}{V_m} \right] - \alpha \quad (2.18)$$

where I_{dc} is the load current in steady state.

These characteristics are modified when the load includes a counter-EMF, as in the case of a DC machine.

There is an additional feature in discontinuous operation, with the induced EMF appearing across the output of the converter during zero-current intervals, but, if the source EMF is instantaneously greater than the back emf, then the conduction starts but will **NOT** end immediately when the source EMF becomes less than the induced emf, due to the energy stored in the machine inductance and in the external inductance connected in series to the armature of the machine. Therefore, conduction will be prolonged until the energy in these inductances is depleted.

The three-phase controlled full-bridge converter is similar in operation to the single-phase controlled rectifier. Three-phase converters are widely used for both DC and ac motor control. The emphasis is placed on the three-phase converter-controlled DC motor drive. The following section contains the principle of operation, design features of the control circuit, and the characteristics of this converter.

2.3.2. Three-Phase Controlled Converter

A three-phase SCR converter is shown in Figure 1.10 as a Simulink Simulation, and its voltage and current waveforms in the rectifier model of operation are shown in Figure 3.11. For simplicity the current is **assumed continuous** for the present.

At a given instant two-thirds ($2/3$) of the thyristors are conducting.

Assuming that the voltage between phases a and b is maximum, then the transistors T_1 and T_6 are conducting. The next line voltage to get more positive than ab is ac . At that time, the triggering signal for T_6 will be disabled and that of T_2 will be enabled.

the anode of T_2 is more negative than the cathode of T_6 , because line voltage ac is greater than the line voltage ab .

That will turn off T_6 and transfer the current from T_6 to T_2 . The delay in current transfer from T_6 to T_2 is dependent on the source inductance. During this current transfer, T_1 , T_6 and T_2 are all conducting, and the load voltage is the average of the line voltages ab and ac .

This phenomenon is the commutation overlap, resulting in a reduction in the load voltage.

The load current will remain the same during commutation of T_6 . The current in T_6 declines by the same proportion as current in T_2 rises. It is to be observed that the current transfer is effected by the source voltages: voltage ac become greater than the voltage ab , resulting in the reverse biasing of T_6 and forward biasing of T_2 . Similarly, it could be seen that the firing/gating sequence is:

$$T_1 \rightarrow T_2 \rightarrow T_3 \rightarrow T_4 \rightarrow T_5 \rightarrow T_6$$

and so on. Also, each of these gating signals is spaced by 60° ($\pi/3$) electrical degrees.

The thyristors require small reactors in series to limit the rate of rise of currents and snubbers, which are resistors in series with capacitors across the devices. to limit the rate of rise of voltages when the devices are commutated.

A typical inversion model of operation is shown in Figure 3.1.2. Note that this corresponds to a second-quadrant operation of the DC motor drive. The transfer characteristic of the three-phase controlled rectifier is derived using the following relation.

$$V_{dc} = \frac{1}{(\pi/3)} \int_{-\pi/6+\alpha}^{+\pi/6+\alpha} V_{ab} d(\omega_s t) = \int_{-\pi/6+\alpha}^{+\pi/6+\alpha} V_m \sin(\omega_s t) d(\omega_s t) = \frac{3}{\pi} V_m \cos \alpha. \quad (2.19)$$

The transfer characteristics are quite similar to those of the single-phase converter in both the continuous and the discontinuous mode of conduction. The transfer characteristic for the continuous mode of conduction is shown in Figure 3.13.

The characteristic is non-linear. Therefore, the use of this converter as a component in a feedback-control system will cause an oscillatory response with this trait also occurs when transistors are being used [16].

This can be explained as follows.

The delay angle will be made a function of **speed**, **current**, or **position error** in a motor-drive system. The error variable is expected to increase or decrease the DC output voltage proportionally. The gain of the converter to a delay angle is **NOT** a constant, so it will either overreach or fall short of

the required output voltage. This necessitates one more correction in the error signal, causing both time delay and oscillatory response.

Such oscillatory responses have been known to create ripple instability in converters.

A control technique to overcome this non-linear characteristic and the accompanying undesirable dynamic behavior is given in the following. The control input to determine the delay angle is modified to be

$$\alpha = \cos^{-1} \left(\frac{v_c}{V_{cm}} \right) = \cos^{-1} (v_{cn})$$

where v_c is the control input and V_{cm} is the maximum of the absolute value of the control voltage. Then the DC output voltage is:

$$V_{dc} = \frac{3}{\pi} V_m \cos \alpha = \frac{3}{\pi} V_m \cos (\cos^{-1} v_{cn}) = \left(\frac{3}{\pi} V_m \right) v_{cn} = \left(\frac{3}{\pi} \frac{V_m}{V_{cm}} \right) v_c = K_r v_c \quad (2.20)$$

where v_{cn} is the normalised control voltage and K_r is the gain of the converter, defined as

$$K_r = \frac{3}{\pi} \frac{V_m}{V_{cm}} = \frac{3\sqrt{2}V}{\pi V_{cm}} = 1.35 \frac{V}{V_{cm}} \quad (2.21)$$

where V is the rms line-to-line voltage. Then the modified transfer characteristic is linear with a slope of K_r .

The control voltage is normalised to keep its magnitude less than or equal to 1, to be able to obtain the inverse cosine of it.

2.3.3. Control Circuit

The control circuit for the three-phase thyristor converter can be realised in numerous ways. A schematic of a generic implementation is shown in Figure X. The synchronisation signal is obtained from the line voltage between a and c . The positive-zero crossing of this line voltage formed by the starting point for the controller design. The synthesized signal is used to correspond to each gate equivalent pulses at 60° intervals.

The delay angle is obtained from the normalised control voltage v_m through a function generator, so as to make the overall gain of the thyristor converter **constant**. The delay is incorporated into the synchronised control signal and amplified and fed to the gates of the thyristors.

Therefore, the maximum limit on the delay angle has to be externally set or commanded.

It is essential that sufficient time is given for the thyristor to recover its forward blocking capability. Otherwise, a short of the load and source will occur.

Therefore, the maximum practical limit for the delay angle is usually set in the range of from 150 to 155 degrees.

Many adaptive control schemes adjust this maximum triggering angle as a function of load current. The feature to handle the identification of phase sequence in the AC supply has to be built in, so that the reference synchronisation voltage v_{ac} matches with the control circuit.

2.3.4. Control Modelling of the Three-Phase Converter

For simplicity, we can consider the converter as a black box with a certain gain and phase delay for modelling and use in developing a controller. The gain of the linear controller-based converter for a maximum control voltage V_{cm} is given in equation Eq. (2.21) as

$$K_r = 1.35 \frac{V}{V_{cm}} \quad \text{VV}^{-1} \quad (2.22)$$

The converter is a sampled-data system. The sampling interval gives an indication of its time delay. Once a thyristor is switched on, its triggering angle cannot be changed. The new triggering delay can be implemented with the succeeding thyristor gating. In the meanwhile, the delay angle can be corrected and will be ready for implementation within 60° ¹¹. Statistically speaking, we may treat the delay as one half of this interval; in time, it is equal to:

$$T_r = \frac{60/2}{360} \times (\text{time period of one cycle}) = \frac{1}{12} \times \frac{1}{f_s} \quad \text{s} \quad (2.23)$$

As an example, for a 50-Hz supply, note that the time delay is equal to 0.02 ms. The converter is then modeled with its gain and time delay as

$$G_r(s) = K_r e^{-T_r s} \quad (2.24)$$

and Eq. (2.24) can also be approximated as a first-order time lag and given as¹²:

$$G_r(s) = \frac{K_r}{1 + sT_r} \quad (2.25)$$

Most low-performance systems have a simple controller with no linearisation of its transfer characteristic¹³. The transfer characteristic in such a case is non-linear. Then, the gain of the converter is obtained as a small-signal gain given by

$$K_r = \frac{\delta V_{dc}}{\delta \alpha} = \frac{\delta}{\delta \alpha} (1.35V \cos \alpha) = -1.35V \sin \alpha \quad (2.26)$$

The gain is dependent on the operating delay angle denoted by α_0 . The converter delay is modeled as an exponential function in Laplace operator s or a first-order lag, describing the transfer function of the converter as in Eq. (2.25).

Current Source

The key to effectively control the machine is to control the electromagnetic torque (T_e) with sufficient accuracy. This control is achieved in the separately-excited DC machine by controlling its

armature current, but the phase-controlled converter provides only a variable voltage output.

To make it a controllable current source, we need a closed-loop control of the DC link current, which in this case is the armature current. A current source and a load-output current can be loaded, so when in Figure X.

Consider a resistive and inductive load combination. The reference current is enforced on the load by comparing it with the actual current in the load. The error current is amplified by a proportional-plus-integral (PI) controller and its output is limited so that the control signal will be constrained to be within the maximum triggering angle, α_{\max} . The control signal is processed to correspond to linearized operation by the inverse cosine function, and the signals are processed through gate power amplifiers and the converter.

Assume current reference is a step function and the converter is at rest to start with.

The current error will be maximum, which would correspond to minimum triggering angle, thus providing a large voltage across the DC link, i.e., load. This will build up the current in the load, and, when it exceeds the reference value, the current error will reduce from maximum positive to zero. This will enable the triggering angle to be close to $\pi/2$ in this present case, where the DC link voltage, v_{dc} , is **NOT** allowed to go below zero. The DC link is constrained to be positive, as the passive load cannot provide for regeneration, and only an active source such as a DC motor will provide the induced EMF with the appropriate polarity so that energy can be transferred from the load to source. An implementation can be seen in Figure X.

The maximum control voltage is 0.7 V, and the control voltage is normalized with respect to this for realizing a linearized controller. The step command of the reference current produces a maximum control voltage, and, correspondingly, the triggering angle is driven to zero to produce the maximum voltage across the DC link. The voltage across the resistor, v_R , starts to increase and that across the inductance, v_L , begins to decrease. When the current exceeds the reference, the control voltage goes to zero and the triggering angle reaches 90° , to provide an average voltage of zero across the DC link. The current is maintained around the reference value, on average, with a dither, and that dithering is a function of the current controller gains and the load time constant. When the reference current goes to zero, the control voltage becomes zero, and the triggering angle goes to 90° permanently. That forces the current to decay to zero, as the entire voltage of the DC link is **NOT** by the current, so the current is the voltage of the current source is realized in the 100,000-A range at low voltages for electrolysis in the control processing plants and in a few-twisting-A range at voltages of 600 V to 4,000 V for DC and ac motor drives.

2.3.5. Half-Controlled Converter

The converter under study is a fully controlled bridge converter. Low-power applications can make do with a half-controlled converter, shown in Figure 3.17. The lower half of the bridge has diodes in place of transistors, thus reducing the cost of the converter. The control circuit is simplified also.

Such a configuration is also possible with a single-phase converter. The half-controlled converters are employed up to 100 kW rating in practice.

This converter has only first-quadrant operational capability.

Converters with Freewheeling

In this configuration, a diode is connected across the load as shown in Figure 3.18. Due to the configuration, the reversal of voltage is **NOT** possible, making the converter operate only in the first quadrant, delivering a positive voltage and current. Even though the converter is limited in its capability, the current conduction interval is prolonged by the energy stored in the load inductance.

The current continuity has the positive effects of reducing the current ripples in the motor and hence the torque ripples.

The waveforms of this free-weeling circuit are shown in Figure 3.19.

There is an alternative way to obtain free-weeling without using a diode across the load. The thyristors of a phase leg can be triggered together and short the load. This, in turn, requires modification of the control circuitry.

Using this method has the advantage of minimising the cost of the converter and making optimal use of the power devices.

Converter Configuration for a Four-Quadrant DC Drive

Up to now, we have only worked with converters possessing one- or two-quadrant operational capabilities. Figure 3.20 shows the converter configuration for a four-quadrant DC motor drive. It consists of dual three-phase controlled bridge converters in parallel, with their output polarities reversed. Converter 1 gives both positive and negative DC output voltages with a positive current output, scattering to the first- and second-quadrant operation of the dc motor drive, respectively.

This converter is hereafter referred to as the **forward converter**.

Similarly, Converter 2 delivers negative current to the motor with positive and negative DC output voltages. Such operation encompasses the fourth- and third-quadrant performance of the DC motor drive, respectively. Because of this, from hereon it is referred as the **reverse converter**.

Adequate care must be given to make sure short circuiting does **NOT** happen when switching from forward to reverse operation.

The phase-controlled converter has two (2)quadrants of operation:

- Quadrants I and II,
- Quadrants III and IV

depending on the connection of the converter relative to the machine armature.

Quadrants I and IV or quadrants II and III are more useful in many unidirectional motion control applications than the ones things provided by the converter. That will enable both the motoring and gear-in-opars have to provide a torque contribution to cluster acceleration and deceleration in one direction of rotation.

2.4. Steady State Analysis of 3-Phase Converter Drive

2.4.1. Average Analysis

A separately-excited DC motor is fed from a three-phase converter and is operated in one rotational direction, say, in Quadrant I and IV of torque-speed characteristics.

Now we will describe its steady-state performance.

The steady-state performance, when combined with the load characteristics, provides the basis for evaluating the suitability of the motor drive for the given application. The steady-state performance is developed by assuming that only the average values are considered. Indirectly, it is implied that the average current produces an average torque, which, in combination with load torque, determines the average speed.

In this analysis we will disregard the quasi-transients as it is a steady state analysis.

Then the armature voltage (V_a) for the motor in steady state is:

$$v_a = R_a i_a + e \quad (2.27)$$

and, in terms of average values¹⁴,

$$V_a = R_a I_a + K\phi_f \omega_{m(av)} \quad (2.28)$$

¹⁴For brevity we denote the variables in capital letters or with a subscript 'av'

Average electromagnetic torque is given by

$$T_{av} = K\phi_f I_a \quad (2.29)$$

and, from a previous derivation, the average DC-link voltage is:

$$V_{dc} = 1.35V \cos \alpha \quad (2.30)$$

where V is the rms line-to-line ac voltage in a three-phase system. Then the electromagnetic torque is expressed in terms of delay angle and speed, from Eq. (2.28) to Eq. (2.30), as

$$T_{av} = K\phi_f \left(\frac{V_a - K\phi_f \omega_{max}}{R_a} \right) = K\phi_f \left(\frac{1.35V \cos \alpha - K\phi_f \omega_{max}}{R_a} \right) \quad (2.31)$$

The equation Eq. (2.31) is then normalised by dividing the average torque by the rated torque:

$$T_{\text{en}} = \frac{T_{\text{av}}}{T_{\text{er}}} = \frac{T_{\text{av}}}{K\phi_{\text{fr}} I_{\text{ar}}} = \frac{K\phi_f (1.35V \cos \alpha - K\phi_f \omega_{\text{mav}})}{K\phi_{\text{fr}} I_{\text{ar}} R_a} = \frac{(1.35V \cos \alpha - K\phi_f \omega_{\text{mav}})}{I_{\text{ar}} R_a} \phi_{\text{fn}} \quad (2.32)$$

Dividing the numerator and denominator of Eq. (2.32) by the rated motor voltage (V_r) leads to:

$$T_{\text{en}} = \left(\frac{\frac{1.35}{V_r} V \cos \alpha - \frac{K\phi_f \omega_{\text{mav}}}{V_r}}{\frac{I_{\text{ar}} R_a}{V_r}} \right) \phi_{\text{fn}} \quad (2.33)$$

and, noting that

$$V_r = K\phi_{\text{fr}} \omega_{\text{mr}} \quad \text{p.u.} \quad \text{and} \quad R_{\text{an}} = \frac{R_a I_a}{V_r} \quad \text{p.u.} \quad (2.34)$$

the normalised electromagnetic torque, then, is given by

$$T_{\text{en}} = \left(\frac{1.35V_n \cos \alpha - \phi_{\text{fn}} \omega_{\text{mn}}}{R_{\text{an}}} \right) \phi_{\text{fn}} \quad \text{p.u.} \quad (2.35)$$

where:

$$\phi_{\text{fn}} = \frac{\phi_r}{\phi_{\text{fr}}} \quad \text{p.u.}, \quad \omega_{\text{mn}} = \frac{\omega_{\text{mav}}}{\omega_{\text{mr}}} \quad \text{p.u.} \quad \text{and} \quad V_n = \frac{V}{V_r} \quad \text{p.u..} \quad (2.36)$$

The normalized Eq. (2.35) deserves careful look for use in steady-state performance computation. Positive or motoring torque is produced when the numerator of Eq. (2.35) is positive, i.e.,

$$1.35V_n \cos \alpha - \phi_{\text{fn}} \omega_{\text{mn}} > 0 \quad \text{or} \quad \cos \alpha > \frac{\phi_{\text{fn}} \omega_{\text{mn}}}{1.35V_n} \quad (2.37)$$

If $\cos \alpha$ is less than the Right Hand Side (RHS) of Eq. (2.37), then there is no torque generation in the machine. For some positive values of α , the numerator can become negative, but that will **NOT** produce regeneration, since there will be no current flow from the machine to the source with only one converter. The induced EMF of the machine will be greater than the applied voltage, thus blocking the conduction of this resistor. If an appropriate counter is available on the capacitor of the machine, the reflection coefficient is achieved by decreasing the applied voltage compared with the value of the induced emf. That enables the machine to generate current from the difference between its induced EMF and the applied voltage. This step results in power flow from the machine to the ac source.

The electromagnetic torque in Eq. (2.35) expressed as a function of normalised flux, speed, and triggering angle delay has design use. The resolution of the control law, is a certain precision in its triggering angle delay to resolution (as before), but for instance, finding the minimum and maximum speed depends on the torque requirements at the minimum and maximum speeds of operation by using this expression. The range of triggering delay angle and the finesse with which it needs to be controlled is given by the resolution of speed or torque control.

2.5. Two Quadrant 3-Phase Converter Control

The control schematic of a two-quadrant converter-controlled separately-excited DC motor drive is shown in Figure 3.26. The motor drive shown is a speed-controlled system. The transistor bridge converter gets its ac supply through a three-phase transformer and fast-acting ac conductors. The DC output is fed to the armature of the DC motor. The field is separately excited, and the field supply can be kept constant or regulated, depending on the need for the field-weakeening mode of operation. The DC motor has a tachogenerator whose output is utilized for closing the speed loop. The motor is driving a load considered to be frictional for this treatment. The output of the tachogenerator is filtered to remove the ripples to provide the signal, ω_{net} . The speed command ω_r is compared to the speed signal to produce a speed error signal. This signal is processed through a proportional-plus-integral (PI) controller to determine the torque command. The torque command is limited, to keep it within the safe current limits, and the current command is obtained by proper scaling. The armature current command i_t is compared to the actual armature current i_t to have a zero current error. In case there is an error, a PI current controller processes it to alter the control signal v_c . The control signal accordingly modifies the triggering angle α to be sent to the converter for implementation. The implementation of v_c to α in the converter is discussed under control circuit in section 3.3.3.

The inner current loop assures a fast current response and hence also limits the current to a safe preset level. This inner current loop makes the converter a linear current amplifier. The outer speed loop ensures that the actual speed is always equal to the commanded speed and that any transient is overcome within the short-test feasible time without exceeding the motor and converter capability.

The operation of the closed-loop speed-controlled drive is explained from one or two particular instances of speed command. A speed from zero to rated value is commanded, and the motor is assumed to be at standstill. This will generate a large speed error and a torque command and in turn an armature current command. The armature current error will generate the triggering angle to supply a perfect maximum DC voltage across the motor terminals. The inner current loop will maintain the current at the level permitted by its commanded value, producing a corresponding torque. As the motor starts running, the torque and current are maintained at their maximum level, thus accelerating the motor rapidly. When the rotor attains the commanded value, the torque command will settle down to a value equal to the sum of the load torque and other motor losses to keep the motor in steady state. The design of the gain and time constants of the speed and current controllers is of paramount importance in meeting the dynamic specifications of the motor drive. Their systematic designs are considered in the next section.

2.6. Transfer Functions of the Subsystems

2.6.1. DC Motor with Load

The DC machine contains an **inner loop** caused by the induced emf.

It is not physically observed as it is magnetically coupled phenomenon.

The inner current loop will cross this back-emf loop, creating a complexity in the development of the model which we can see in Figure XX.

The interactions of these loops can be decoupled by suitably redrawing the block diagram. The load is assumed to be proportional to speed and is given as

$$T_l = B_l \omega_m \quad (2.38)$$

For us to decouple the inner current loop from the induced-emf loop, it is necessary to split the transfer function between the speed and voltage into two (2) cascade transfer functions:

- first between speed and armature current,
- then between armature current and input voltage.

These are both represented as:

$$\frac{\omega_m(s)}{V_a(s)} = \left(\frac{\omega_m(s)}{I_a(s)} \right) \left(\frac{I_a(s)}{V_a(s)} \right) \quad (2.39)$$

where,

$$\frac{\omega_m(s)}{I_a(s)} = \frac{K_b}{B_r(1+sT_m)}$$

$$\frac{I_a(s)}{V_a(s)} = K_t \frac{(1+sT_m)}{(1+sT_1)(1+sT_2)}$$

$$T_m = \frac{J}{B_t}$$

$$B_t = B_1 + B_t$$

$$-\frac{1}{T_1}, -\frac{1}{T_2} = -\frac{1}{2} \left[\frac{B_t}{J} + \frac{R_a}{L_a} \right] \pm \sqrt{\frac{1}{4} \left(\frac{B_t}{J} + \frac{R_a}{L_a} \right)^2 - \left(\frac{K_a^2 + R_a B_t}{J L_a} \right)}$$

$$K_1 = \frac{B_t}{K_b^2 + R_a B_t}$$

2.6.2. Converter

The converter after linearisation is represented as:

$$G_r(s) = \frac{V_{a(s)}}{v_{a(s)}} = \frac{K_r}{1 + sT_r}$$

The delay time T_r and gain are evaluated and given in section 3.3.4.

2.6.3. Current and Speed Controllers

The current and speed controllers are of proportional-integral type. They are represented as

$$G_c(s) = \frac{K_c(1 + sT_c)}{sT_c} \quad \text{and} \quad G_s(s) = \frac{K_s(1 + sT_s)}{sT_s} \quad (2.40)$$

where the subscripts c and s correspond to the current and speed controllers, respectively. The K and T correspond to the gain and time constants of the controllers.

2.6.4. Current Feedback

The gain of the current feedback is H_c . No filtering is required in most cases. In the case of a filtering requirement, a low-pass filter can be included in the analysis. Even, then, the time constant of the filter might not be greater than a millisecond.

2.6.5. Speed Feedback

Most high performance systems use a DC tachogenerator, and the filter required is low-pass, with a time constant under 10 ms. The transfer function of the speed feedback filter is

$$G_u(s) = \frac{K_u}{1 + sT_u}$$

where K_u is the gain and T_u is the time constant.

2.7. Designing Controllers

The overall closed-loop system is shown in Figure 3.29. It is seen that the current loop does not contain the inner induced-ent loop. The design of control loop starts from the innermost (faster) loop and proceeds to the slowest loop, which in this case is the outer speed loop. The reason to proceed from the inner to the outer loop in the design process is that the gain and time constants

f only one controller at a time are solved, instead of solving for the gain and time constants of all the controllers simultaneously. Not only is that logical; it also has a practical implication. Note that every motor drive need not be speed-controlled but may be torque-controlled, such as for a traction application. In that case, the current loop is essential and exists regardless of whether the speed loop is going to be closed. Additionally, the performance of the outer loop is dependent on the inner loop; therefore, the tuning of the inner loop has to precede the design and tuning of the outer loop. That way, the dynamics of the inner loop can be simplified and the impact of the outer loop on its performance could be minimized. The design of the current and speed controllers is considered in this section.

2.7.1. Current Controller

The current-control loop is shown in Figure 3.30. The loop gain function is

$$GH_i(s) = \left\{ \frac{K_I K_c K_r H_c}{T_c} \right\} \frac{(1+sT_c)(1+sT_m)}{s(1+sT_1)(1+sT_2)(1+sT_r)} \quad (2.41)$$

As we can see, this is a 4th-order system, and simplification is necessary to synthesise a controller without resorting to a computer. Noting that T_m is on the order of a second and in the vicinity of the gain crossover frequency, we see that the following approximation is valid:

$$(1+sT_m) \approx sT_m \quad (2.42)$$

which reduces the loop gain function to:

$$GH_i(s) \approx \frac{K(1+sT_c)}{s(1+sT_1)(1+sT_2)(1+sT_r)} \quad \text{where} \quad K = \frac{K_I K_c K_r H_c T_m}{T_c} \quad (2.43)$$

The time constants in the denominator are seen to have the relationship

$$T_r < T_2 < T_1 \quad (2.44)$$

The Eq. (2.43) can be reduced to second order, to facilitate a simple controller synthesis, by judiciously selecting:

$$T_c = T_2 \quad (2.45)$$

Then the loop function is

$$GH_i(s) \approx \frac{K}{(1+sT_1)(1+sT_r)} \quad (2.46)$$

The characteristic equation or denominator of the transfer function between the armature current and its command is

$$(1+sT_1)(1+sT_r) + K \quad (2.47)$$

This equation is expressed in standard form as:

$$T_1 T_r \left\{ s^2 + s \left(\frac{T_1 + T_r}{T_1 T_r} \right) + \frac{K+1}{T_1 T_r} \right\} \quad (2.48)$$

from which the natural frequency (ζ) and damping ratio are obtained as:

$$\omega_n^2 = \frac{K+1}{T_1 T_r} \quad \zeta = \frac{\left(\frac{T_1+T_r}{T_1 T_r}\right)}{2\sqrt{\frac{K+1}{T_1 T_r}}} \quad (2.49)$$

where ω_n and ζ are the natural frequency and damping ratio, respectively. For good dynamic performance, it is an accepted practice to have a damping ratio of 0.707. Therefore equating the damping ratio to 0.707 in Eq. (2.49), we get:

$$K+1 = \frac{\left(\frac{T_1+T_r}{T_1 T_r}\right)^2}{\left(\frac{2}{T_1 T_r}\right)} \quad (2.50)$$

Realising that

$$K \gg 1 \quad T_1 \gg T_r \quad (2.51)$$

tells us that K is approximated as:

$$K \approx \frac{T_1^2}{2T_1 T_r} \approx \frac{T_1}{2T_r} \quad (2.52)$$

By equating (3.76) to Eq. (2.52), the current-controller gain is evaluated as

$$K_c = \frac{1}{2} \frac{T_1 T_c}{T_r} \left(\frac{1}{K_l K_r H_c T_m} \right) \quad (2.53)$$

Exercise 2.1: Designing a Speed Controller

Design a speed-controlled DC motor drive maintaining the field flux constant. The motor parameters and ratings are as follows:

$$\begin{aligned} & 220 \text{ V} & 1470 \text{ min}^{-1} & R_a = 4 \text{ } \Omega \\ & J = 0.00607 \text{ kg m}^2 & L_a = 0.074 \text{ H} & B_l = 0.0869 \text{ N m s rad}^{-1} \\ & K_b = 1.26 \text{ V s rad}^{-1} \end{aligned}$$

The converter is supplied from 230V,3-phase AC at 60 Hz. The converter is linear, and its maximum control input voltage is $\pm 10 \text{ V}$. The tachogenerator has the transfer function:

$$G_\omega(s) = \frac{0.065}{1 + 0.002s}$$

The speed reference voltage has a maximum of 10V. The maximum current permitted in the motor is 20 A.

Solution

Converter transfer function:

$$\begin{aligned} K_r &= \frac{1.35V}{V_{cm}} = \frac{1.35 \times 230}{10} = 31.05 \text{ V V}^{-1} \\ V_{dc(max)} &= \sqrt{2} \times 220 \approx 310.5 \text{ V} \end{aligned}$$

The rated DC voltage required is 220 V, which corresponds to a control voltage of 7.09 V. The transfer function of the converter is

$$G_r(s) = \frac{31.05}{1 + 0.00138s} \text{ V V}^{-1}$$

(ii): Current transducer gain: The maximum safe control voltage is 7.09 V, and this has to correspond to the maximum current error:

$$\begin{aligned} i_{max} &= 20 \text{ A} \\ H_c &= \frac{7.09}{I_{max}} = \frac{7.09}{20} = 0.355 \text{ V/A} \end{aligned}$$

(iii): Motor transfer function:

$$K_1 = \frac{B_1}{K_b^2 + R_a B_1} = \frac{0.0869}{1.26^2 + 4 \times 0.0869} = 0.0449$$

$$-\frac{1}{T_1} = -\frac{1}{T_2} = -\frac{1}{2} \left[\frac{B_1}{J} + \frac{R_a}{L_a} \right] \pm \sqrt{\frac{1}{4} \left(\frac{B_1}{J} + \frac{R_a}{L_a} \right)^2 - \left(\frac{K_b^2 + R_a B_1}{J L_a} \right)}$$

$$T_1 = 0.1077 \text{ sec}$$

$$T_2$$

The subsystem transfer functions are

$$\frac{I_s(s)}{V_s(s)} = K_i \frac{(1 + sT_m)}{(1 + sT_i)(1 + sT_2)} = \frac{0.0449(1 + 0.7s)}{(1 + 0.0208s)(1 + 0.1077s)}$$

$$\frac{\omega_m(s)}{I_s(s)} = \frac{K_h/B_1}{(1 + sT_m)} = \frac{14.5}{(1 + 0.7s)}$$

(iv): Design of current controller:

$$T_c = T_2 = 0.0208 \text{ sec}$$

$$K = \frac{T_1}{2T_f} = \frac{0.1077}{2 \times 0.001388} = 38.8$$

$$K_c = \frac{KT_c}{K_1 H_c K_c T_m} = \frac{38.8 \times 0.0208}{0.0449 \times 0.355 \times 31.05 \times 0.7} = 2.33$$

(v): Current-loop approximation:

$$\frac{I_s(s)}{I'_s(s)} = \frac{K_i}{(1 + sT_i)}$$

where

$$K_i = \frac{K_{fi}}{H_c} \cdot \frac{1}{(1 + K_{fi})}$$

$$K_{fi} = \frac{K_e K_i T_m H_e}{T_c} = 38.8$$

$$\therefore K_i = \frac{27.15}{28.09} \frac{1}{0.355} = 2.75$$

$$T_i = \frac{T_i}{1 + K_{fi}} = \frac{0.109}{1 + 38.8} = 0.0027 \text{ sec}$$

The validity of the approximations is evaluated by plotting the frequency response of the closed-loop current to its command, with and without the approximations. This is shown in Figure 3.34. From this figure, it is evident that the approximations are quite valid in the frequency range of interest.

(vi) Speed-controller design:

$$T_t = T_t + T_w = 0.0027 + 0.002 = 0.0047 \text{ sec}$$

$$K_2 = \frac{K_s K_b H_w}{B_t} = \frac{275 \times 1.26 \times 0.065}{0.0869 \times 0.7} = 3.70$$

$$K_s = \frac{1}{2K_2 T_t} = \frac{1}{2 \times 3.70 \times 0.0047} = 28.73$$

$$T_t = 4T_t = 4 \times 0.0047 = 0.0188 = \text{sec}$$

The frequency responses of the speed to its command are shown in Figure 3.35 for cases with and without approximations. That the model reduction with the approximations has given a transfer function very close to the original is obvious from this figure. Further, the smoothing of the overshoot by the cancellation of the zero with a pole at $-1/4T_4$ is shown in Figure 3.36. This figure contains the approximated transfer function of third order for the speed to its command-transfer function and the one without any approximations. Again, the closeness of these two solutions justifies the approximations.

The time responses are important to verify the design of the controllers, and they are shown in Figure 3.37 for the case without smoothing and with smoothing. The case without any approximation is included here for the comparison of all responses.

Part II.

Induction Machines

Chapter 3

Induction Motor Dynamics and Control

Table of Contents

3.1. Introduction	49
3.2. Steady-State Analysis	50
3.3. Construction	53
3.4. Dynamic Modelling	59
3.5. Dynamic Simulation Equations	76

3.1. Introduction

An IM is type of electro-mechanical device¹ whereby AC is supplied to the stator **directly** and to the rotor by the process of **induction** from the stator, when excited from a balanced poly-phase source². During operation, it will produce a magnetic field in its air gap rotating at **synchronous speed** as determined by the number of stator poles and the applied stator frequency f_e which can either be fed from the grid or from an inverter. A cross sectional view of an IM can be seen in **Fig. 3.1.**

IMs are the go-to choice for AC machines in industry [18] and are a commonplace in a wide variety of applications such as mining [19, 20], power generation [21], and electric cars [22]. The benefits of IM over other types of electrical machines is its optimised manufacturing, cheap production, and simple construction.

¹some consider it as a rotating transformer

²either by star or delta connection if it is a three-phase connection, however there are applications which more than three (3) phases are used, which are in places where high traction is needed.

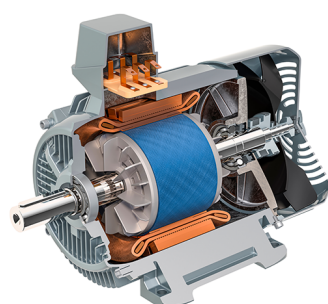


Figure 3.1.: Cross-sectional view of IM [17].

³known in literature as $dq0$ axes [23].

In this section, the dynamic model of the IM in direct, quadrature, and zero-sequence axes³ is derived from fundamentals.

To simplify the problems we will face in modelling an AC system we will use certain transformations. These transformations used in the derivation of various dynamic models are based on simple trigonometric relationships obtained as projections on a set of axes⁴. The dynamic model is derived with the frames of the observation starting at an arbitrary speed. The same idea is used to obtain transient responses, small-signal equations, and a multitude model is used to obtain transient responses, small-signal equations, and a multitude of transfer functions, all of which are useful in the study of converter-fed induction-motor drivers [25]. Space-phasor approach has further simplified the polyphase IM model to one equivalent stator and one rotor winding, thereby evolving a powerful similarity to the DC machine to correspond with its armature and field windings⁵.

⁵This is the main goal of any AC machine analysis: to create a mathematical analogy with a DC machine.



Figure 3.2.: A wound-rotor IM [24].

3.2. Steady-State Analysis

The rotor of a poly-phase IM may be one of two (2) types⁶.

Wound Rotor built with a polyphase winding similar to, and wound with the same number of poles as, the stator. The terminals of the rotor winding are connected to **insulated** slip rings mounted on the shaft. Carbon brushes bearing on these rings make the rotor terminals available **external** to the machine, which can be seen in **Fig. 3.2.**

Wound-rotor IM are relatively uncommon, being found only in a limited number of specialised applications where good control of speed is required.

Squirrel Cage rotor windings consist of conducting bars embedded in slots in the rotor iron and short-circuited at each end by conducting end rings⁷. The extreme simplicity, ruggedness, and a century of industrial optimisation makes the squirrel-cage construction the **dominant** type of IM ranging from a less than a kW to a MW.

3.2.1. Speed of Operation

To understand the operation principle of an IM, let us assume the rotor is turning at the steady speed of n_r rpm in the same direction as the rotating stator field. Let the synchronous speed of the stator field be n_s rpm. This difference between synchronous speed and the rotor speed is commonly referred to as the **slip** of the rotor⁸.

⁷These bars are usually made from aluminium or copper.

⁸For more information, please look at the B.Sc Drive Technology Repo.

Slip is more usually expressed as a fraction of synchronous speed⁹.

⁹i.e., 0 – 100 %

The **fractional slip**, ranging between 0 and 1, (s) is:

$$s = \frac{n_s - n_r}{n_s} \quad (3.1)$$

The slip is often expressed in percent (%), simply equal to 100 percent times the fractional slip of Eq. (3.1) whereas the rotor speed in rpm can be expressed in terms of the slip and the synchronous speed as:

$$n_r = (1 - s) n_s \quad (3.2)$$

Similarly, the mechanical angular velocity (ω_r) can be expressed in terms of the synchronous angular velocity (ω_s) and the slip as:

$$\omega_r = (1 - s) \omega_s \quad (3.3)$$

A final relationship could be made with regards to the stator frequency (f_s) and rotor frequency (f_r):

$$f_r = sf_s \quad (3.4)$$

The electrical behaviour of an IM is similar to a transformer but with the additional feature of **frequency transformation** produced by the relative motion of the stator and rotor windings. A useful application of wound-rotor IM is as a frequency changer as the frequency of the rotor and the stator is **different**.

Starting Up the Motor

The terminals of an squirrel-cage IM rotors are **internally short circuited** whereas in a wound-rotor IM it is short circuited **externally**. The rotating air-gap flux induces slip-frequency voltages in the rotor windings. The rotor currents are then determined by the magnitudes of the induced voltages and the rotor impedance at slip frequency.

During startup, the rotor is stationary ($n_r = 0$), the slip is **unity** ($s = 1$), and the rotor frequency equals the stator frequency (f_s). The field produced by the rotor currents therefore revolves at the same speed as the stator field, and a starting torque results, ending to turn the rotor **in the direction of the stator field rotation**. If this torque is sufficient to overcome the opposition to rotation created by the shaft load, the machine will come up to its operating speed.

The operating speed can never equal the synchronous speed as the rotor conductors would then be stationary **with respect to** the stator field; no current would be induced in them, and therefore no torque would be produced.

With rotor revolving in the same direction of the stator field, the frequency of the rotor currents is sf_s and they will produce a rotating flux wave which will rotate at sn_s rpm with respect to the rotor

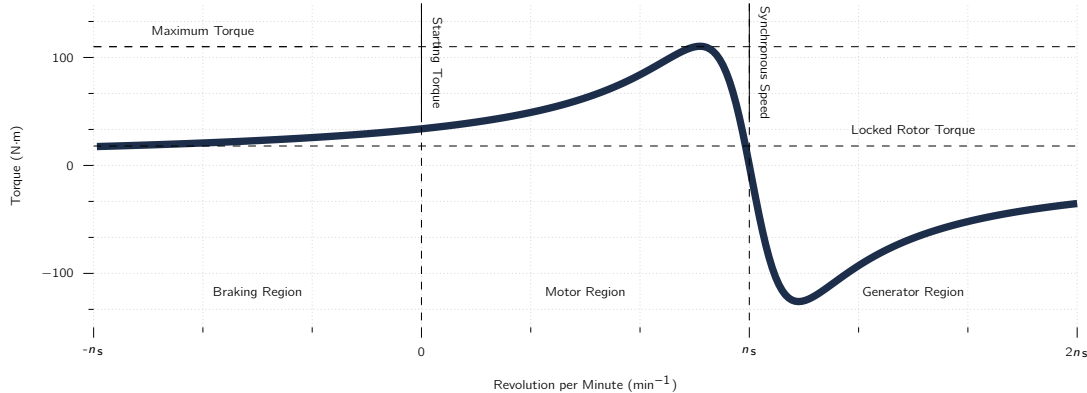


Figure 3.3.: Steady-state torque behaviour of an IM. Here important parameters and concepts can be observed. An important aspect is to mention is the stability of an IM only occurs between %2 to %8 slip during normal operation.

in the forward direction. But superimposed on this rotation is the mechanical rotation of the rotor at n rpm.

Therefore, with respect to the stator, the speed of the flux wave produced by the rotor currents is the sum of these two (2)speeds and equals

$$sn_s + n_r = sn_s + n_s(1 - s) = n_s \quad (3.5)$$

From Eq. (3.5) we see the rotor currents produce an air-gap flux wave which rotates at synchronous speed and is synchronised with that produced by the stator currents. Because the stator and rotor fields each rotate synchronously, they are stationary with respect to each other and produce a steady torque, thus maintaining rotation of the rotor. Such torque, which exists for any mechanical rotor speed n_s other than synchronous speed, is called an **asynchronous torque**.

3.2.2. Normal Operation

Under normal running conditions the slip s is small¹⁰. As the rotor frequency is directly related to slip the frequency ($f_r = sf_s$) of the current flowing in the rotor is very low, around 1 to 5 Hz in 50-Hz machines. In this range the rotor impedance is largely resistive and independent of slip. as reactance element is proportional to $2\pi f_r L$.

Approximate proportionality of torque with slip is therefore to be expected in the range where the slip is small. As slip increases, the rotor impedance increases due to the increasing contribution of the rotor leakage inductance. Therefore, the rotor current is less than proportional to slip. The result is that the torque increases with increasing slip up to a maximum value and then decreases. The maximum torque, or **breakdown torque**, which is typically a factor of two larger than the rated machine torque, limits the short-time overload capability of the machine.

The slip at which the peak torque occurs is proportional to the rotor resistance.

For squirrel-cage machines this peak-torque slip is relatively small. Therefore, the squirrel-cage IM is substantially a constant-speed machine having a few percent drop in speed from no load to full load. In the case of a wound-rotor IM, the rotor resistance can be increased by inserting external resistance, hence increasing the slip at peak-torque, and thus decreasing the machine speed for a specified value of torque. The speed-torque plot of a squirrel-cage IM can be seen in **Fig. 3.3.**

Wound-rotor¹¹ IM are generally made to be larger, and therefore are more expensive and require significantly more maintenance than squirrel-cage IMs, this method of speed control is rarely used, and IMs driven from constant-frequency sources tend to be limited to essentially constant-speed applications.

¹¹While wound-rotor has significant merits compared to that of a squirrel-cage the market-share is around %5 compared to squirrel-cages' %95. Therefore, the dynamic modelling usually takes a squirrel cage into account.

3.3. Construction

Magnetic Part

The stator and rotor of IM are made up of magnetic steel laminations of thickness varying from 0.0185 to 0.035 inch¹², machine-punched with slots at the inner periphery for the stator and at the outer periphery for the rotor [27] which can be seen in **Fig. 3.4.** These slots can be partially closed or fully open in the stator laminations to adjust the leakage inductance¹³ of the stator windings. In the rotor dimensions, the stator can be arbitrarily small enough to move from the rotor. The rotor stops can be seen as the path length of the rotor.

The rotor will cross-part networks to be bold rotor bars of different shapes placed in them. In such a case, the rotor is known as a deep bar rotor. Depending on the number of parallel copper bars placed in a slot, the machine is referred to as a double-, triple-, or multiple-age IM.

The multiple-cage rotor is intended to maximise the electromagnetic torque during starting and to minimise the rotor copper losses during steady-state operation. The stator laminations are aligned and stacked in a future and pressed by heavy presses of capacity varying from 40 to 80 tons, to pack the laminations very closely and to remove the air gap between them. With these steps, the stator magnetic part of the machine is ready for insertion of windings [28].

The rotor windings are **skewed** by one half or a full slot pitch from one end to the other, to minimise or to completely cancel some of the time harmonics¹⁴. To accommodate such skewing, the rotor laminations are assembled with a skew in a jig and fixture and then pressed to make the rotor magnetic block [29, 30].



¹²0.47 to 0.875 mm

¹³an inductive component that results from the imperfect magnetic linking of one winding to another

Figure 3.4.: Lamination on a stator is done to reduce eddy currents [17].

¹⁴harmonics in the input supply given to the three phase machine.

Windings

Stator & Rotor Windings

Consider a three-phase IM having three (3) windings each on its stator and rotor. The phase windings are displaced in space from each other by 120° electrical degrees¹⁵, where

¹⁵or $\pi/3$ if you prefer radians.

$$\text{Electrical degrees} = \text{Pairs of poles} \times \text{Mechanical degrees} \quad (3.6)$$

The three-phase rotor windings are **short-circuited** either within the rotor or outside of the rotor, with or without external resistances connected to them. If the rotor windings are connected through slip rings mounted on the shaft and adjacent to the rotor of the IM to provide external access to the rotor windings, the machine is referred to as a **slip-ring induction** motor, as mentioned previously. Alternately, the rotor windings can be bars of copper or aluminium, with two (2) end rings attached to short-circuit the bars on the rotor itself, thus making the rotor very compact [31]. Such a construction is known as **squirrel-cage IM**.

The numbers of slots in the stator and rotor are unequal to avoid harmonic crawling torques¹⁶ [33]. The windings are distributed in the slots across the periphery of the stator and rotor. The windings can have different progressions, such as **concentric** or **lap** windings. In concentric windings, the windings are centred around slots within a pole pitch. In the case of lap windings, a coil is spread over a fixed pitch angle, for example, 180 electrical degrees, and connected to the coil in the adjacent slot, and so on. With a coil pitch of 180 electrical degrees, the induced EMF of the coil side under the south pole. The inductance of the coil is equal to the sum of the incidence of the rotor. The induced emf in the coil is equal to the sum of the incidence of the coils. The winding number of the coil is equal to the sum of the coils. The windings need not have a pitch of 180 electrical degrees and might have less than that, to eliminate some fixed number of harmonics. This case is known as short-charged winding. Short chlorine reduces the resultant voltage, because the coils are not displaced by 180 degrees but by less, with the outcome that their phasor sum is less than their algebraic sum. Such an effect is included in the **pitch factor**, c_p .

The slots have a phase shift, both to allow for mechanical integrity and to control the short-chording angle, so the induced EMF in the adjacent coils of a phase will have a phase displacement. When the EMF is the noise coils of a phase are summed up, the resultant induced EMF is the sum of the phasor voltages induced in the tensile coils. A reduction in the voltage results because of the phasor addition compared to their algebraic sum. The factor to account for this aspect is known as the **distribution factor**, c_d . The resultant voltage in a phase winding is reduced both by the pitch and distribution factors. Therefore, the winding factor, k_w , which reflects the effectiveness of the winding, is given as:

$$k_w = c_d c_p,$$

where c_d is the winding distribution factor.

Induced EMF

With this understanding, the induced EMF in a stator phase winding is derived from the first principles¹⁷. The mutual flux linkages are distributed sinusoidal. The induced EMF is equal in magnitude to the rate of change of mutual flux linkages, which in turn is equal to the product of the effective number of turns in the winding and the mutual flux.

From this, the induced EMF in a phase winding is derived as:

$$e_{as} = -\frac{d\lambda}{dt} = -\frac{d}{dt} \left[(k_{w1} T_1) \Phi_m \sin(2\pi f_s t) \right] = -2\pi f_s k_{w1} T_1 \Phi_m \cos(2\pi f_s t),$$

where f_s is the supply frequency in Hz, Φ_m is the peak value of the mutual flux, T_1 is the total number of turns in phase a , and k_{w1} is the stator winding factor. The rms value of the induced emf is given by

$$E_{as} = \frac{|e_{as}|}{\sqrt{2}} = 4.44 k_{w1} T_1 \Phi_m f_s \quad (3.7)$$

The expression for the induced EMF in the rotor phase windings is very similar to Eq. (3.4) if appropriate winding factor, number of turns, and frequency for the induced EMF in the rotor are inserted into Eq. (3.4).

Winding Methods

There are two (2) types of winding methods are common in IMs.

- Random-wound,
- Form-wound.

Let's look at them in a bit more detail:

Random-Wound Winding

The coils are placed in the slots and separated from the magnetic steel with an insulation paper, such as a mica sheet, which can be seen in **Fig. 3.5**. Each coil in a slot contains a number of circular but stranded empty wires which are wound on a former. This type of winding is referred to as random-wound. They are used for low-voltage (< 600 V) motors. The disadvantages of this method of winding the coil are:

- The adjacent round wires in the worst case can be the first and the last turn in the coil. Because of this, the turn-to-turn voltage can be maximum in such a case and will equal the full coil voltage but not equal the sequential turn-to-turn voltage, which is only a small fraction of the full coil voltage.

¹⁷In this case we derive it from Faraday's law taught in M.Sc Electrodynamics.

- They are likely to have considerable air pockets, the full coil voltages. These air pockets form capacitors between strands of wire. With rotational of repetitive voltages at high frequency with high rate of change of voltages from the inverter, a discharge current flows into the air capacitor. This is known as partial discharge and can cause insulation failures.

However, random-wound machines are economical, have low losses, and hence have a higher efficiency and tend to run cooler. Random-wound machines use a semi-closed slot, which reduces the flux density in the teeth, resulting in lower core losses¹⁸. Some methods have very recently been suggested to reduce the partial-discharge possibility of random-wound machines.

The methods recommend using:

- heavier insulation,
- a wind-in-place insertion method, making the wire placement sequential
- extra strategically placed insulation within a phase of the motor
- extra insulating steves on the turns nearer to the line leads

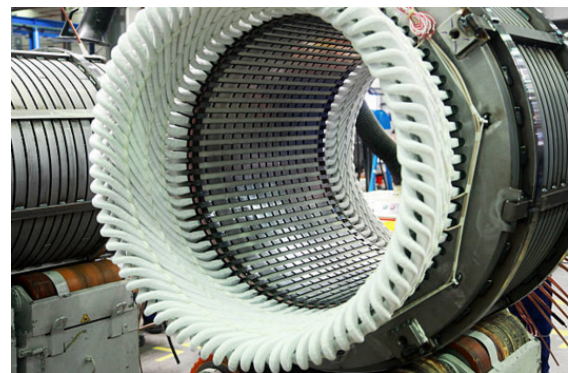


Figure 3.5.: Form winding.

Form-Wound Winding

Higher-voltage (>600 V) IMs are usually wound in form, meaning, each wire of rectangular cross section is placed in sequence with a strand of insulation in between them and then the bundle is wrapped with mica ground wall insulation, over which an armour covering is applied to keep all the wire arrangement firmly in place. The form-wound coils are placed in a fully open slot, as it is not possible to use the semi-closed slot for this arrangement.

This wound has higher core losses.

This is because the tooth flux density increases as there is a sizable reduction of its cross sectional area compared to a semi-closed slotted tooth. On the other hand, form-wound windings have a much higher resistance to partial discharges, as their turn-to-turn voltage is minimal and a heavier insulation bound between them also helps mitigate them.

The disadvantage of this winding is that it is relatively expensive compared to random windings.

Rotor Construction

There are two (2) methods of rotor construction are used for IMs. They are fabrication and die casting of the rotor. Fabricated rotor construction is possible for both aluminium and copper bar rotors but aluminium fabricated rotors are hardly ever used.

The reason is that a fabricated aluminium rotor is expensive, whereas a die-cast aluminium rotor is inexpensive.

The fabricated copper-bar rotor is used in large machines where the aluminium die-cast rotor is not available or in high-inertia loads demanding frequent starts, such as in cruisers and shredders. Frequent line-supply starts of the IM result in higher-inrush currents¹⁹ that are multiple times the rated currents and hence produce more losses and forces capable of disclosing the rotor bars.

The aluminium die-cast rotor construction is used in applications having lower-load inertia than recommended by National Electrical Manufacturers Association (NEMA) and **NOT** required to meet stall condition or very high starting torques [34].

This rotor type is dominant in applications and covers as much as 90% of applications.

Insulation

Wounded stator and rotor windings are immersed in varnish and heat-treated for drying. The insulation sheets between slots and coils and on the enamelled²⁰ wires and between turns in the coil consist of insulation materials of different classes, known as **A**, **B**, **F**, and **H**. The choice depends on the maximum temperature rise permissible for each class. The NEMA [MG1](#) and American National Standards Institution (ANSI) [CR50.41](#) specifies for allowable stator temperature rise for various insulation classes, with the European standard regulated by International Electrotechnical Commission (IEC) 60034-1:2022 [35].

Service factor is the ratio between the steady-state maximum power output capability and the rated power output of the machine. As an example, a service factor of 1.15 means the machine can practically generate %15 more power than what is written on its nameplate.

Because of the uncertainty of measuring certain loads, service factor greater than 1 is recommended in field applications.

most IM have insulation class **F**, whereas motors for servo-drive applications usually need class **H** insulation.

If the machine is not going to be in constant operation or has no overload application, lower class insulation can be chosen to save on cost.

¹⁹the high current a highly inductive load draws when it is first energised.

²⁰enamelling is the process of applying varnish on the surface of copper or aluminium wires to form electrical insulation film. This process also increases mechanical strength, thermal resistant and chemical resistant properties.

Higher winding temperatures usually result in transmission of heat to bearings, resulting in failures and frequent replacements. Therefore, higher operating winding temperature is not preferred, and that is the reason for a majority of motors to have an insulation class of **F** or lower.

Rotor Shaft

The rotor shaft is usually made of **forged steel** for higher speeds (i.e., $n_r > 3600$ rpm) and has to conform to sizes recommended for power levels by NEMA or other applications-specific industrial standards such as American Petroleum Institute (API) standard [541](#) for American markets and IEC 60072-1:2022 [36] for European.

Enclosure

Windings are inserted in the stator laminations and the stator laminations are fitted inside of a non-magnetic steel housing. Two end covers will be attached to the steel housing with part of the bearings attached to them. They then will be assembled with through bolts after inserting the rotor with shaft. The non-magnetic steel housing is intended for protecting the stator and rotor assembly from an inertial forces²¹. Commonly used enclosures are:

²¹such as pin, water, snow, insect, birds, ...

- open dip-proof (ODP)
- weather-protected types I and II (WPLWPI)
- totally enclosed air-to-air cooled (TEAC),
- totally enclosed fan cooled (TEFC),
- totally enclosed water-to-air cooled (TEAC)

These provide varying degrees of protection from environment and core with cost different widely between them.

Rotor Balancing

Before final assembly, the rotor is dynamically balanced so no eccentricities of any kind are presented to the bearings. The balancing is achieved either by **removing some magnetic iron material** in smaller motors or by **adding a magnetically and electrically inert material** compound in larger machines. To close this topic of, here is a diagram showing the materials generally used in the construction of the IM, shown in **Fig. 3.6**.

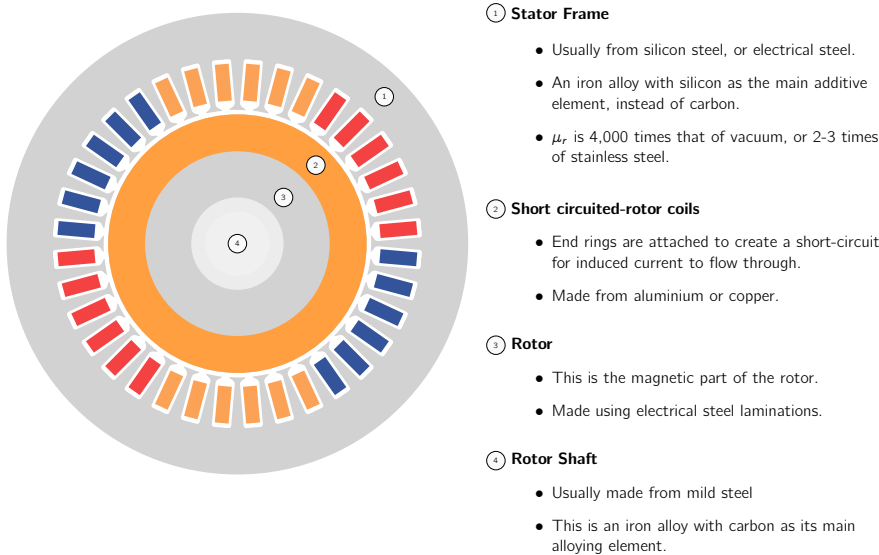


Figure 3.6.: The materials used in the construction of an IM.

3.4. Dynamic Modelling

The steady-state model and equivalent circuit developed in **B.Sc Drive Technology** are useful for studying the performance of an IM in **normal operation**. This implies all electrical transients are **neglected** during load changes and stator frequency variations. Such variations arise in applications involving variable-speed drives.

The variable-speed drives are converter-fed from finite sources, unlike the utility sources, due to the limitations of the switch ratings and filter sizes.

This results in their incompatibility to supply large transient power. Therefore, it is in our best interest, to evaluate the dynamics of converter-fed variable-speed drives to assess the adequacy of the converter switches and the converters for a given motor and their interaction to determine the excursions of currents and torque in the converter and motor.

The dynamics model considers the three (3) major properties of an IM:

1. instantaneous effects of varying voltages/currents,
2. stator frequency, and
3. torque disturbance.

The dynamic model of the IM is derived using a two-phase motor in direct and quadratic (**d, q**) effects. This approach is desirable because of the conceptual simplicity obtained with two (2) sets of windings, one on the stator and the other on the motor.

For this transformation to work we need to introduce the concept of **power invariance**; the power

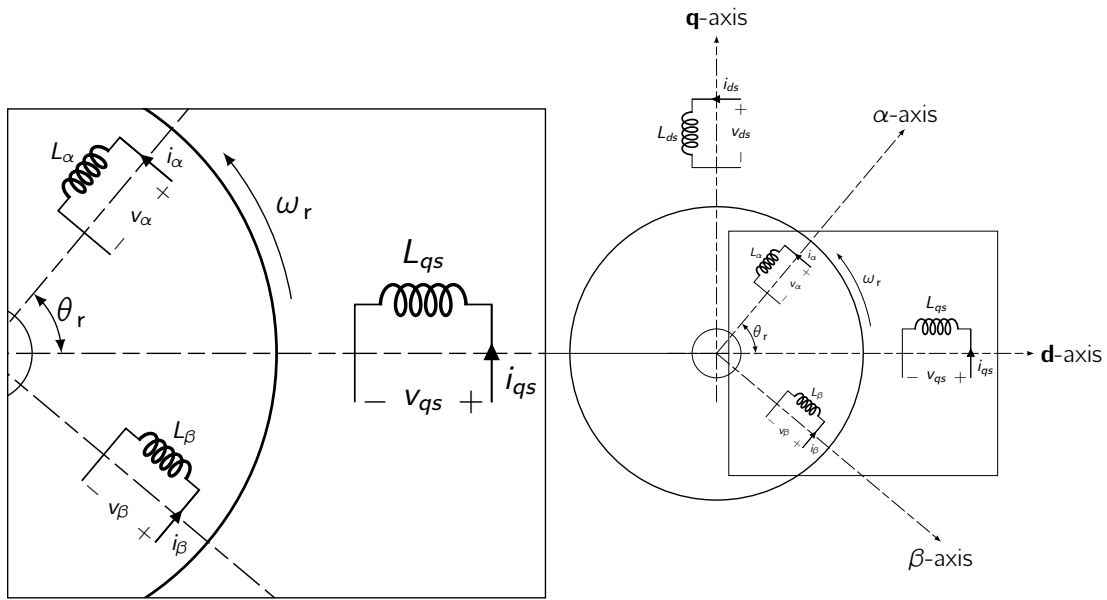


Figure 3.7.: Stator and rotor winding of a two-phase IM. The model shows the stator inductances as L_{qs} and L_{ds} , and the rotor as L_α and L_β . As the rotor spins these inductances will interact with one another and produce mutual inductance.

must be equal in the three-phase machine and its equivalent two-phase model. The required transformation in voltages, currents or flux linkages is derived in a generalised way. The reference frames are chosen to be **arbitrary**, and particular cases such as stationary, rotor, and synchronous reference frames, are simple instances of the general case. Deviations for electromagnetic torque involving the currents and flux-linkages are given.

The differential equations describing IM are **non-linear**. For stability and designing controllers it is important to linearise the machine equations around a steady-state operating point to obtain small-signal equations. Time to start derive the two-phase equivalent model.

3.4.1. Real Time Model of a Two-Phase Induction Machine

²²These assumptions allow us to disregard non-symmetrical geometries or non-linear behaviour of materials.

The following assumptions are necessary to derive the dynamic model²² [37]:

- The machine has **uniform air gap** (i.e., δ is constant across circumference),
- Balanced rotor and stator windings with sinusoidally distributed MMF. This permits us to assume the system to be void of any **spatial harmonics**.
- Inductance v. rotor position is **sinusoidal**²³.
- Saturation and parameter changes are neglected (i.e., material is assumed linear)

A two (**2**)phase IM with stator and rotor windings is shown in **Fig. 3.7.** The windings are displaced in space by 90° electrical, and the rotor winding, α , is at an angle θ_r , from the stator **d** axis winding.

It is assumed that the d-axis (**d**) is **leading** q-axis (**q**) for clockwise direction of rotation of the rotor. If the clockwise phase sequence is **dq**, the rotating magnetic field will be revolving at the angular speed of the supply frequency but counter to the phase sequence of the stator supply. Therefore, the rotor is **pulled in the direction of the rotating magnetic field**. For this case it is counter-clockwise. The currents and voltages of the stator and rotor windings are marked in **Fig. 3.7**. The number of turns per phase in the stator and rotor windings respectively are T_1 and T_2 .

A pair of poles is assumed for **Fig. 3.7**, but it is applicable with the slight modification for the rotation of the rotor position at drawn in terms of electrical heterogeneity.

θ_r is the electrical rotor position at any instant, obtained by multiplying the rotation of the rotor position by pairs of electrical poles.

The terminal voltages of the stator and rotor windings can be expressed as the sum of the voltage drops in resistances and rates of change of flux linkages, which are the products of currents and inductance [38].

The equations are as follows:

$$v_{qs} = R_q i_{qs} + p_t (L_{qq} i_{qs}) + p_t (L_{qd} i_{ds}) + p_t (L_{q\alpha} i_\alpha) + p_t (L_{q\beta} i_\beta) \quad (3.8)$$

$$v_{ds} = p_t (L_{dq} i_{qs}) + R_d i_{ds} + p_t (L_{dd} i_{ds}) + p_t (L_{d\alpha} i_\alpha) + p_t (L_{d\beta} i_\beta) \quad (3.9)$$

$$v_\alpha = p_t (L_{\alpha q} i_{qs}) + p_t (L_{\alpha d} i_{ds}) + R_\alpha i_\alpha + p_t (L_{\alpha\alpha} i_\alpha) + p_t (L_{\alpha\beta} i_\beta) \quad (3.10)$$

$$v_\beta = p_t (L_{\beta q} i_{qs}) + p_t (L_{\beta d} i_{ds}) + p_t (L_{\beta\alpha} i_\alpha) + R_\beta i_\beta + p_t (L_{\beta\beta} i_\beta) \quad (3.11)$$

where p_t is the **short-hand notation** for the differential operator²⁴ d/dt , and the various inductances are explained as follows:

²⁴Which makes this a system of ODEs, if we recall Higher Mathematics I.

- v_{qs} , v_{ds} , v_α , v_β are the terminal voltages of the stator **d** axis, **q** axis, and rotor α and β windings respectively.
- i_α , i_β are the rotor α , β winding currents respectively.
- L_{qq} , L_{dd} , $L_{\alpha\alpha}$, $L_{\beta\beta}$ are the stator **d**, and **q** axis winding and rotor α and β winding self inductances respectively.

The mutual inductances between any two (2) windings are denoted by L with two (2) subscripts:

First subscript denoting the winding at which the cut is measured due to the current in the other winding, indicated by the second subscript. For example, L_{qd} is the mutual inductance between q and d axes windings due to a current in the d axis winding.

Under the predefined assumption of **uniform air gap**, the self-inductances are **independent** of angular positions which makes them **constants**.

$$L_{\alpha\alpha} = L_{\beta\beta} = L_{rr} \quad L_{dd} = L_{qq} = L_s. \quad (3.12)$$

The mutual inductances between stator and rotor windings are zero (0), as the flux set up by a current in one winding will not link with the other winding displaced in space by 90 degrees. This leads to the following simplifications.

$$L_{\alpha\beta} = L_{\beta\alpha} = 0$$

$$L_{dq} = L_{qq} = 0$$

The mutual inductances between the stator and rotor windings are a function of the rotor position, θ_r , and they are assumed to be sinusoidal functions based on our previous assumption of sinusoidal MMF distribution in the windings. Symmetry in windings and construction causes the mutual inductances between one stator and one rotor winding to be the same whether they are viewed from the stator or the rotor.

$$L_{\alpha d} = L_{d\alpha} = L_{sr} \cos \theta_r \quad (3.13)$$

$$L_{\beta d} = L_{d\beta} = L_{sr} \sin \theta_r \quad (3.14)$$

$$L_{\alpha q} = L_{q\alpha} = L_{sr} \sin \theta_r \quad (3.15)$$

$$L_{\beta q} = L_{q\beta} = -L_{sr} \cos \theta_r \quad (3.16)$$

where L_{sr} is the peak value of the mutual inductance between a stator and a rotor winding. The last equation has a negative term, because a positive current in β winding produces a negative flux linkage in the q axis winding, and vice versa. Substitution of equations from Eq. (3.12) to Eq. (3.13) into equations from Eq. (3.8) to Eq. (3.11) results in a system of differential equations with time-varying inductances. The resulting equations are as follows:

$$v_{qs} = (R_s + L_s p_t) i_{qs} + L_{sr} p_t (i_\alpha \sin \theta_r) - L_{sr} p_t (i_\beta \cos \theta_r) \quad (3.17)$$

$$v_{ds} = (R_s + L_s p_t) i_{ds} + L_{sr} p_t (i_\alpha \cos \theta_r) + L_{sr} p_t (i_\beta \sin \theta_r) \quad (3.18)$$

$$v_\alpha = L_{sr} p_t (i_{qs} \sin \theta_r) + L_{sr} p_t (i_{ds} \cos \theta_r) + (R_{rr} + L_{rr} p_t) i_\alpha \quad (3.19)$$

$$v_\beta = -L_{sr} p_t (i_{qs} \cos \theta_r) + L_{sr} p_t (i_{ds} \sin \theta_r) + (R_{rr} + L_{rr} p_t) i_\beta \quad (3.20)$$

where:

$$R_s = R_q = R_d \quad \text{and} \quad R_{rr} = R_\alpha = R_\beta$$

The solution of these equations is time-consuming, because of their dependence on the product of the instantaneous rotor-position-dependent cosine functions and winding currents, and an elegant set of equations leading to a simple solution procedure is necessary.

Transformations performing such a step are discussed subsequently.

3.4.2. Transformations for Constant Matrices

The transformation to obtain constant inductance values is achieved by replacing the actual with a fictitious rotor on the **q** and **d** axes as shown in Fig. 3.8.

In that process, the fictitious rotor will have the same number of turns for each phase as the actual rotor phase windings and should produce the same MMF. That leads to a calculation of the number

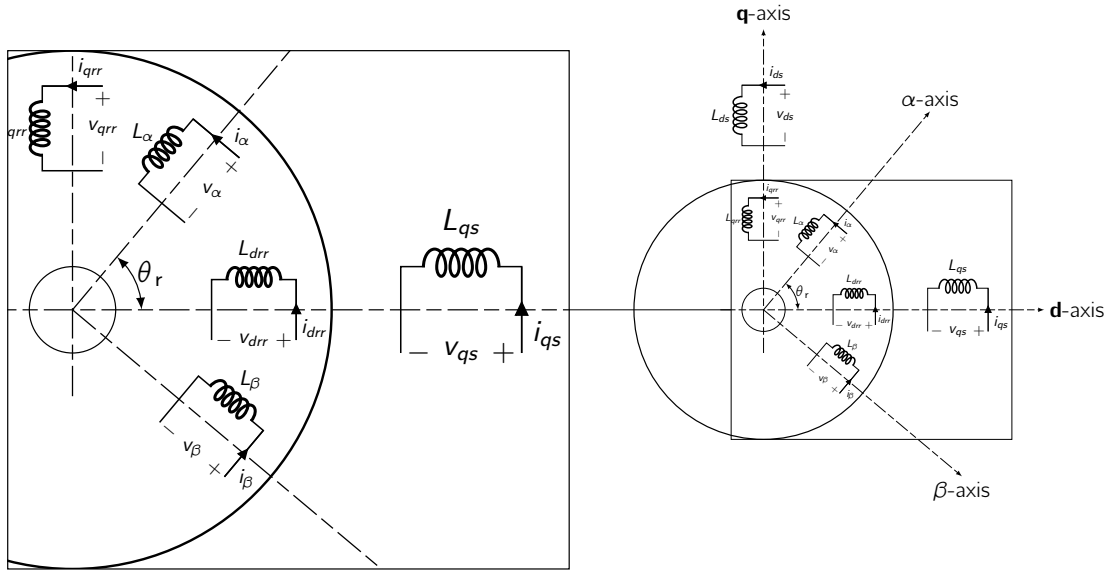


Figure 3.8.: Transformation on actual to fictitious rotor variables.

of turns on both sides of that equation, resulting in a relationship of the actual currents to fictitious rotor currents i_{qrr} and i_{drr} . Then the fictitious rotor currents i_{qrr} and i_{drr} are equal to the sum of the projections of i_α and i_β on the q and d axis, respectively, as given below:

$$\begin{bmatrix} i_{drr} \\ i_{qrr} \end{bmatrix} = \begin{bmatrix} \cos \theta_r & \sin \theta_r \\ \sin \theta_r & -\cos \theta_r \end{bmatrix} \begin{bmatrix} i_\alpha \\ i_\beta \end{bmatrix} \quad (3.21)$$

Eq. (3.21) is written compactly as:

$$\vec{i}_{dqrr} = [\mathbf{T}_{\alpha\beta}] \mathbf{i}_{\alpha\beta}$$

where

$$\vec{i}_{dqrr} = [i_{drr} \quad i_{qrr}]^T \quad \text{and} \quad \mathbf{i}_{\alpha\beta} = [i_\alpha \quad i_\beta]^T$$

and

$$\mathbf{T}_{\alpha\beta} = \begin{bmatrix} \cos \theta_r & \sin \theta_r \\ \sin \theta_r & -\cos \theta_r \end{bmatrix}$$

This transformation is valid for voltages, currents, and flux-linkages in a machine.

This transformation from α, β axes to d, q axes and vice versa is quite useful as:

$$\mathbf{T}_{\alpha\beta} = \mathbf{T}_{\alpha\beta}^{-1}$$

It is worth mentioning, that this matrix is both orthogonal and symmetric.

Applying this transformation to the α and β rotor-winding currents and rotor voltages in Eq. (3.19) and Eq. (3.20), the following matrix equation is obtained:

$$\begin{bmatrix} v_{qs} \\ v_{ds} \\ v_{qrr} \\ v_{dr} \end{bmatrix} = \left[\begin{array}{cc|cc} R_s + L_s p_t & 0 & L_s p_t & 0 \\ 0 & R_s + L_s p_t & 0 & L_{sr} p_t \\ \hline L_s p_t & -L_s \dot{\theta}_r & R_{rr} + L_{rr} p_t & -L_{rr} \dot{\theta}_r \\ L_s \dot{\theta}_r & L_s p_t & L_{rr} \dot{\theta}_r & R_{rr} + L_{rr} p_t \end{array} \right] \begin{bmatrix} i_{qs} \\ i_{ds} \\ i_{qrr} \\ i_{dr} \end{bmatrix}$$

where $\dot{\theta}_r$ is the time derivative of θ_r . The rotor equations need to be referred to the stator, as in the case of the transformer-equivalent circuit. This step removes the physical isolation and facilitates the corresponding stator and rotor **d** and **q** axes, windings in becoming physically connected. The steps involved in referring these rotor parameters and variables to the stator are as follows:

$$\begin{aligned} R_r &= a^2 R_{rr} & L_r &= a^2 L_{rr} & i_{qr} &= \frac{i_{qrr}}{a} \\ i_{dr} &= \frac{i_{dr}}{a} & v_{qr} &= a v_{qrr} & v_{dr} &= a v_{dr} \end{aligned}$$

where:

$$a = \frac{\text{Stator effective turns per phase}}{\text{Rotor effective turns per phase}} = \frac{k_{w1} T_1}{k_{w2} T_2} \quad (3.22)$$

Please be aware of the magnetising and mutual inductances as:

$$L_m \propto T_1^2 \quad L_{sr} \propto T_1 T_2 \quad (3.23)$$

From Eq. (3.22) and Eq. (3.23), the magnetising inductance of the stator as:

$$L_m = a L_{sr}$$

Using the aforementioned relations we can derive the machine equations referred to the stator as:

$$\begin{bmatrix} v_{qs} \\ v_{ds} \\ v_{qr} \\ v_{dr} \end{bmatrix} = \left[\begin{array}{cc|cc} R_s + L_s p_t & 0 & L_m p_t & 0 \\ 0 & R_s + L_s p_t & 0 & L_m p_t \\ \hline L_m p_t & -L_m \dot{\theta}_r & R_r + L_r p_t & -L_r \dot{\theta}_r \\ L_m \dot{\theta}_r & L_m p_t & L_r \dot{\theta}_r & R_r + L_r p_t \end{array} \right] \begin{bmatrix} i_{qs} \\ i_{ds} \\ i_{qr} \\ i_{dr} \end{bmatrix} \quad (3.24)$$

This equation is in the form where the voltage vector is equal to the product of the impedance matrix and current vector.

The impedance matrix has constant inductance terms and is no longer dependent on the rotor position.

Some of the impedance matrix elements are dependent on the rotor speed, and only when they are constant, as in steady state, does the system of equations become linear. In the case of varying rotor speed and if its variation is dependent on the currents, then the system of equations becomes non-linear. It is derived later that the electromagnetic torque, as a function of winding currents and rotor speed, is determined by the electromagnetic and load torques along with load parameters such as inertia and friction. In that case, it can be seen that the induction-machine system is non-linear.

3.4.3. Three-Phase to Two-Phase Transformation

We have now a model for a two-phase IM, however compared to a 3-phase it is seldom used. Therefore we need to be able to create a bridge between 2-phase and 3-phase model. For this, we need to establish and equivalence. This equivalence is based on the equality of the MMF produced in the two-phase and three-phase windings and equal current magnitudes.

Assuming each of the three-phase windings has T_1 turns per phase and equal current magnitudes, the two-phase windings will have $3T_1/2$ turns per phase for MMF equality. The **d** and **q** axes MMFs are found by resolving the MMFs of the three phases along the **d** and **q** axes.

The common term, the number of turns in the winding, is cancelled on either side of the equations, leaving the current equality.

The **q** axis is assumed to be lagging the **a** axis by θ_c . The relationship between **dq0** and **abc** currents is as follows:

$$\begin{bmatrix} i_{qs} \\ i_{ds} \\ i_0 \end{bmatrix} = \frac{2}{3} \begin{bmatrix} \cos \theta_c & \cos \left(\theta_c - 2\frac{\pi}{3} \right) & \cos \left(\theta_c + 2\frac{\pi}{3} \right) \\ \sin \theta_c & \sin \left(\theta_c - 2\frac{\pi}{3} \right) & \sin \left(\theta_c + 2\frac{\pi}{3} \right) \\ \frac{1}{2} & \frac{1}{2} & \frac{1}{2} \end{bmatrix} \begin{bmatrix} i_{as} \\ i_{bs} \\ i_{cs} \end{bmatrix} \quad (3.25)$$

The current i_0 , represents the **imbalances** in the *a*, *b*, and *c* phase currents and can be recognised as the zero-sequence component of the current. Eq. (3.23) can be expressed in a compact form by

$$\vec{i}_{qd0} = \vec{T}_{abc} \vec{i}_{abc}$$

where

$$\vec{i}_{qd0} = [i_{qs} \quad i_{ds} \quad i_0]^T \quad \vec{i}_{abc} = [i_{as} \quad i_{bs} \quad i_{cs}]^T$$

and the transformation from **abc** to **qdo** variables is [39]:

$$\vec{T}_{abc} = \frac{2}{3} \begin{bmatrix} \cos \theta_c & \cos \left(\theta_c - 2\frac{\pi}{3} \right) & \cos \left(\theta_c + 2\frac{\pi}{3} \right) \\ \sin \theta_c & \sin \left(\theta_c - 2\frac{\pi}{3} \right) & \sin \left(\theta_c + 2\frac{\pi}{3} \right) \\ \frac{1}{2} & \frac{1}{2} & \frac{1}{2} \end{bmatrix} \quad (3.26)$$

The zero-sequence current, i_0 , does not produce a resultant magnetic field.

The transformation from two-phase currents to three-phase currents can be obtained as:

$$\vec{i}_{abc} = \vec{T}_{abc}^{-1} \vec{i}_{qd0}$$

This transformation could also be thought of as a transformation from three (3) (**abc**) axes to three new (**qdo**) axes; for uniqueness of the transformation from one set of axes to another set of axes, including unbalanced in the **abc** variables requires three (3) variables:

... such as the **dq0**.

The reason for this is that it is easy to interpret from the **abc** variables to **qd** variables if the **abc** variables have an inherent relationship among the two (2) variables as the equal-phase idea here and magnitude. Therefore, in such a case, there are only two independent variables in **abc** with the third being a dependent variable, obtained as the negative sum of the other two variables.

Therefore a **dq0-to-abc** transformation is unique under the aforementioned circumstance. When the **abc** variables have no such inherent relationship, then there are three distinct and independent variables; hence, the third variable cannot be recovered from the knowledge of the other two variables only. It also means that they are not recoverable from two (2) variables **qd** but require another variable, such as the zero-sequence component, to recover the **abc** variables from the **dq0** variables.

Under balanced conditions only, there are four (4) system equations, as given in Eq. (3.24). Under unbalanced conditions, note that two (2) more system equations, one for the stator zero-sequence voltage and the other for the rotor zero-sequence voltage, emerge. They are given as:

$$v_{os} = R_s + L_{ls} p_t i_{os} \quad v_{or} = R_r + L_{lr} p_t i_{or}$$

where in the variables the first subscript (*o*) denotes the **zero-sequence component** and the second subscript denotes the stator and rotor by *s* and *r*, respectively. They could be derived from the stator and rotor inductance matrices in the **abc** frames, then converted into **dq0** frames by using the transformation derived above.

It is interesting to observe that only leakage inductances and phase resistances influence the zero-sequence voltages and currents, unlike in the **dq** component variables, which are influenced by the self and mutual inductances and phase resistances.

It is usual to align the **q** axis with the phase *a* winding; this implies that the **qd** frames are fixed to the stator²⁵. In that case, $\theta_c = 0$, and the transformation from **abc** to **qd0** variables is given as

$$T_{abc}^s = \frac{2}{3} \begin{bmatrix} 1 & -\frac{1}{2} & -\frac{1}{2} \\ 0 & -\frac{\sqrt{3}}{2} & \frac{\sqrt{3}}{2} \\ \frac{1}{2} & \frac{1}{2} & \frac{1}{2} \end{bmatrix} \quad (3.27)$$

In a balanced three-phase machine, the sum of the three-phase currents is zero and is given as

$$i_{as} + i_{bs} + i_{cs} = 0$$

leading to a zero-sequence current of zero value:

$$i_0 = \frac{1}{3} (i_{as} + i_{bs} + i_{cs}) = 0 \quad (3.28)$$

With Eq. (3.26), the equivalence²⁶ between the two-phase and three-phase IMs is established.

²⁵The model is known as Stanley's model or the *stator reference frames* model [40].

²⁶It is instructive to know that the transformation derived is applicable to currents, voltages, and flux-linkages.

Exercise 3.1: Calculating d-q currents

An IM has the following parameters:

$$\begin{array}{lllll} \text{5 hp} & \text{3-phase} & \text{4-pole} & \text{star-connected} \\ R_s = 0.277 \Omega & R_r = 0.183 \Omega & L_m = 0.0538 \text{ H} & L_s = 0.0533 \text{ H} \\ L_r = 0.056 \text{ H} & a = 3 \end{array}$$

where a is the effective stator to rotor turns ratio. The motor is supplied with its rated and balanced voltages. Find the v_{qs} , v_{ds} axes steady-state voltages and currents when the rotor is locked. Use the stator-reference-frame model of the IM.

Solution

The applied phase voltages are as follows:

$$\begin{aligned} v_{as} &= \frac{200}{\sqrt{3}} \times \sqrt{2} \sin \omega_s t = 163.3 \sin \omega_s t \\ v_{bs} &= 163.3 \sin \left(\omega_s t - \frac{2\pi}{3} \right) \\ v_{cs} &= 163.3 \sin \left(\omega_s t + \frac{2\pi}{3} \right) \end{aligned}$$

The v_d and v_q axes voltages are

$$\begin{bmatrix} v_{qs} \\ v_{ds} \\ v_0 \end{bmatrix} = \vec{T}_{abc}^s \begin{bmatrix} v_{as} \\ v_{bs} \\ v_{cs} \end{bmatrix}$$

Therefore,

$$v_{qs} = \frac{2}{3} \left[v_{as} - \frac{1}{2} (v_{bs} + v_{cs}) \right]$$

For a balanced three-phase input:

$$v_{as} + v_{bs} + v_{cs} = 0$$

Substituting for v_{bs} , and v_{cs} in terms of v_{as} gives

$$v_{qs} = \frac{2}{3} \left[\frac{3}{2} v_{as} \right] = v_{as}$$

Similarly,

$$v_{ds} = \frac{1}{\sqrt{3}} (v_{cs} - v_{bs})$$

and $v_0 = 0$

$$v_{qs} = v_{as} = 163.3 \sin \omega_s t = 163.3 \angle 0^\circ = 163.3 \text{ V}$$

$$v_{ds} = \frac{1}{\sqrt{3}} (v_{cs} - v_{bs}) = 163.3 \cos \omega_s t = 163.3 \angle 90^\circ = j 163.3 \text{ V}$$

The rotor is locked, therefore:

$$\dot{\theta}_r = 0$$

For steady-state evaluation:

$$p_t = j \omega_s = j 2\pi f_s = j 2\pi 60 = j 377 \text{ rad s}^{-1}$$

The system equations are:

$$\begin{bmatrix} v_{qs} \\ v_{ds} \\ 0 \\ 0 \end{bmatrix} = \begin{bmatrix} R_s + j \omega_s L_s & 0 & j \omega_s L_m & 0 \\ 0 & R_s + j \omega_s L_s & 0 & j \omega_s L_m \\ j \omega_s L_m & 0 & R_r + j \omega_s L_r & 0 \\ 0 & j \omega_s L_m & 0 & R_r + j \omega_s L_r \end{bmatrix} \begin{bmatrix} i_{qs} \\ i_{ds} \\ i_{qr} \\ i_{dr} \end{bmatrix} \quad (3.29)$$

Note that the rotor windings are **short-circuited**, and hence rotor voltages are zero. The numerical values for the parameters and variables are substituted to solve for the currents. The currents are

$$i_{qs} = 35.37 - j 108.18 = 113.81 \angle -71.90^\circ$$

$$i_{ds} = 108.18 + j 35.37 = 113.81 \angle 18.90^\circ$$

$$i_{qr} = -34.88 + j 103.63 = 109.34 \angle 108.60^\circ$$

$$i_{dr} = -103.63 - j 34.88 = 109.34 \angle -161.40^\circ$$

Note that the stator and rotor currents are displaced by 90° among themselves, as expected in a two-phase machine. The zero-sequence currents are zero because zero-sequence voltages are non-existent with balanced supply voltages ■.

3.4.4. Power Equivalence

The power input to the three-phase motor must be equal to the power input to the two-phase machine for it to have a meaningful interpretation in the modelling, analysis, and simulation.

The three-phase **instantaneous power input** is:

$$p_i = \vec{v}_{abc}^t \vec{i}_{abc} = v_{as} i_{as} + v_{bs} i_{bs} + v_{cs} i_{cs} \quad (3.30)$$

From Eq. (3.25), the **abc** phase currents and voltages are transformed into their equivalent **qd** currents and voltages as:

$$\vec{i}_{abc} = [\vec{T}_{abc}]^{-1} \vec{i}_{qd0} \quad \text{and} \quad \vec{v}_{abc} = [\vec{T}_{abc}]^{-1} \vec{v}_{qd0} \quad (3.31)$$

Substituting Eq. (3.31) into Eq. (3.30) gives the power input as:

$$p_i = \vec{v}_{qd0}^t \left([\vec{T}_{abc}]^{-1} \right)^t [\vec{T}_{abc}^{-1}]^{-1} \vec{i}_{qd0}. \quad (3.32)$$

Expanding the RHS of Eq. (3.32) gives the power input in **dq0** variables:

$$p_i = \frac{3}{2} \left((v_{qs} i_{qs} + v_{ds} i_{ds}) + 2v_0 i_0 \right) \quad (3.33)$$

For a **balanced three-phase machine**, the zero-sequence current does not exist. Therefore, the power input is compactly represented by

$$p_i = \frac{3}{2} (v_{qs} i_{qs} + v_{ds} i_{ds}) \quad (3.34)$$

The model we have developed thus far kept the **dq** axes **stationary with respect to the stator**. These axes or frames are known as reference frames.

The input power given by Eq. (3.33) remains valid for all occasions, provided that the voltages and currents correspond to the frames under consideration.

3.4.5. Generalised Model in Arbitrary Reference Frame

Reference frames are very much like observer platforms, in that each of the platform gives a unique view of the system at hand as well as a dramatic simplification of the system equations.

For the purposes of control, it is desirable to have the system variables as DC quantities, although the actual variables are sinusoidal.

This could be accomplished by having a reference frame revolving at the same angular speed as that of the sinusoidal variable. As the reference frames are moving at an angular speed equal to the

angular frequency of the sinusoidal supply, say, then the differential speed between them is reduced to zero, resulting in the sinusoidal being perceived as a DC signal from the reference frames. Then, by moving to that plane, it becomes easier to develop a small-signal equation out of a non-linear equation, as the operation is described only by DC values. This then leads to the linearised system around an operating point. Now, it is easier to create a compensator for the system by using standard linear control-system techniques.

the independent rotor-field position determines the induced EMF and affects the dynamic system equations of both the wound-rotor and PMSM.

Therefore, looking at the entire system from the rotor²⁷, the system inductance matrix becomes **independent of rotor position**, therefore leading to the simplification and compactness of the system equations. Such advantages are many from using reference frames. Instead of deriving the transformations for each and every particular reference frame, it is advantageous to derive the general transformation for an arbitrary rotating reference frame. Then any particular reference frame model can be derived by substituting the appropriate frame speed and position in the generalised reference model.

²⁷rotating reference frames applied

Reference frames rotating at an arbitrary speed are hereafter called **arbitrary reference frames**. Other reference frames are particular cases of these arbitrary reference frames. From now on, the three-phase machine is assumed to have balanced windings and balanced inputs, thus making the zero-sequence components be zero (0) and eliminating the zero-sequence equations from further consideration.

the zero-sequence equations have to be included only for unbalanced operation of the motor, a situation common with a fault in the machine²⁸ or converter.

²⁸which could be a very interesting M.Sc thesis topic

Assuming the windings have **equal number of turns** on both of the reference frames, the arbitrary reference frame currents are resolved on the **d, q** axes to find the currents in the stationary reference frames. The relationships between the currents are written as:

$$i_{qds} = [T^c] i_{qds}^c$$

where:

$$i_{qds} = \begin{bmatrix} i_{qs} & i_{ds} \end{bmatrix}^T \quad i_{qds}^c = \begin{bmatrix} i_{qs}^c & i_{ds}^c \end{bmatrix}^T$$

and:

$$T^c = \begin{bmatrix} \cos \theta_c & \sin \theta_c \\ -\sin \theta_c & \cos \theta_c \end{bmatrix}$$

The speed of the arbitrary reference frames is:

$$\dot{\theta}_c = \omega_c$$

Similarly, the fictitious rotor currents are transformed into arbitrary frames by using T^c , and they are written as

$$i_{qdr} = [T^c] i_{qdr}^c$$

where:

$$i_{\text{qdr}} = \begin{bmatrix} i_{\text{qr}} & i_{\text{dr}} \end{bmatrix}^T \quad i_{\text{qdr}}^c = \begin{bmatrix} i_{\text{qr}}^c & i_{\text{dr}}^c \end{bmatrix}^T$$

And similarly, the voltage relationships are:

$$v_{\text{qds}} = [T^c] v_{\text{qds}}^c \quad v_{\text{qdr}} = [T^c] v_{\text{qdr}}^c$$

where, as usual:

$$\begin{aligned} v_{\text{qds}} &= \begin{bmatrix} v_{\text{qs}} & v_{\text{ds}} \end{bmatrix}^T & v_{\text{qds}}^c &= \begin{bmatrix} v_{\text{qs}}^c & v_{\text{ds}}^c \end{bmatrix}^T \\ v_{\text{qdr}} &= \begin{bmatrix} v_{\text{qr}} & v_{\text{dr}} \end{bmatrix}^T & v_{\text{qdr}}^c &= \begin{bmatrix} v_{\text{qr}}^c & v_{\text{dr}}^c \end{bmatrix}^T \end{aligned}$$

By substituting the aforementioned equations into Eq. (3.24), the IM in arbitrary reference frame is obtained which is shown as:

$$\begin{bmatrix} v_{\text{qs}}^c \\ v_{\text{ds}}^c \\ v_{\text{qr}}^c \\ v_{\text{dr}}^c \end{bmatrix} = \left[\begin{array}{cc|cc} R_s + L_s p_t & \omega_c L_s & L_m p_t & \omega_c L_m \\ -\omega_c L_s & R_s + L_s p_t & -\omega_c L_m & L_m p_t \\ \hline L_m p_t & (\omega_c - \omega_r) L_m & R_r + L_r p_t & (\omega_c - \omega_r) L_r \\ -(\omega_c - \omega_r) L_m & L_m p_t & -(\omega_c - \omega_r) L_r & R_r + L_r p_t \end{array} \right] \begin{bmatrix} i_{\text{qs}}^c \\ i_{\text{ds}}^c \\ i_{\text{qr}}^c \\ i_{\text{dr}}^c \end{bmatrix} \quad (3.35)$$

where:

$$\omega_r = \dot{\theta}_r$$

ω_r is the rotor speed in electrical rpm. The relationship between the arbitrary reference frame variables and the a , b , and c variables is derived by using

$$i_{\text{qds}}^c = [T^c]^{-1} i_{\text{qds}}$$

By substituting from Eq. (3.27) for i_{qds} in terms of a , b , and c phase currents in the stator reference frames, the **qd0** currents in the arbitrary reference frames are obtained as:

$$i_{\text{qd0}}^c = \begin{bmatrix} [T^c]^{-1} & 0 \\ [0] & 1 \end{bmatrix} [T_{abc}^s] [i_{abc}] = [T_{abc}] [i_{abc}]$$

where $[0]$ is a 1×2 null vector. Note that the zero-sequence currents remain unchanged in the arbitrary reference frames. This transformation is valid for currents, voltages, and flux-linkages for both the stator and the rotor. Particular cases of the reference frames are derived in a later section. The next section contains the derivation of the electromagnetic torque in terms of the current variables in the arbitrary reference frames.

3.4.6. Electromagnetic Torque

The electromagnetic torque (T_e) is an important output variable which determines such mechanical dynamics of the machine as the rotor position and speed. Therefore, its importance cannot be overstated in any of the simulation studies. It is derived from the machine matrix equation by looking at the input power and its various components, such as:

resistive losses, mechanical power, rate of change of stored magnetic energy, and reference-frame power [41]

Elementary reasoning leads to the fact that there cannot be a power component due to the introduction of reference frames. Similarly, the rate of change of stored magnetic energy must be zero in steady state. Hence, the output power is the difference between the input power and the resistive losses in steady state. Dynamically, the rate of change of stored magnetic energy need **NOT** be zero (0).

Based on these observations, the derivation of the electromagnetic torque is made as follows. The equation (5.114) can be written as

$$\vec{V} = \vec{R}\vec{i} + \vec{L}\vec{p}_t\vec{i} + \vec{G}\omega_r\vec{i} + \vec{F}\omega_c\vec{i}$$

where the vectors and matrices are identified by observation. Pre-multiplying the equation Eq. (3.4.6) by the transpose of the current vector (\vec{i}^T) gives the instantaneous input power as,

$$\vec{p}_i = \vec{i}^T \vec{V} = \vec{i}^T \vec{R}\vec{i} + \vec{i}^T \vec{L}\vec{p}_t + \vec{i}^T \vec{G}\omega_r\vec{i} + \vec{i}^T \vec{F}\omega_c\vec{i}$$

where:

\vec{R} consists of resistive elements,

\vec{L} consists of the coefficients of the derivative operator \vec{p}_t ,

\vec{G} elements that are the coefficients of the electrical rotor speed ω_r ,

\vec{F} frame matrix in terms of the coefficients of the reference frame speed, ω_c

$\vec{i}^T \vec{R}\vec{i}$ Stator and rotor resistive losses.

$\vec{i}^T \vec{F}\omega_c\vec{i}$ The reference frame power,²⁹

$\vec{i}^T \vec{L}\vec{p}_t$ The rate of change of stored magnetic energy.

Therefore, what is left of the power component must be equal to the air gap power, given by the term $\vec{i}^T \vec{G}\omega_r\vec{i}$. From fundamentals, it is known the air gap power has to be associated with the rotor speed.

The air gap power is the product of the mechanical rotor speed and air gap or electromagnetic torque.

²⁹upon expansion is found to be identically equal to zero, as it should be, because there cannot be a power associated with a fictitious element introduced for the sake of simplifying the model and analysis.

Therefore the air-gap torque, T_e , is derived from the terms involving the rotor speed, ω_m in mechanical rad s⁻¹, as

$$\omega_m \vec{T}_e = P_{\text{air-gap}} = \vec{i}^T \vec{G}\vec{i} \times \omega_r$$

Substituting for ω_r in terms of ω_m leads to electromagnetic torque as

$$\vec{T}_e = \frac{\vec{P}}{2} \vec{i}^T \vec{G}\vec{i} \quad (3.36)$$

By substituting for \vec{G} in equation Eq. (3.36) by observation from Eq. (3.35), the electromagnetic torque is obtained as:

$$\vec{T}_e = \frac{3}{2} \frac{\bar{P}}{2} L_m (i_{qs}^c i_{dr}^c - i_{ds}^c i_{qr}^c) \quad (3.37)$$

The factor $3/2$ is introduced into the right-hand side of equation Eq. (3.37) from the power-equivalence condition between the three-phase and two-phase IMs. The next section considers the frequently used models in various reference frames and their derivation from the generalised induction-motor model in arbitrary reference frames.

3.4.7. Derivation of Commonly Used Induction-Machine Models

There are three (3) particular cases of the generalised model of the IM in arbitrary reference frames are of general interest:

1. stator reference frames model;
2. rotor reference frames model;
3. synchronously rotating reference frames model.

Let's look at each of them in more detail.

Stator Reference

The speed of the reference frames is that of the stator, which is zero.

$$\omega_c = 0 \quad (3.38)$$

This is substituted to Eq. (3.35) to derive the following model:

$$\begin{bmatrix} v_{qs} \\ v_{ds} \\ v_{qr} \\ v_{dr} \end{bmatrix} = \begin{bmatrix} R_s + L_s p_t & 0 & L_m p_t & 0 \\ 0 & R_s + L_s p_t & 0 & L_m p_t \\ L_m p_t & -\omega_r L_m & R_r + L_r p_t & -\omega_r L_r \\ \omega_r L_m & L_m p_t & \omega_r L_r & R_r + L_r p_t \end{bmatrix} \begin{bmatrix} i_{qs} \\ i_{ds} \\ i_{qr} \\ i_{dr} \end{bmatrix} \quad (3.39)$$

For convenience, the superscript is omitted for the stator reference frames model hereafter.

The torque equation is

$$\vec{T}_e = \frac{3}{2} \frac{\vec{P}}{2} L_m (i_{qs} i_{dr} - i_{ds} i_{qr}) \quad (3.40)$$

Note that Eq. (3.39) and Eq. (3.24) are identical. The transformation for variables is obtained by substituting $\theta_c = 0$ in $[T_{abc}]$ and will be the same as $[T_{abc}^S]$, defined in Eq. (3.27).

This model is used when stator variables are required to be actual³⁰, and rotor variables can be fictitious. This model allows simple simulation of stator-controlled IM drives, such as phase-controlled and inverter-controlled induction-motor drives, as the input variables are well defined and could be used to find the stator **qd** axes voltages through a set of simple algebraic equations, for a **balanced** poly-phase supply input, given by:

$$v_{qs} = v_{as} \quad \text{and} \quad v_{ds} = \frac{(v_{cs} - v_{bs})}{\sqrt{3}}$$

³⁰i.e., the same as in the actual machine stator

These algebraic relationships reduce the number of computations and therefore lend themselves to real-time control applications in high-performance variable-speed drives requiring the computation of stator currents, stator flux linkages, and electromagnetic torque for both control and parameter adaptation.

Rotor Reference

The speed of the rotor reference frame is:

$$\omega_c = \omega_r \quad (3.41)$$

and the angular position is:

$$\theta_c = \theta_r \quad (3.42)$$

Substituting in the upper subscript *r* for rotor reference frames and Eq. (3.41) in Eq. (3.35), the induction-motor model in rotor reference frames is obtained. The equations are given by

$$\begin{bmatrix} v_{qs}^r \\ v_{ds}^r \\ v_{qr}^r \\ v_{dr}^r \end{bmatrix} = \begin{bmatrix} R_s + L_s p_t & \omega_r L_s & L_m p_t & \omega_r L_m \\ -\omega_r L_s & R_s + L_s p_t & -\omega_r L_m & L_m p_t \\ L_m p_t & 0 & R_r + L_r p_t & -0 \\ 0 & L_m p_t & 0 & R_r + L_r p_t \end{bmatrix} \begin{bmatrix} i_{qs}^r \\ i_{ds}^r \\ i_{qr}^r \\ i_{dr}^r \end{bmatrix} \quad (3.43)$$

The torque equation is

$$\vec{T}_e = \frac{3}{2} \frac{P}{2} L_m (i_{qs}^r i_{dr}^r - i_{ds}^r i_{qr}^r) \quad (3.44)$$

The transformation from **abc** to **dq0** variables is obtained by substituting Eq. (3.42) to $[T_{abc}]$,

defined in Eq. (3.26) as:

$$[T_{abc}^r] = \frac{2}{3} \begin{bmatrix} \cos \theta_r & \cos(\theta_r - 2\frac{\pi}{3}) & \cos(\theta_r + 2\frac{\pi}{3}) \\ \sin \theta_r & \sin(\theta_r - 2\frac{\pi}{3}) & \sin(\theta_r + 2\frac{\pi}{3}) \\ \frac{1}{2} & \frac{1}{2} & \frac{1}{2} \end{bmatrix} \quad (3.45)$$

The rotor reference frames model is useful where the switching elements and power are controlled on the rotor side. Slip-power recovery scheme is one example where this model will find use in the simulation of the motor-drive system.

Synchronous Rotation Reference

The reference frames is

$$\omega_c = \omega_s = \text{Stator supply angular frequency} \quad (3.46)$$

and the instantaneous angular position is

$$\theta_c = \theta_s = \omega_s t \quad (3.47)$$

By substituting Eq. (3.47) into Eq. (3.35), the induction-motor model in the synchronous reference frames is obtained. By using the superscript *e* to denote this electrical synchronous reference frame, the model is obtained as

$$\begin{bmatrix} v_{qs}^e \\ v_{ds}^e \\ v_{qr}^e \\ v_{dr}^e \end{bmatrix} = \begin{bmatrix} R_s + L_s p_t \\ -\omega_s L_s \\ L_m p_t \\ -(\omega_s - \omega_r) L_m \end{bmatrix} \begin{bmatrix} \omega_s L_s \\ R_s + L_s p_t \\ (\omega_s - \omega_r) L_m \\ L_m p_t \end{bmatrix} \begin{bmatrix} i_{qs}^e \\ i_{ds}^e \\ i_{qr}^e \\ i_{dr}^e \end{bmatrix} \quad (3.48)$$

The torque equation is

$$\vec{T}_e = \frac{3}{2} \frac{P}{2} L_m (i_{qs}^e i_{dr}^e - i_{ds}^e i_{qr}^e) \quad \text{Nm} \quad (3.49)$$

The transformation from *abc* to *dqo* variables is found by substituting Eq. (3.47) into Eq. (3.26) and is given as:

$$[T_{abc}^e] = \frac{2}{3} \begin{bmatrix} \cos \theta_e & \cos(\theta_e - 2\frac{\pi}{3}) & \cos(\theta_e + 2\frac{\pi}{3}) \\ \sin \theta_e & \sin(\theta_e - 2\frac{\pi}{3}) & \sin(\theta_e + 2\frac{\pi}{3}) \\ \frac{1}{2} & \frac{1}{2} & \frac{1}{2} \end{bmatrix} \quad (3.50)$$

It may be seen that the synchronous reference frames transform the sinusoidal inputs into DC signals. This model is useful where the variables in steady state need to be DC quantities, as in the development of small-signal equations. Some high-performance control schemes use this model to estimate the control inputs.

This led to a major breakthrough in induction-motor control, by decoupling the torque and flux channels for control in a manner similar to that for separately-excited DC motor drives. This is dealt with in detail on vector control schemes on the next chapter.

3.4.8. Equations in Flux Linkages

The dynamic equations of the IM in arbitrary reference frames can be represented by using flux linkages as variables. This involves the reduction of a number of variables in the dynamic equations.

Even when the voltages and currents are discontinuous, the flux linkages are continuous.

This gives the advantage of differentiating these variables with numerical stability. In addition, the flux-linkages representation is used in motor drives to highlight the process of the decoupling of the flux and torque channels in the induction and synchronous machines.

The stator and rotor flux linkages in the arbitrary reference frames are defined as

$$\lambda_{qs}^c = L_s i_{qs}^c + L_m i_{qr}^c, \quad \lambda_{ds}^c = L_s i_{ds}^c + L_m i_{dr}^c, \quad \lambda_{qr}^c = L_r i_{qr}^c + L_m i_{qs}^c, \quad \lambda_{dr}^c = L_r i_{dr}^c + L_m i_{ds}^c \quad (3.51)$$

The zero-sequence flux linkages are

$$\lambda_{os} = L_{ls} i_{os}, \quad \lambda_{or} = L_{lr} i_{or}.$$

The **q** axis stator voltage in the arbitrary reference frame is

$$v_{qs}^c = R_s i_{qs}^c + \omega_c (L_s i_{ds}^c + L_m i_{dr}^c) + L_m p_t i_{qr}^c + L_s p_t i_{qs}^c$$

Substituting from the defined flux-linkages into the voltage equation gives:

$$v_{qs}^c = R_s i_{qs}^c + \omega_c \lambda_{ds}^c + p_t \lambda_{qs}^c \quad (3.52)$$

Similarly, the stator **d** axis voltage, the **dq**-axes rotor voltages, and the zero-sequence voltage equations are derived as:

$$v_{ds}^c = R_s i_{ds}^c - \omega_c \lambda_{qs}^c + p_t \lambda_{ds}^c \quad (3.53)$$

$$v_{os} = R_s i_{os} + p_t \lambda_{os} \quad (3.54)$$

$$v_{qr}^c = R_r i_{qr}^c + (\omega_c - \omega_r) \lambda_{dr}^c + p_t \lambda_{qr}^c \quad (3.55)$$

$$v_{dr}^c = R_r i_{dr}^c - (\omega_c - \omega_r) \lambda_{qr}^c + p_t \lambda_{dr}^c \quad (3.56)$$

$$v_{or} = R_r i_{or} + p_t \lambda_{or} \quad (3.57)$$

To simplify these expression we can represent them as per-unit values. The normalisation of the variables is made via reactances rather than inductances. To facilitate such a step, a modified flux linkage is defined whose unit in volts is

$$\Psi_{qs}^c = \omega_b \lambda_{qs}^c = \omega_b (L_s i_{qs}^c + L_m i_{qr}^c) = X_s i_{qs}^c + X_m i_{qr}^c$$

where ω_b is the base frequency in rad s^{-1} . The other modified flux linkages can be written as:

$$\Psi_{ds}^c = X_s i_{ds}^c + X_m i_{dr}^c$$

$$\Psi_{ds}^c = X_s i_{qr}^c + X_m i_{qs}^c$$

$$\Psi_{ds}^c = X_r i_{dr}^c + X_m i_{ds}^c$$

$$\Psi_{os} = X_{ls} i_{os}$$

$$\Psi_{or} = X_{lr} i_{or}$$

Substituting the flux linkages in terms of the modified flux linkages gives:

$$\lambda_{qs}^c = \frac{\Psi_{qs}^c}{\omega_b}, \lambda_{ds}^c = \frac{\Psi_{ds}^c}{\omega_b}, \lambda_{os}^c = \frac{\Psi_{os}^c}{\omega_b}, \lambda_{qr}^c = \frac{\Psi_{qr}^c}{\omega_b}, \lambda_{dr}^c = \frac{\Psi_{dr}^c}{\omega_b}, \lambda_{or}^c = \frac{\Psi_{or}^c}{\omega_b} \quad (3.58)$$

and by substituting equation Eq. (3.58) into equations from Eq. (3.52) to Eq. (3.57), the resulting equations in the modified flux linkages are:

$$\begin{aligned} v_{qs}^c &= R_s i_{qs}^c + \frac{\omega_c}{\omega_b} \Psi_{ds}^c + \frac{p_t}{\omega_b} \Psi_{qs}^c \\ v_{ds}^c &= R_s i_{ds}^c - \frac{\omega_c}{\omega_b} \Psi_{qs}^c + \frac{p_t}{\omega_b} \Psi_{ds}^c \\ v_{os}^c &= R_s i_{os}^c + \frac{p_t}{\omega_b} \Psi_{os}^c \\ v_{qr}^c &= R_r i_{qr}^c + \frac{(\omega_c - \omega_r)}{\omega_b} \Psi_{dr}^c + \frac{p_t}{\omega_b} \Psi_{qr}^c \\ v_{dr}^c &= R_r i_{dr}^c - \frac{(\omega_c - \omega_r)}{\omega_b} \Psi_{qr}^c + \frac{p_t}{\omega_b} \Psi_{dr}^c \\ v_{or}^c &= R_r i_{or}^c + \frac{p_t}{\omega_b} \Psi_{or}^c \end{aligned}$$

The electromagnetic torque in flux linkages and currents is derived as:

$$T_e = \frac{3P}{2} L_m \left(i_{qs}^c i_{dr}^c - i_{ds}^c i_{qs}^c \right) = \frac{3P}{2} \left(i_{qs}^c (L_m i_{dr}^c) - i_{ds}^c (L_m i_{qr}^c) \right)$$

The rotor current can be substituted in terms of the stator currents and stator flux linkages from the basic definitions of the flux linkages. From Eq. (3.51):

$$L_m i_{dr}^c + L_s i_{ds}^c = \lambda_{ds}^c \quad (3.59)$$

Which makes

$$L_m i_{dr}^c = (\lambda_{ds}^c - L_s i_{ds}^c) \quad \text{and} \quad L_m i_{qr}^c = (\lambda_{qs}^c - L_s i_{qs}^c) \quad (3.60)$$

Substituting Eq. (3.59) and Eq. (3.60) to X gives the electromagnetic torque in stator flux linkages and stator currents as:

$$T_e = \frac{3P}{2} \left(i_{qs}^c (\lambda_{ds}^c - L_s i_{ds}^c) - i_{ds}^c (\lambda_{qs}^c - L_s i_{qs}^c) \right) = \frac{3P}{2} \left(i_{qs}^c \lambda_{ds}^c - i_{ds}^c \lambda_{qs}^c \right)$$

Or we can write electromagnetic torque in terms of modified flux linkages and currents as:

$$T_e = \frac{3P}{2} \frac{1}{\omega_b} \left(i_{qs}^c \Psi_{ds}^c - i_{ds}^c \Psi_{qs}^c \right)$$

The electromagnetic torque can also be expressed using only rotor variables which has been left to the reader as exercise.

3.5. Dynamic Simulation Equations

The dynamic simulation of the IM is explained in this section. The equations of the IM in arbitrary reference frames in p.u. are cast in the state-space form as:

$$\vec{P}_1 p_t \vec{X}_1 + \vec{Q}_1 \vec{X}_1 = u_1$$

where

$$\vec{P} = \begin{bmatrix} \frac{X_{sn}}{\omega_b} & 0 & \frac{X_{mn}}{\omega_b} & 0 \\ 0 & \frac{X_{sn}}{\omega_b} & 0 & \frac{X_{mn}}{\omega_b} \\ \frac{X_{mn}}{\omega_b} & 0 & \frac{X_{rn}}{\omega_b} & 0 \\ 0 & \frac{X_{mn}}{\omega_b} & 0 & \frac{X_{rn}}{\omega_b} \end{bmatrix} \quad \vec{X} = \begin{bmatrix} i_{qsn}^c \\ i_{dsn}^c \\ i_{qrn}^c \\ i_{drn}^c \end{bmatrix} \quad \vec{u} = \begin{bmatrix} v_{qsn}^c \\ v_{dsn}^c \\ v_{qrn}^c \\ v_{drn}^c \end{bmatrix}$$

$$\vec{Q} = \begin{bmatrix} R_{sn} & \omega_{cn} X_{sn} & 0 & \omega_{cn} X_{mn} \\ -\omega_{cn} X_{sn} & R_{sn} & -\omega_{cn} X_{mn} & 0 \\ 0 & (\omega_{cn} - \omega_{rn}) X_{mn} & R_{rn} & (\omega_{cn} - \omega_{rn}) X_{mn} \\ -(\omega_{cn} - \omega_{rn}) X_{mn} & 0 & -(\omega_{cn} - \omega_{rn}) X_{rn} & R_{rn} \end{bmatrix}$$

The equations can be re-arranged in the state-space form as:

$$p_t \vec{X} = \vec{P}^{-1} (\vec{u} - \vec{Q} \vec{X})$$

Which can be re-written as:

$$p_t \vec{X} = \vec{A} \vec{X} + \vec{B} \vec{u} \quad \text{where} \quad \vec{A} = -\vec{P}^{-1} \vec{Q} \quad \text{and} \quad \vec{B} = \vec{P}^{-1}$$

These aforementioned expressions are evaluated to be:

$$\vec{B} = \vec{P}^{-1} = \frac{1}{\Delta} \begin{bmatrix} X_{rn} & 0 & -X_{mn} & 0 \\ 0 & X_{rn} & 0 & -X_{mn} \\ -X_{mn} & 0 & X_{sn} & 0 \\ 0 & -X_{mn} & 0 & X_{sn} \end{bmatrix} \quad \text{where} \quad \Delta = \left(\frac{X_{sn} X_{rn} - X_{mn}^2}{\omega_b} \right)$$

and let's not forget the matrix \vec{A} :

$$\vec{A} = \frac{1}{\Delta} \begin{bmatrix} R_{sn} X_{rn} & k + \omega_{rn} X_{mn}^2 & -R_{rn} X_{mn} & \omega_{rn} X_{rn} X_{mn} \\ -k - \omega_{rn} X_{mn}^2 & R_{sn} X_{rn} & -\omega_{rn} X_{rn} X_{mn} & -R_{rn} X_{mn} \\ -R_{sn} X_{mn} & -\omega_{rn} X_{mn} X_{sn} & R_{rn} X_{sn} & k - \omega_{rn} X_{sn} \\ \omega_{rn} X_{mn} X_{sn} & -R_{sn} X_{mn} & -k + \omega_{rn} X_{rn} X_{sn} & R_{rn} X_{sn} \end{bmatrix}$$

where:

$$k = \omega_{cn} (X_{sn} X_{rn} - X_{mn}^2)$$

The electromechanical equation is:

$$T_{en} = \frac{T_e}{T_b} = 2 \left(\frac{1}{2} \frac{J \omega_b^2}{P_b (P/2)^2} \right) p_t \omega_{rn} + T_{ln} + B_n \omega_{rn}$$

where J is the moment of inertia, P_b is the base power, T_{ln} is the normalised load torque, B_n is the normalised friction coefficient of the load and motor and ω_{rn} is the normalised mechanical rotor speed, and

$$T_{en} = i_{qsn}^c \Psi_{dsn}^c - i_{dsn}^c \Psi_{qsn}$$

The modified flux linkages require additional computation. The torque can be conveniently expressed in terms of the normalised currents as:

$$T_{en} = X_{mn} \left(i_{qsn}^c i_{drn}^c - i_{dsn}^c i_{qrn}^c \right)$$

Solving these equations require numerical methods which are out of scope for this lecture. However, no one said one can't use SIMULINK which will be the topic of the next section.

3.5.1. Simulation Example

To get a better understanding of the equations derived previously, it is useful to do an example. To start let's define some parameters to use: We assume the motor stands at standstill. We apply a set of balanced three-phase voltages with a frequency of 50 Hz. The simulation diagram drawn in SIMULINK can be seen in **Fig. 3.9**.

As can be seen the initial model is relatively abstracted under sub-blocks. On the upper left part is the scopes of the variables which are of interest and on the upper-right is the variables which are to be saved to the work space. On the input block we define the other initial values for the simulation which are not defined in the **.m** file which are the step response torque load, three-phase voltage input, and the initial speed.

Before we start with the SIMULINK we need to initialise some variables which are as follows:

```

1 % Initialization
2
3 Rr      =1.15;           %Rotor resistance
4 Rs      =0.855;          %Stator resistance
5 Lls     =3.92e-3;        %Stator inductance
6 Llr     =3.92e-3;        %Rotor inductance
7 Lm      =30e-3;          %Magnetizing Inductance
8 fb      =50;              %Base frequency
9 p       =6;                %Number of poles
10 J       =0.06;             %Moment of inertia
11
12 Lr     = Llr + Lm;
13 Tr     = Lr / Rr;
14 we     =2*pi*fb;
15
16 % Impedance and angular speed calculations

```

C.R. 1
matlab

	200 V	4 pole	3 phase	60 Hz
star connected	$R_s = 0.183 \Omega$	$R_r = 0.277 \Omega$	$L_m = 0.0538 H$	
$L_s = 0.0553 H$	$L_r = 0.056 H$	$B = 0$	$T_i = 0 Nm$	
$J = 0.0165 kg m^2$	$P = 4 kW$			

Table 3.1.: Simulation parameters for the IM example.

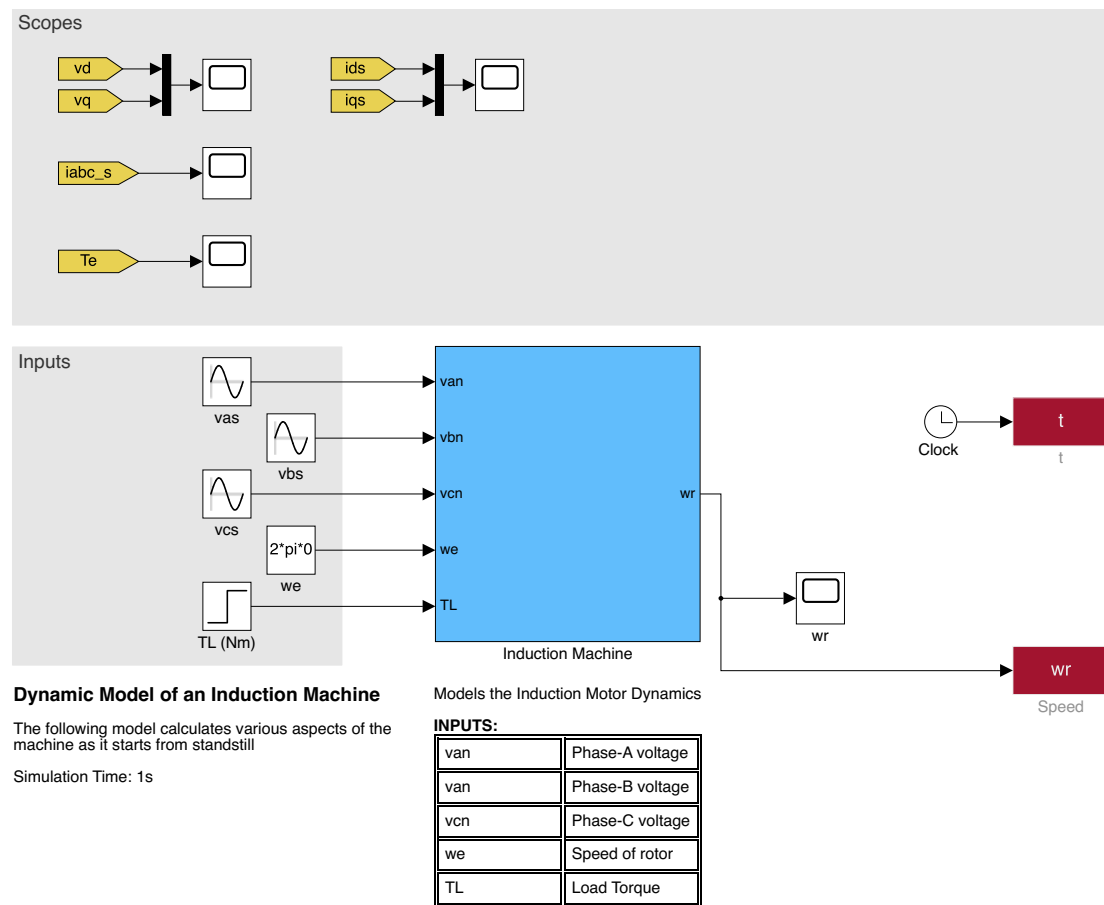


Figure 3.9.: A Simulink Model of an Induction Machine.

```

17
18 wb      =2*pi*fb;           %Base speed
19 Xls     =wb*Lls;            %Stator impedance
20 Xlr     =wb*Llr;            %Rotor impedance
21 Xm      =wb*Lm;             %Magnetizing impedance
22 Xmstar  =1/(1/Xls+1/Xm+1/Xlr);

```

C.R. 2
matlab

3.5.2. No-load Startup

We assume for this simulation the motor is not connected to any load but its own inertia. Before the simulation start, we should be aware, the rotor speed should be around %99-%98 of the synchronous speed. The results can be seen in **Fig. 3.12**.

Let's look at the figures from top to bottom. As can be seen the three-phase currents experiences a massive surge of current during its initial startup. This effect can be attributed to the inrush current experienced by any IM, where the inductive elements require a significant amount of current flow to generate the internal magnetic field to operate. Obviously, this can cause problem if **NOT**

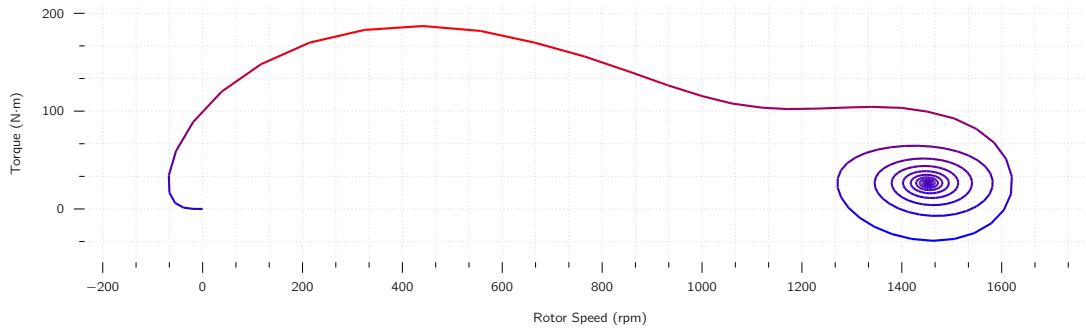


Figure 3.10.: The parametric plot of rotor speed v. torque when the motor starts from standstill without an external load.

taken care of as a massive surge of current during startup can cause the stator winding to melt and cause short circuit. There are methods to control this behaviour which was discussed in **B.Sc Drive Technology** course.

Next plot explains the torque development. As massive current surge happens, the motor experiences a significant torque production for a very brief time and as the rotor builds up speed the motor reaches a stable torque production.

The **dq0** transform allows us to remove the AC component of the signal and allows us to treat them as DC signal which we can easily observe.

The final plot to discuss is the i_d , i_q current which shows the effect of the induced current frequency. Observe in the beginning, the current has a relatively similar frequency value to that of the stator, but as the speed develops, the frequency dies down which is also observed.

The final aspect worth looking at is the **stability**. Of course if the motor does not produce stable torque at a given speed it's industrial relevance would be questionable. To that end let's observe it's speed v. torque given in **Fig. 3.10**. As can be seen there is only one (1) attractor and the system **converges** to that point without any oscillation or any orbit around a central point. This shows the stable behaviour of the motor.

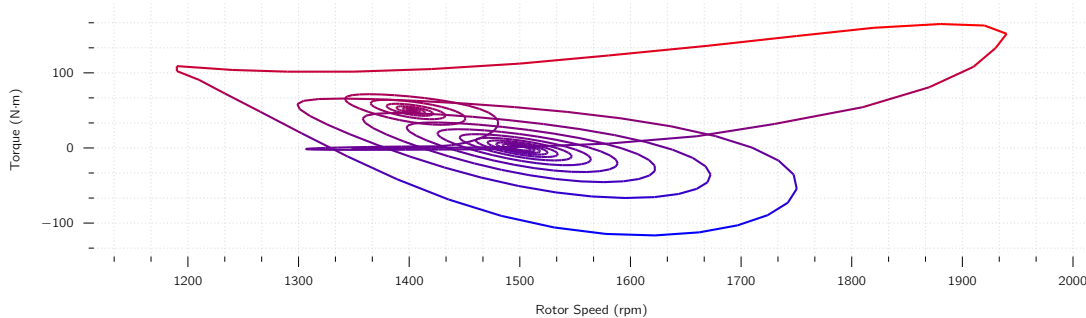


Figure 3.11.: The parametric plot of rotor speed v. torque when an instantenous load is applied to the motor at 0.4 s.

3.5.3. Application of a Step Torque Load

It is of course normal for something to be **NOT** constant as the load experienced by the motor can change. This could be for situation such as the elevator, or any kind of transportation task where the load can change. This entails the study of these machines under different loads.

The previous simulation assumed a standard load connected to the shaft and the motor starts from standstill. Now, we will introduce a load of 50 N m to the shaft of the motor at the time s. Think of adding a shovel of cement to the cement mixer or dropping of items from a conveyor belt.

The simulation parameters are kept constant for both with only difference being the simulation time has been increased to 1 s to observe the transient effect. The simulation result are shown in X. As can be seen the 3-phase current experience a surge of current flow due to the increase of load the motor is required to handle and the stability is reached within 100 ms.

Looking at the **dq** current values of the it can be seen the sudden shift of the load increased the flow of i_{qs} while the i_{ds} current has just experiences an oscillation without a change in its amplitude. From here it can be seen the **torque-producing** part of the current is i_{qs}^{31} .

Final plot to look is the parametric plot in **Fig. 3.11**. As can be seen there are two (2) points of attraction. The first one on right is the initial stability point when the motor has no load whereas the second one on the left is the second point of stability. This plot tells us these **points of attraction** makes the machine operation stable and allow the safe operation under sudden load change.

³¹We will look into optimising this to control the machine performance, also known as **Vector Control**

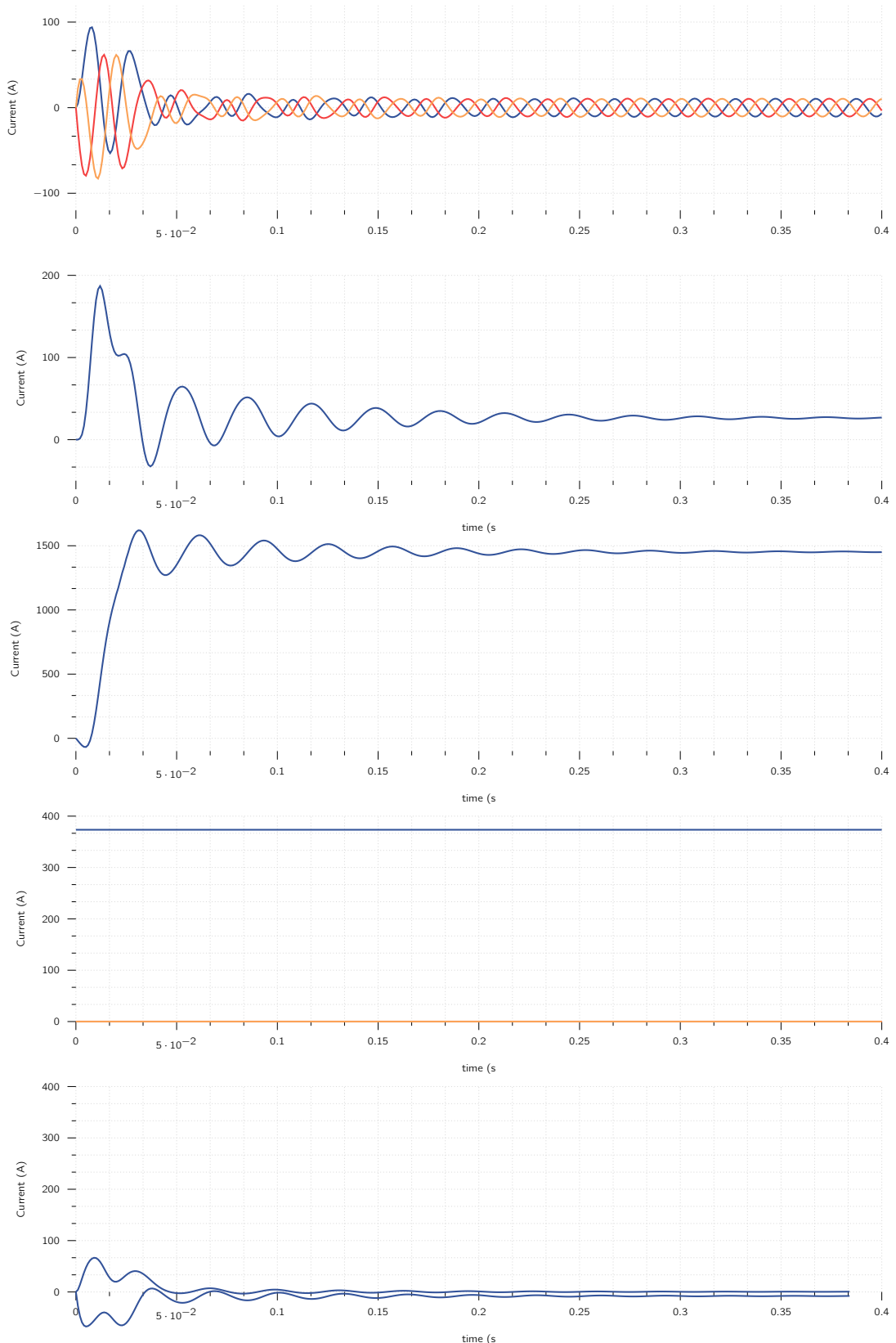


Figure 3.12.: Simulation results for starting IM from standstill.

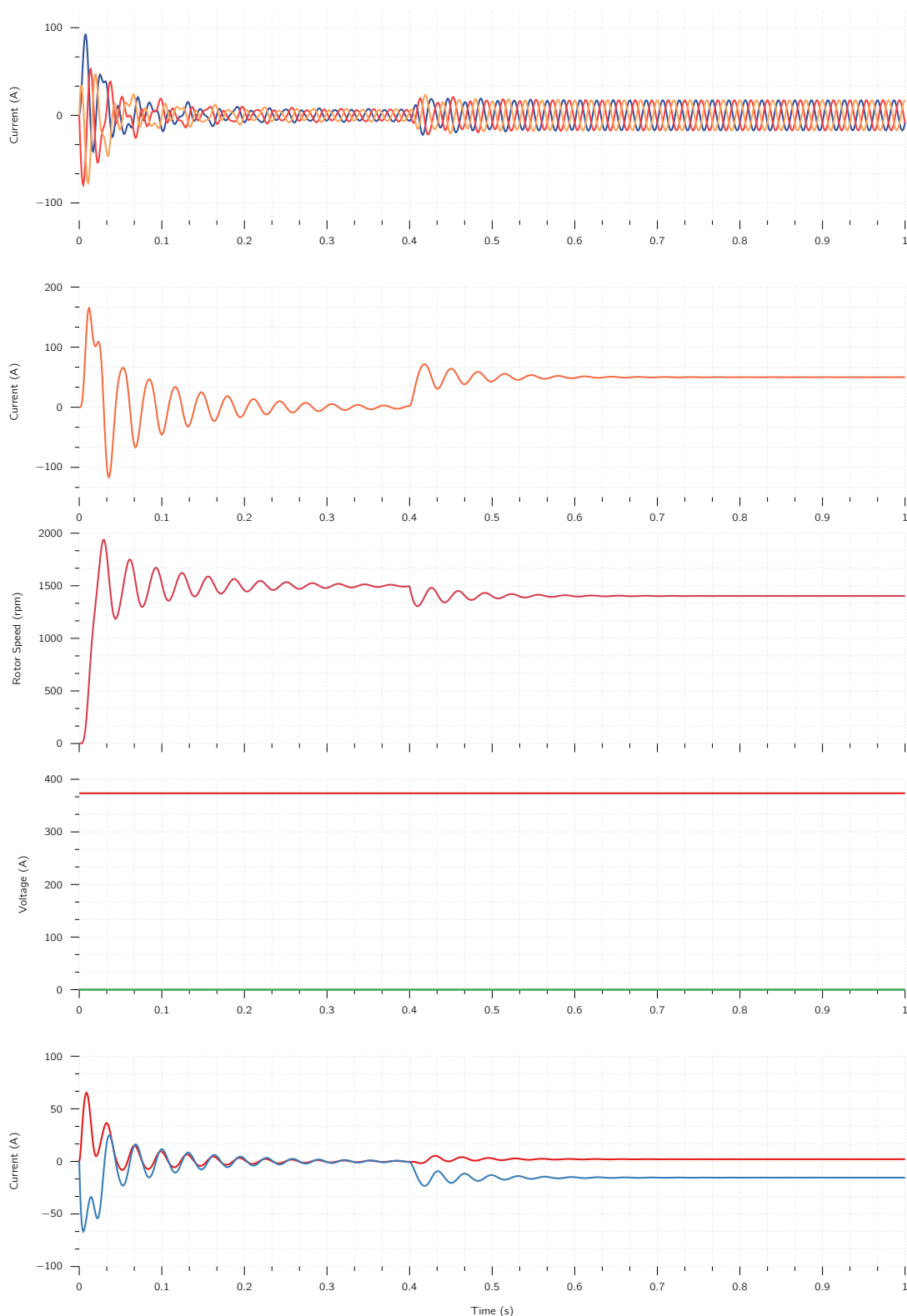


Figure 3.13.: Simulation of the IM when an instantaneous load is applied to the motor at 0.4 s.

Chapter 4

Vector Controlled Induction Machines

Table of Contents

4.1. Introduction	85
4.2. Principles of Vector Control	87
4.3. Direct Vector Control	90

4.1. Introduction

The various control strategies for the control of the inverter-fed IM provide good steady-state performance but poor dynamic response [42].

The cause of such poor dynamic response is found to be that the air-gap flux linkages deviate from their set values with deviation **NOT** only in magnitude but in phase as well.

These variations in the flux linkages (λ) have to be controlled by the **magnitude** and **frequency** of the stator and rotor phase currents and their instantaneous phases. Up to now, the control strategies have utilised the stator-to-phase current magnitude and frequency but **NOT** their phases¹.

This approach resulted in the deviation of the phase and magnitudes of the air-gap flux linkages from their set values.

¹These control methods are known as scalar control methods.

These oscillations in the air-gap flux linkages result in oscillations in electromagnetic torque (T_e) and, if left unneeded, reflect as speed oscillations (ω_r) [43]. These oscillations are undesirable in many high-performance applications:

such as in robotic actuators, centrifuges, metal-rolling mills, ...

where high precision, fast positioning or speed control are required. In addition, air-gap flux variations result in **high stator currents**, requiring large peak converter and inverter ratings to meet the dynamics.

An enhancement of peak inverter rating increases cost and reduces the competitive edge of a drives in the marketplace, in spite of excellent advantages over DC drives.

To play the devils advocate, separately-excited DC drives are simpler in control because they **independently** control flux, which, when maintained constant, contributes to an independent control of torque. This is made possible with separate control of field and armature currents which, in turn, control the field flux and the torque independently. Moreover, the DC motor control requires **only** the control of the field or armature current magnitudes, providing a simplicity **NOT** possible with AC machine control.

By contrast, AC drives require a coordinated control of stator current magnitudes, frequencies, and their phases, making it a relatively complex control method compared to its DC counterpart. As with the DC drives, independent control of the flux and torque is possible in AC drives. The stator current phasor can be resolved along the rotor flux linkages, and the component along the rotor flux lines is the field-producing current, but this requires the knowledge of rotor flux linkage position at all times.

This process is **dynamic** unlike that of a DC motor.

If position information is known, the control of AC machines is very similar to that of separately-excited motors.

The requirement of phase, frequency, and magnitude control of the currents and hence of the flux phasor is made possible by **inverter control**. The control is achieved in field coordinates² sometimes it is known as **vector control**, as it relates to the phasor control of the rotor flux linkages.

²hence the name of this control strategy, **field-oriented control**

Vector control made the AC drives equivalent to DC drives in the independent control of flux and torque and superior to them in their dynamic performance. These developments positioned the AC drives for high-performance applications, which was reserved for separately-excited dc motor drives.

This section of the Lecture Book discusses the basic principles, classifications, modelling, analysis, and design of vector-control schemes. The parameter sensitivity of vector-control schemes is

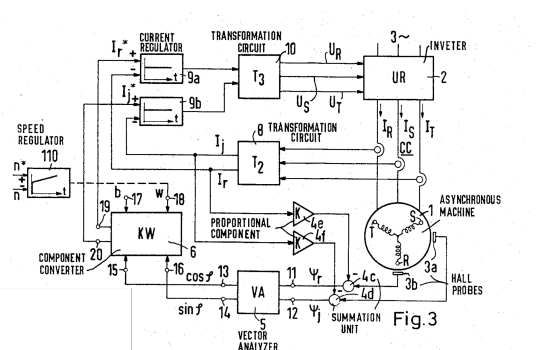


Figure 4.1.: Block diagram from Blaschke's 1971 US patent application [44].

analysed, and methods for its compensating are described. The design of the speed controller for a vector controller is systematically derived by using symmetric optimum technique.

4.2. Principles of Vector Control

To understand vector control, we have to make an assumption:

the position of the rotor flux linkages phasor (λ_r) is known.

λ_r is at position θ_f from a **stationary reference** and θ_f is referred to as **field angle** from now on.

The three (3) current can be transformed into its **qd0** form in synchronous reference form as³:

$$\begin{bmatrix} i_{qs}^e \\ i_{ds}^e \end{bmatrix} = \frac{2}{3} \begin{bmatrix} \sin \theta_r & \sin \left(\theta_r - \frac{2\pi}{3} \right) & \sin \left(\theta_r + \frac{2\pi}{3} \right) \\ \cos \theta_r & \cos \left(\theta_r - \frac{2\pi}{3} \right) & \cos \left(\theta_r + \frac{2\pi}{3} \right) \end{bmatrix} \begin{bmatrix} i_{as} \\ i_{bs} \\ i_{cs} \end{bmatrix}$$

³We can easily disregard the zero-sequence as we assume the system is balanced.

from which the stator current phasor (i_s) is derived as:

$$i_s = \sqrt{(i_{qs}^e)^2 + (i_{ds}^e)^2} \quad (4.1)$$

and the stator phasor angle (θ_s) is:

$$\theta_s = \tan^{-1} \left(\frac{i_{qs}^e}{i_{ds}^e} \right) \quad (4.2)$$

where i_{qs}^e , i_{ds}^e are the **q**, **d** axes currents in the **synchronous reference frames** that are obtained by projecting the stator current phasor on the **q** and **d** axes, respectively.

The current phasor magnitude remains the same regardless of the reference frame which can be seen in Fig. 4.2.

The current phasor i_s produces the rotor flux (λ_r) and the electromagnetic torque (T_e). The component of the current producing the rotor flux phasor has to be in phase with λ_r . Therefore, resolving the stator current phasor along λ_r reveals⁴:

⁴which can also be observed in Fig. 4.2.

- The component i_f is the field-producing component,
- The perpendicular component i_r is hence the torque-producing component.

By writing rotor flux linkages and torque in terms of these components as

$$\lambda_r \propto i_f \quad \text{and} \quad T_e \propto \lambda_f i_T \propto i_f i_T$$

it can be seen that i_f and i_T have **only** DC components in steady-state, because the relative speed with respect to that of the rotor field is zero (**0**) the rotor flux-linkages phasor has a speed equal to the sum of the rotor and slip speeds, which is equal to the synchronous speed. Orientation of λ_r , amounts to considering the synchronous reference frames, and hence the flux- and torque-producing components of current are DC quantities. Because they are DC quantities, they are ideal for use as control variables:

The bandwidth of the computational control circuits will have no effect on the processing of these DC control signals.

Crucial to the implementation of vector control, then, is the determination of the instantaneous rotor flux phasor position, θ_f . This field angle can be written as:

$$\theta_f = \theta_r + \theta_{sl}$$

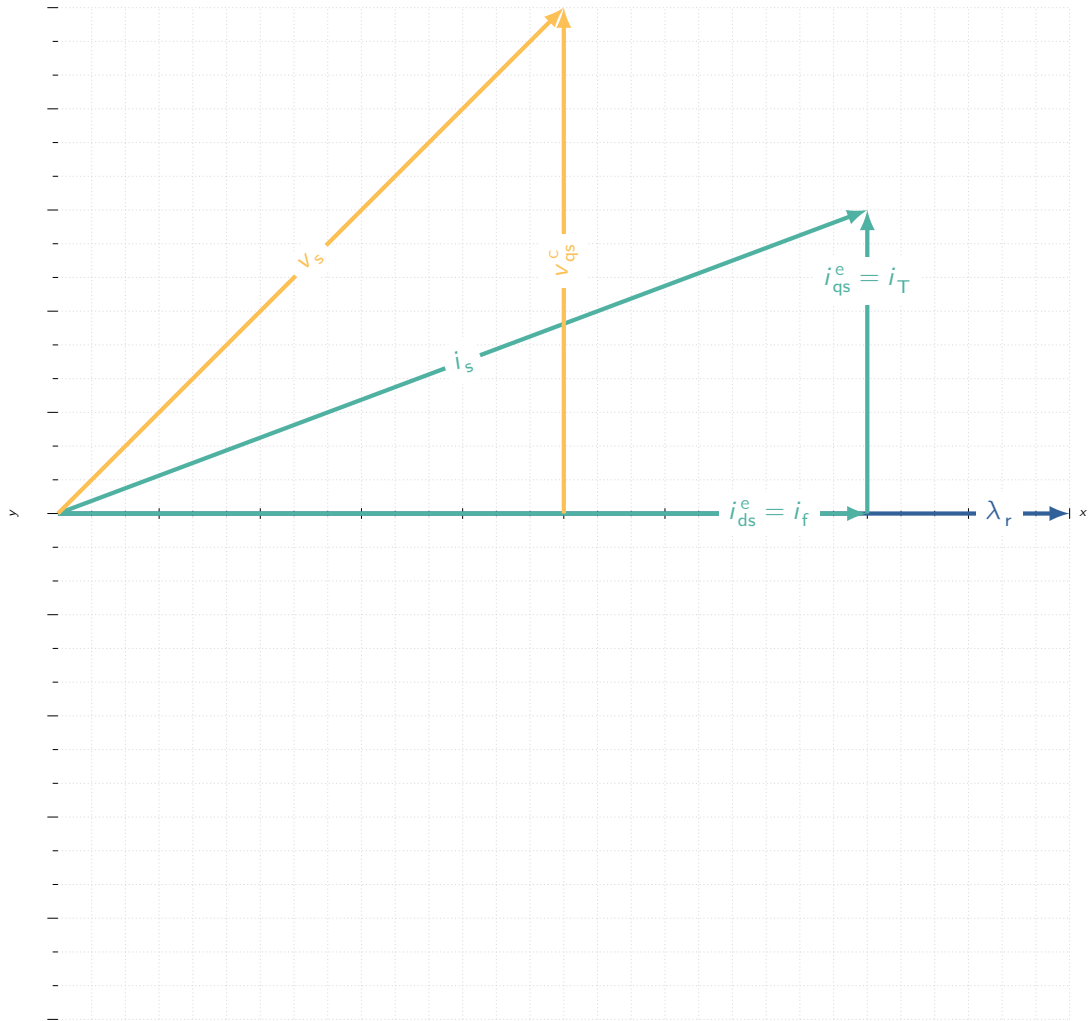


Figure 4.2.: Phasor diagram of the vector controller. Observe that regardless of the reference frame, the magnitude stays the same.

where θ_r is the rotor position, and $\theta[s]$ is the slip angle. In terms of the speeds and time, the field angle is written as:

$$\theta_f = \int (\omega_r + \omega_{sl}) dt = \int \omega_s dt$$

Vector-control schemes are classified according to **how the field angle is acquired**⁵.

⁵Both vector-control schemes are explained in the following sections

- If the field angle is calculated by using terminal voltages, currents, Hall sensors or flux-sensing windings, it is known as **direct vector control**.
- If the field angle is calculated by using rotor position measurement and partial estimation with only machine parameters and **NOT** any other variables i.e., voltages or currents⁶, then it is known as **indirect vector control**.

⁶

To summarise the methods, vector control works as follows:

- i. Obtain the field angle.
- ii. Calculate the flux-producing component of current (i_f^*), for a required rotor flux linkage (λ_r^*). By controlling only this field current, the rotor flux linkages are controlled.

It is very similar to the separately-excited DC machine, in that the field current controls the field flux. The armature current has **NO** impact on it.

- iii. From (λ_r^*) and the required T_e^* , calculate the torque-producing component of stator current (i_T^*). Controlling the torque-producing component current when the **rotor flux linkages phasor is constant** gives an independent control of electromagnetic torque.

It is very similar to the case of the armature current's controlling the electromagnetic torque in a separately-excited dc machine with the field current maintained constant.

Steps (ii) and (iii) gives a complete decoupling of flux from torque producing channels in the IM.

- iv. Calculate the stator-current phasor magnitude, (i_s^*), from the vector sum of i_T^* and i_f^* .
- v. Calculate torque angle from the flux- and torque-producing components of the stator-current commands,

$$\theta_T = \tan^{-1} \frac{i_T^*}{i_f^*}$$

- vi. Add θ_T and θ_f to obtain the stator current phasor angle, θ_e .
- vii. By using the stator-current phasor angle and its magnitude, θ_s and i_s^* , the required stator-current commands are found by going through the **dq0** transformation to **abc** variables:

$$i_{as}^* = i_s^* \sin \theta_s \quad i_{bs}^* = i_s^* \sin \left(\theta_s - \frac{2\pi}{3} \right) \quad i_{cs}^* = i_s^* \sin \left(\theta_s + \frac{2\pi}{3} \right)$$

viii. Synthesise these currents by using an inverter; when they are supplied to the stator of the IM, the commanded rotor flux linkages and torque are produced.

The analogy between the separately-excited DC motor and the IM is complete:

i_f and i_T correspond to the field and armature currents of the DC machine, respectively.

Even though the IM does not have separate field and armature windings, finding equivalent field and armature currents as components of the stator-current phasor has resulted in the **decoupling** of flux from torque-producing channels in a machine that is highly coupled.

Unlike the scalar control involved in DC machines, phasor or vector control is employed in IM. In the DC machine, the field and armature are **fixed** in space by the commutator, whereas, in the IM, no such additional component exists to separate the field (to produce the flux) from the armature (to produce the torque) channels to the optimum space angle of 90 electrical degrees between them.

⁷and for that matter any AC machine.

In the place of the commutator, the IM⁷ acquires the functionality of the commutator with the use of an inverter. The inverter controls both the magnitude of the current and its phase, allowing the machine's flux and torque channels to be decoupled by controlling precisely and injecting the flux- and torque-producing currents in the IM to match the required rotor flux linkages and electromagnetic torque. The phasor control of current further adds to the complexity of computation involving phase and magnitude and of transformations to orient i_f and i_T with respect to rotor flux linkages.

The orientation need not be on rotor flux linkages as the computations can be carried out in stator or rotor or arbitrary reference frames. However, generally synchronous reference frames are used.

4.3. Direct Vector Control

4.3.1. Description

A block diagram of the direct vector-control scheme with a current-source inverter is shown in Figure 8.2. The electrical rotor speed, ω_r , is compared to the reference speed, ω_r^* , and the error is amplified and limited to generate the reference torque (T_e^*). The rotor flux linkages reference (λ_r^*) is derived from the rotor speed via an absolute-value function generator.

λ_i^* is kept at 1 p.u. for from 0- to 1 p.u. rotor speed. Beyond 1 p.u. speed, it is varied as a function of the rotor speed. This is to ensure that the rotor speed is extended beyond the base speed with the available DC voltage to the inverter, by weakening the rotor flux linkages, therefore reducing the induced EMF to lower than that of the available output voltage from the inverter. By reducing the rotor flux linkages for the same torque-producing component of the stator current, the electromagnetic torque is reduced, which, in combination with the increasing rotor speed, can be controlled to produce the constant power output, say a rated value of the machine in steady

state. The torque and rotor flux-linkages are compared to the torque, T_e , and the rotor flux-linkages, λ_r , respectively. Their errors are amplified and limited to generate the reference torque- and flux-producing components of stator current, i_T^* and i_s^* , respectively. Phasor addition of i_t^* and i_T^* yields the stator-current phasor reference i_t^* , and the angle between i_T^* and i_t^* gives the torque-angle reference, $\theta_t[*]$. The sum of torque angle and field angle gives the position of the stator-current phasor, θ_c . Together with i_t^* , this generates the stator-phase current references, i_{as}^* , i_b^* , and i_s^* . These stator-phase-current requests are simplified by using an inverter and current feedback loops. The phase-current control loops can use one of the following switching techniques:

- PWM
- Hysteresis
- Space-Vector Modulation

By using one of these aforementioned control techniques, the inverter output currents are made to correspond to the reference inputs. The feedback variables θ_f , T_e , and λ_r are obtained from the flux and torque processor block. This is the key to the direct vector-control scheme.

Let's look at how we can calculate these variables.

4.3.2. Calculating the Torque and Flux

The inputs to this block are two (2) stator phase currents and one (1) set of the following: either:

- i. terminal voltages, or
- ii. induced EMF from the flux-sensing coils or Hall sensors.

The selection of (i) or (ii) will determine the computational approach.

Case I: Terminal Voltages

By using terminal voltages, the air-gap torque, flux, and field angle can be calculated with either rotor or stator flux linkages⁸.

Rotor-flux-based Calculator Two line-to-line voltages can be measured, from which the phase (line to neutral) voltages can be calculated⁹. The q and d stator voltages in the stator reference frames are obtained from the phase voltages as

$$v_{qs} = v_{as} \quad \text{and} \quad v_{ds} = \frac{1}{\sqrt{3}} (v_{cs} - v_{bs}) \quad (4.3)$$

⁸The choice has significant impact on the performance of the drive system in terms of its parameter sensitivity.

⁹provided that the voltages are balanced.

Similarly, the currents are obtained in the same way as these equations hold true for them, too. From the stator-reference-frame equations of the IM, the stator equations are:

$$\begin{aligned} v_{qs} &= (R_s + L_s p_t) i_{qs} + L_m p_t i_{qr} \\ v_{ds} &= (R_s + L_s p_t) i_{ds} + L_m p_t i_{dr} \end{aligned} \quad (4.4)$$

from which the rotor currents, (i_{qr} , i_{dr}), are calculated to be:

$$\begin{aligned} i_{qr} &= \frac{1}{L_m} \left\{ \int (v_{qs} - R_s i_{qs}) dt - L_s i_{qs} \right\} \\ i_{dr} &= \frac{1}{L_m} \left\{ \int (v_{ds} - R_s i_{ds}) dt - L_s i_{ds} \right\} \end{aligned} \quad (4.5)$$

From all the stator and rotor currents, torque, the flux and field angle can be computed as follows:

$$\begin{aligned} T_e &= \frac{3}{2} \frac{P}{2} L_m (i_{qs} i_{dr} - i_{ds} i_{qr}) \\ \lambda_{qr} &= L_r i_{dr} + L_m i_{ds} \\ \lambda_{dr} &= L_r i_{qr} + L_m i_{qs} \\ \lambda_r &= \sqrt{(\lambda_{qr})^2 + (\lambda_{dr})^2} \\ \theta_f &= \tan^{-1} \left(\frac{\lambda_{qr}}{\lambda_{dr}} \right) \end{aligned} \quad (4.6)$$

Eq. (4.3) to Eq. (4.6) can be implemented using any kind of electronic circuits or a microprocessor.

Note the methods dependence on the motor parameters R_s , L_s , L_r , L_m

In practice, the changes in stator resistance could be tracked **indirectly** with inexpensive temperature sensors. As for the inductances, they would have no significant variations in this scheme since flux control is implemented. Hence, parameter sensitivity would **NOT** greatly plague the accuracy of the measurement and calculation of flux, torque, and field angle.

Stator-Flux-Based Calculator Computational steps and dependence on many motor parameters could be very much reduced by using the stator flux linkages and calculating the electromagnetic torque, using only the stator flux linkages and stator currents. Then only stator resistance is employed in the calculation of the stator flux linkages, thereby removing the dependence of mutual and rotor inductances of the machine on its calculation. The steps involved are summarized briefly as follows.

$$\begin{aligned} \lambda_{ds} &= - \int (v_{ds} - R_s i_{ds}) dt \\ \lambda_{qs} &= - \int (v_{qs} - R_s i_{qs}) dt \\ \lambda_s &= \sqrt{(\lambda_{qs})^2 + (\lambda_{ds})^2} \angle \theta_{fs} \\ \theta_{fs} &= \tan^{-1} \left(\frac{\lambda_{qs}}{\lambda_{ds}} \right) \\ T_e &= \frac{3}{2} \frac{P}{2} (i_{qs} \lambda_{ds} - i_{ds} \lambda_{qs}) \end{aligned} \quad (4.7)$$

In this case, the flux loop can be closed with the stator flux linkages instead of the rotor flux linkages. The accuracy of the computation might not be high, even though this algorithm depends only on the stator resistance rather than on many other motor parameters, as is proved by an example in the following. The sensitivity of the stator resistance variation and its impact on the accuracy of the stator flux linkages, and hence on the electromagnetic torque is high when the stator voltages are small and of comparable magnitude to the resistive voltage drops. This is the case at low speeds; hence, dynamic operation at such speeds is very poor under this scheme.

4.3.3. Case II: Induced EMF from Flux-Sensing Coils of Hall Sensors

Two sets of sensing coils can be placed in stator slots having 90° electrical displacement, and one set can be placed on the MMF axis of one phase, say phase *a*. These coils can be concentric, making the layout easier. The sensing coils are isolated from the power circuit, to help in tying the outputs of those coils to the logic level-control circuits directly. Two Hall sensors can also be placed very similarly to the sensing coils; Hall sensors reflect the rate of change of the stator flux linkages. Let the induced EMFs of the *q* and *d* axes be e_{qs} , and e_{ds} , respectively. The stator *q* and *d* axes flux linkages, λ_{qs} , and λ_{ds} , respectively, are defined as

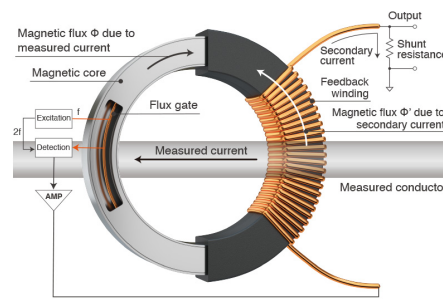


Figure 4.3.: An example of a flux sensing coil [45].

$$\begin{aligned}\lambda_{qs} &= L_s i_{qs} + L_m i_{qr} \\ \lambda_{ds} &= L_s i_{ds} + L_m i_{dr}\end{aligned}\tag{4.8}$$

In terms of induced EMFs, they are

$$\begin{aligned}\lambda_{qs} &= \int e_{qs} dt \\ \lambda_{ds} &= \int e_{ds} dt\end{aligned}\tag{4.9}$$

from which the rotor *q* and *d* axes currents are derived as,

$$i_{qr} = \frac{\lambda_{qs}}{L_m} - \frac{L_s}{L_m} i_{qs} = \frac{1}{L_m} \left\{ \int e_{qs} dt - L_s i_{qs} \right\} \tag{4.10}$$

$$i_{dr} = \frac{\lambda_{ds}}{L_m} - \frac{L_s}{L_m} i_{ds} = \frac{1}{L_m} \left\{ \int e_{ds} dt - L_s i_{ds} \right\} \tag{4.11}$$

From the rotor q and d axes currents and stator flux linkages, the rotor flux linkages and torque are obtained as

$$\begin{aligned}\lambda_{qr} &= L_r i_{qr} + L_m i_{qs} \\ \lambda_{dr} &= L_r i_{dr} + L_m i_{ds} \\ \lambda_r &= \sqrt{\left(\lambda_{qr}\right)^2 + \left(\lambda_{dr}\right)^2} \angle \theta_f \\ \theta_f &= \tan^{-1} \left(\frac{\lambda_{qr}}{\lambda_{dr}} \right) \\ T_e &= \frac{3P}{2} \left(i_{ds} \lambda_{qs} - i_{qs} \lambda_{ds} \right)\end{aligned}\tag{4.12}$$

The torque equation does not involve machine parameters for its calculation.

The rotor flux linkages and the field angle are **dependent** on machine parameters:

$$L_m, L_s \text{ and } L_r$$

¹⁰i.e., due to saturation. When there is a change¹⁰ in these parameters, they will introduce an error in the computation of λ_r and θ_f . In particular, the error in the computation of field angle will generate **significant errors** in the vector control; that is the most crucial information for control.

The flux and torque processor realised with terminal or sensing coils or Hall sensors have some advantages and disadvantages. These are discussed in the following.

The merits of these forms of measuring and computing the rotor flux linkages, its position, and the electromagnetic torque are as follows.

- i. The sensing schemes use only electronic transducers and do **NOT** use any with moving or rotating parts, such as synchors or optical encoders. The absence of moving parts in the transducers makes the reliability of these schemes more robust than from employing mechanical/optical transducers.
- ii. Further, the costly process of mechanical mounting and the loss of valuable space and volume inside or outside the machine enclosure for the rotating sensor parts are avoided. The compactness afforded increases the overall power density of the motor drive system. A saving in labor and parts makes these sensing schemes very attractive at the low-cost, low-power end of industrial applications.

Some disadvantages are as follows:

- i. At zero (0) stator frequency, there is no induced EMF in all the measurement schemes. The result is that neither flux linkages nor their positions are available for vector control. Therefore, torque production at zero speed is **NOT** precisely controllable, thus making it unsuitable for positioning applications such as servo.

- ii. The same problem in a different form appears at low speeds. At these speeds, the induced-EMF signals can be so small that signal-processing circuits cannot use them; they are comparable to quantisation errors in digital circuits and will be affected by drift in the analog circuits. This, combined with factor (i) makes the direct vector-control drive unsuitable for precise positioning and low-speed operation.
- iii. The installation of sensing windings or of Hall-effect sensors, even though it is an inexpensive production process, adds to the number of wires coming out of the machine frame. This is not acceptable in high-volume applications, such as HVAC, because of the cost involved in the hermetic sealing¹¹. Extra wires are also not desirable in high-reliability applications, such as defense actuators and nuclear-plant pump drives.
- iv. In the case of using voltage and current transducers, the filtering required to obtain the fundamental at high frequencies will produce a large phase shift and inaccuracy in the computation of field angle, which will deteriorate the decoupling of flux and torque controls. It is relevant to observe here that voltage sensing with galvanic isolation can be easily and cost-effectively realised from the logic-level switching signals of the inverter, the phase currents and an indication of the DC link voltage magnitude.

¹¹any type of sealing that makes a given object airtight.

Part III.

Permanent Magnet Synchronous Machines

Chapter 5

Permanent Magnet Machine Dynamics and Control

Table of Contents

5.1. Introduction	99
5.2. Properties of Permanent Magnets	100
5.3. Permanent Magnet Synchronous Machines	106
5.4. Vector Control	111
5.5. Control Strategies	114
5.6. Flux Weakening Operation	116
5.7. Speed-Controller Design	120
5.8. Sensorless Control	122
5.9. Brushless DC Motor	123

5.1. Introduction

The availability of modern PM with considerable energy density led to the development of dc machines with PM field excitation in the 1950s [46]. Introduction of PM to replace electromagnets, which have windings and require an external electric energy source, resulted in compact DC machines.

The Synchronous Machine (SynM), with its conventional field excitation in the rotor, is replaced by the PM excitation; the slip rings and brush assembly are dispensed with. With the advent of switching power transistor and SCR devices in later part of 1950s, the replacement of the mechanical commutator with an electronic commutator in the form of PM systems happened with significant speed¹. Therefore, the armature of the machine can be on the stator, enabling better cooling and allowing higher voltages to be achieved as significant clearance space is available for insulation in

¹These two (2) major developments are given as the primary reasons to the development of PM systems as well as the development of the mechanical commutator being replaced by its electronic version.

the stator. The excitation field that used to be on the stator is transferred to the rotor with the PM poles. These machines are nothing but an **inside out** DC machine with the field and armature interchanged from the stator to rotor and rotor to stator, respectively.

This part of the book will focus the description of the PMSM solutions and brush-less DC machines, derivation of their respective dynamic models, principle of control, analysis of the drive system, various control strategies, design of speed controller, flux-weakening operation, and position-sensors-less operation.

5.2. Properties of Permanent Magnets

Before we go into the details of the machine it is important we look at the material property which makes it all possible: PM. Therefore, here, we will focus on their characteristics and their operation within a magnetic circuits. The air gap or load line to determine the operating point of the magnet is derived. The energy-density definition and magnet-volume calculation are given to clarify the rudiments of application considerations for the magnet in machine design.

The design process for the rotor magnet in AC machines is outside the scope of this lecture.

Types of Permanent Magnets

There are a couple of options when it comes to PMs for use with electrical machines. Depending on the environment, operation temperature or the load the choice of magnet can change, therefore it is important to know the general characteristics of PMs. A quick overview table is shown in **Table 5.1** and some important parameters comparison of their properties is seen in **Table 5.2**.

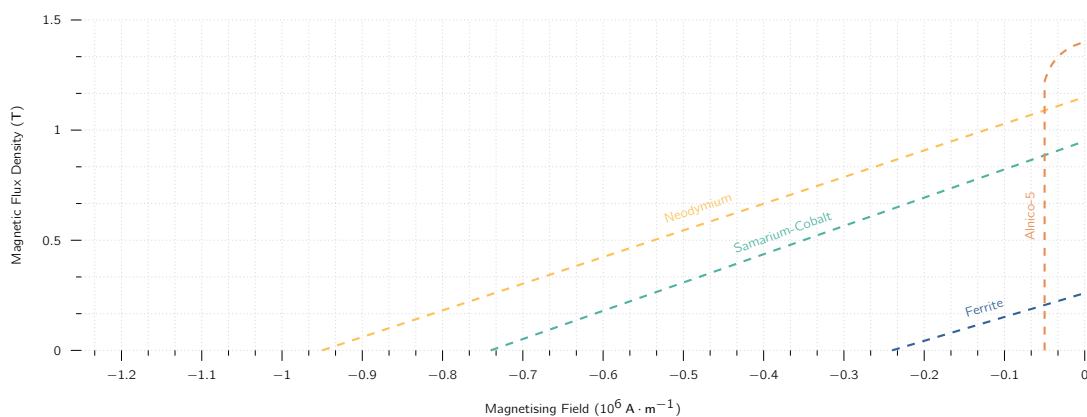


Figure 5.1.: The second quadrant $\vec{B} - \vec{H}$ curve characteristics of PM.

Magnet	Advantages	Disadvantages
Ferrite (Ceramic)	Low Cost	Low Energy Product
	High Coercive Force	Low Mechanical Strength - Brittle
	High Resistance to Corrosion	Resistance to (fairly) high Temperature
AlNiCo	High Corrosion Resistance	High Cost
	High Mechanical Strength	Low Coercive Force
	High Temperature Stability	Low Energy Product
Samarium Cobalt	High Corrosion Resistance	High Cost
	High Energy Product	Low Mechanical Strength - Brittle
		High Temperature Stability
NdFeB	Very High Energy Product	High Cost
	High Coercive Force	Low Mechanical Strength - Brittle
		Moderate Temperature Stability
		Low Corrosion Resistance (When no coating is applied)

Table 5.1.: A quick view on different types of PMs used/produced in industry.

Property	Unit	Sin. NdFeB	Sin. SmCo 2-17	Sin. SmCo 1-5	Sin. Ferrite	AlNiCo
Max. Energy	MGOe	28 - 52	16 - 32	14 - 24	2 - 5	1 - 13
Intrinsic Coercivity	kOe	11 35	8 35	15 30	2 5	1 2
Curie Temperature	°C	310 370	800 850	700 750	450 480	750 890
Maximum Working Temperature	°C	230	350	250	250	500

Table 5.2.: Useful properties of PMs [47] (Here Sin. stands for sintered)

Ceramic

Ceramic, also known as **Ferrite** (Fe) are magnets are made of a composite of iron oxide and barium or strontium carbonate known for their resistance against fairly high temperatures [49]. These materials are readily available and at a lower cost than other types of materials used in PMs making it desirable due to the **lower cost**. Ceramic magnets are made using pressing and sintering. These magnets require care during production as these magnets are brittle and require diamond wheels if these magnets need to be shaped or to remove some imperfections. As with many industrial products, these magnets are also made in different grades.

- Ceramic-1 is an isotropic grade with equal magnetic properties in all directions [50].
- Ceramic grades 5 and 8 are anisotropic grades where the



Figure 5.2.: A stack of ferrite magnets, with stuck metal pieces [48].

magnetisation aligns with the direction of pressing [51].

The anisotropic method delivers the highest energy product among ceramic magnets at values up to 3.5 MGOe (Mega Gauss Oersted). Ceramic magnets have a good balance of magnetic strength, resistance to demagnetising and economy²

²They are the most widely used magnets today.

AlNiCo

Developed in 1931 [53], AlNiCo magnets are made up of a composite of aluminium, nickel and cobalt with small³ amounts of other elements added to enhance the properties of the magnet.

AlNiCo magnets have good temperature stability⁴, good resistance to demagnetisation due to shock but they are easily demagnetised by external fields. AlNiCo magnets are produced by two (2) typical methods:

Casting The molten material is poured into a shell mould or larger green sand moulds. As the molten metal cools, the shell moulds start to burn and by the time the magnets are cold, the shell is almost disintegrated. A shell mould is made using a pattern plate and a moulding machine.

Sintering A process in which particles under pressure chemically bond to themselves in order to form a coherent shape when exposed to a high temperature.

Sintering offers superior mechanical characteristics, whereas casting delivers higher energy products⁵

⁵up to 5.5 MGOe. and allows for the design of intricate shapes.

The two (2) very common grades of AlNiCo magnets are 5 and 8. These are anisotropic grades and provide for a preferred direction of magnetic orientation. AlNiCo magnets have been replaced in many applications by ceramic and rare earth magnets.



Figure 5.3.: A collection of AlNiCo magnets [52].

Samarium Cobalt

Samarium Cobalt (SmCo) is a type of rare earth magnet material that is highly resistant to oxidation, has a higher magnetic strength and temperature resistance than either AlNiCo or Ceramic material [47].

Introduced to the market in the 1970's, samarium cobalt magnets continue to be used today. Samarium cobalt magnets are divided into two (2) main groups⁶ [56]:

⁶Among metallurgist one might encounter them as 1-5 and 2-17.



Figure 5.4.: A collection of SmCo magnets [55].

■ Sm₁Co₅

■ Sm₂Co₁₇

The energy product range for the 1-5 series is 14 to 24 MGOe, with the 2-17 series somewhere between 16 and 32 MGOe (see **Table 5.2**). These magnets offer the best temperature characteristics of all rare earth magnets and can withstand temperatures up to 300°C. Sintered samarium cobalt magnets are brittle and prone to chipping and cracking and may fracture when exposed to thermal shock.

Due to the high cost of the material samarium, samarium cobalt magnets are used for applications where high temperature and corrosion resistance is critical.

Neodymium Iron Boron

Neodymium Iron Boron (NdFeB) is another, but probably the most known type of, rare earth magnetic material. This material has similar properties as the Samarium Cobalt except that it is more easily oxidised and generally doesn't have the same temperature resistance⁷. NdFeB magnets also have the **highest energy products** approaching 50 MGOe. These materials are costly and are generally used in very selective applications due to the cost.

Cost is also driven by existing intellectual property rights of the developers of this type of magnet.

Their high energy products lend themselves to compact designs that result in innovative applications and lower manufacturing costs. A major disadvantage NdFeB magnets are **highly corrosive** [58, 59].

Surface treatments have been developed that allow them to be used in most applications. These treatments include gold, nickel, zinc and tin plating and epoxy resin coating to protect them from the elements.



⁷This is one of the reasons why machine operating temperatures are an important factor during the design process.

Figure 5.5.: A collection of NdFeB magnets [57].

Air Gap Line

To find the operating point on the demagnetisation characteristic of the magnet, consider the flux path in a machine⁸. flux crosses from a north pole of the rotor magnet to the stator across an air gap and then closes the flux path from the stator to the rotor south pole via an air gap. In the process, the flux crosses two (2) times the magnet length and two (2) times the air gap, which the

⁸Preferably one with magnets.

flux lines can be seen in **Fig.** 5.8. The MMF provided by magnets is equal to the MMF received by the air gap if the MMF requirement of stator and rotor iron is considered negligible. Then,

$$H_m l_m + H_g l_g = 0 \quad (5.1)$$

where H_m , H_g are magnetic field strengths in magnet and air, respectively, and, l_m , l_g are the length of the magnet and air gap, respectively. The operating flux density on the demagnetisation characteristic can be modelled, assuming it is a straight line, as

$$B_m = B_r + \mu_0 \mu_r H_m \quad (5.2)$$

Substituting for H_m from Eq. (5.1) into Eq. (5.2) in terms of H_g , and then writing it in terms of the air gap flux density, which is equal to the magnet flux density, gives the operating magnet flux density:

$$B_m = \frac{B_r}{\left(1 + \frac{\mu_r l_g}{l_m}\right)}$$

This clearly indicates the operating flux density is always less than the remnant flux density ($B_r > B_m$), because of the air gap excitation requirement.

The excitation requirements of iron and leakage flux are neglected in this conceptual derivation.

The operating point is shown in **Fig.** 5.6, and the line connecting the operating flux density B_m and origin is known as the air gap line or load line.

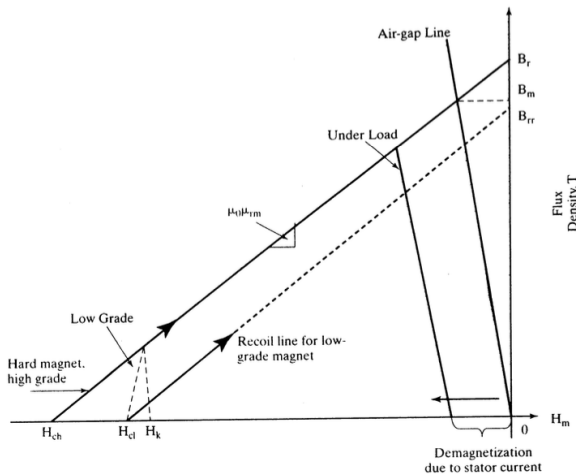


Figure 5.6.: The operating point of a magnet during operation.

The slope of this line is equal to a fictitious permeance coefficient μ_c times the permeance of the air. If the stator is electrically excited, producing demagnetisation, then the load line moves toward the left but remains parallel to the original load line, as shown in the figure. The operating flux density is further reduced from B_m . Note that the permeance coefficient is derived for a operating point defined by B_m and H_m as:

$$B_m = B_r + \mu_0 \mu_m H_m = -\mu_0 \mu_c H_m$$

from which the permeance coefficient is derived as

$$\mu_c = \frac{B_r}{-\mu_0 H_m} - \mu_{rm} = \frac{-\mu_0 \mu_{re} H_m}{-\mu_0 H_m} - \mu_{rm} = \mu_{re} - \mu_{rm}$$

where μ_{re} can be considered as external permeability. The variations in the remnant flux density are due to temperature changes as well as to the impact of the applied magnetic field intensity, both of which are induced by external operating conditions, as is clearly seen from this formulation of μ_c , and therefore it is appropriately labelled as external permeability. As the demagnetising field is introduced by external operating conditions, it is seen that the permeance coefficient will decrease as the external permeability also decreases for that operating point. In hard PMs, the external permeability is on the order of from 1 to 10 in the nominal operating region.

Energy Density

The energy density of the magnet is found as the product of its magnetic field strength and its operating flux density. This measure serves to differentiate magnets for use in machines from those having higher values preferred for high-power-density machines. The peak-energy operating point is optimal from the point of view of magnet utilisation. It is found by differentiating the energy density with respect to magnetic field strength and equating to zero to find the magnetic field strength at which it is the maximum. The maximum energy density for a hard high-grade PM shown in Figure 9.4 is

$$E_{max} = -\frac{B_r^2}{4\mu_0 \mu_{rm}} \quad (5.3)$$

and the flux density at which the maximum energy density available is at $0.5B_r$. The operating line for this flux density is shown as giving the required magnetic field strength.

this operating point for maximum energy density requires a considerable amount of demagnetising field strength from the stator excitation of the machine.

In addition, it will not be possible to maintain this operating point in a variable-speed machine drive; the stator currents will be varying widely over the entire torque-speed region which in turn will change the operating point of the magnets.

Magnet Volume

The magnet volume is found in terms of operating point and air gap volume, as follows:

$$B_g I_g = \mu_0 H_m I_m \quad \text{and} \quad B_m A_m = B_g A_g \quad (5.4)$$

From these ideal relationships, magnet volume is calculated to be:

$$V_m = A_m I_m = \left(\frac{B_g A_g}{B_m} \right) \left(\frac{B_g I_g}{\mu_0 |H_m|} \right) = \frac{B_g^2 (A_g / g)}{\mu_0 (B_m H_m)} = \frac{B_g^2 V_g}{\mu_0 |E[m]|} \quad (5.5)$$

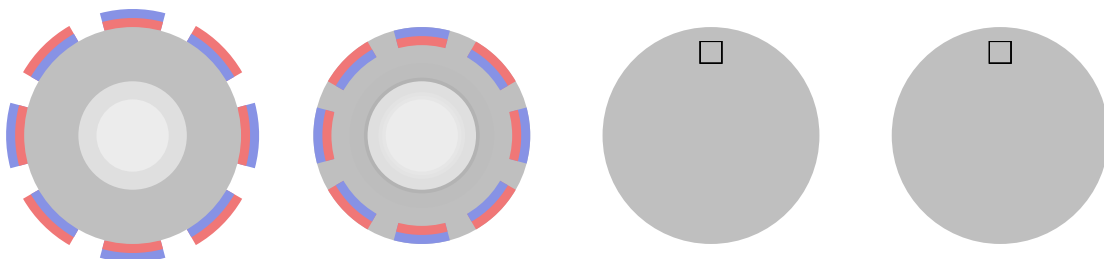


Figure 5.7.: Types of PMSMs.

where V_g is the volume of the air gap, E_m is the magnet operating energy density, and A_m , A_g are the magnet and air gap area. From this relationship, we can infer that, the maximum operating energy density point of the magnet will produce the magnet with the minimum volume and cost.

5.3. Permanent Magnet Synchronous Machines

5.3.1. Machine Configurations

The PMSM can be broadly classified on the basis of the direction of field flux, as follows:

Radial field the flux direction is along the radius of the machine.

Axial field the flux direction is parallel to the rotor shaft.

The radial-field PM machines are common: the axial-field machines are coming into prominence in a small number of applications because of their higher power density and acceleration.

Axial-flux machines are very desirable for high-performance applications.

There are different ways in which magnets can be placed in the rotor. The radial-field versions are shown in **Fig. 5.7.** The high-power-density SynM machines have surface PMs with radial orientation intended generally for low speed applications, whereas the interior-magnet version is intended for high-speed applications.

The operation principle does is the same regardless of how the magnets are mounted.

An important consequence of the method of mounting the rotor magnets is the difference in direct and quadrature axes inductance values. The rotor magnetic axis is called direct axis and the principal path of the flux is through the magnets. The permeability of high-flux-density PMs is almost that of the air. This results in the magnet thickness becoming an extension of air gap by that amount. The stator inductance when the direct axis or magnets are aligned with the stator winding is known as **direct axis inductance**. By rotating the magnets from the aligned position by 90 degrees, the stator flux sees the inter-polar⁹ area of the rotor, containing only the iron path, and the inductance

⁹The region between two consecutive poles

measured in this position is referred to as **quadrature axis inductance**.

The direct-axis reluctance is greater than the quadrature-axis reluctance.

$$L_q > L_d \quad (5.6)$$

where L_d is the inductance along the magnet axis (i.e., direct axis) and L_q is the inductance along an axis in quadrature to the magnet axis.

This is quite contrary to the wound-rotor salient-pole synchronous machine, where the quadrature-axis inductance is always greater than the direct-axis inductance¹⁰.

Lets look at **Fig. 5.7** and define all four (4) rotor types:

- a. shows the magnets mounted on the surface of the outer periphery of rotor limitations. This arrangement provides the highest air gap flux density, but it has the drawback of lower structural integrity and mechanical robustness. Machines with this arrangement of magnets are known as **surface mount** PMSMs.
- b. magnets placed in the grooves of the outer periphery of the rotor lamination, providing a uniform cylindrical surface of the rotor. In addition, this arrangement is much more robust mechanically as compared to surface-mount machines.

¹⁰in the wound-rotor salient-pole SynM machine, the direct axis, having the excitation coils, has a small air gap, whereas the quadrature axis has the large air gap.

The ratio between the quadrature- and direct-axis inductances can be as high as 2 to 2.5 in this configuration. This construction is known as **inset** PMSM.

- c.-d. show the placement of magnets in the middle of the rotor lamination in radial and circumferential orientations, respectively. This construction is mechanically robust and therefore suited for high-speed applications.

The manufacturing of this arrangement is more complex than for the surface-amount or inset-magnet rotors. Note that the ratio between the quadrature- and direct-axis inductances can be higher than that of the inset-magnet rotor but generally does not exceed three in value. This type of machine construction is generally referred to as **interior** PMSM.

The inset-magnet construction has the advantages of both the surface- and interior-magnet structures; easier construction and mechanical robustness, with a high-range between the quadrature- and direct-axis inductances, respectively. Many more arrangements of the magnets on the rotor are possible, but they are very rarely used in general industrial practice.

Flux-reversal machines with magnets and armature windings on the salient stator poles and salient rotors with no windings or magnets are another possible construction.

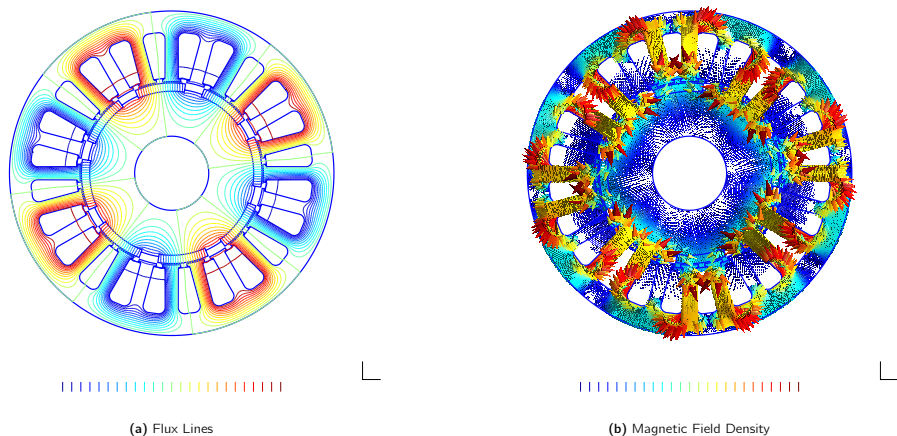


Figure 5.8.: Finite element simulation results of a PMSM with 8-poles (Simulation was done with qetDP).

5.3.2. Flux Density Distribution

The flux plot and flux density v. rotor position of a surface PM with radial orientation are shown in **Fig. 5.8** and **9.7**, respectively. The dips in the flux density at various points occur because of the slot opening of the stator lamination where the reluctance is much higher and, hence, the flux and its density are lower. The slotting effect also affects the induced EMFs in the machine armature, clearly raising design and practical concerns about possible ripple effects. The slotting effect exists regardless of whether the machine is designed with sinusoidal or trapezoidal flux-density distribution. For these distributions, predetermined sinusoidal or rectangular currents are injected to produce the torque. Invariably, that results in ripple air gap torque capable of causing undesirable effects at low speed.

5.3.3. Line-Start PMSM

Some PM synchronous machines are intended and designed for constant-speed applications, to improve efficiency and power factor in comparison to induction and wound-rotor synchronous motors. Such machines have a squirrel-cage winding to provide the torque from standstill to near-synchronous speed. The same cage windings also serve to damp rotor oscillations. Once the motor pulls into synchronism, the cage windings do not contribute to electrical torque, because there are no induced voltages and hence no currents in them at zero slip. Variable-speed PMSM drives have no need for the damper windings to offset hunting and oscillation. The damping is provided by properly controlling the input currents from the inverter. This results in a compact and a smaller rotor than that of the machine with damper windings. The way damping is produced in the PMSM with and without damper windings deserves a mention. The machine with the damper windings operates to suppress the oscillations with no external feedback. The feedback comes internally through the induced EMF due to the slip speed in the cage windings. In the inverter-controlled PMSM drives, the control has to be initiated by an external signal or feedback variable to counter the oscillation.

[ts dependence on an external feedback loop compromises reliability.

5.3.4. Types of PM Synchronous Machines

The PM synchronous motors are classified on the basis of the wave shape of their induced EMF:

Sinusoidal known as PMSM,

Trapezoidal known as BLDC.

Even though the trapezoidal type of induced EMFs have constant magnitude for 120 electrical degrees both in the positive and negative half-cycles, as shown in **Fig. 5.9**, the power output can be uniform by exciting the rotor phases with 120 degrees (electrical) wide currents. The currents cannot rise and fall in the motor windings in zero time¹¹. Therefore, in actual operation, there are power pulsations during the turn-on and turn-off of the currents for each half-cycle.

¹¹This is due to the fact of windings having inductance

The severity of such pulsations is absent in PMSMs.

BLDCs have 15% more power density than PMSMs [60]. This can be attributed to the fact that the ratio of the Root-Mean Square (RMS) value to peak value of the flux density in the BLDC machine is higher than PMSM.

The ratio of the power outputs of these two (2)machines is derived in the following, assuming they both have equal copper losses in their stator.

Let I_{ps} and I_p be the peak values of the stator currents in the PMSM and BLDC. The RMS values of these currents are:

$$I_{sy} = \frac{I_{ps}}{\sqrt{2}} \quad I_d = I_p \sqrt{\frac{2}{3}} \quad (5.7)$$

Equating the copper losses and substituting for the currents in terms of their peak currents gives

$$3I_{sy}^2 R_a = 3I_d^2 R_a, \quad (5.8)$$

$$3\left(\frac{I_{ps}}{\sqrt{2}}\right)^2 R_a = 3\left(\sqrt{\frac{2}{3}} I_p\right)^2 R_a, \quad (5.9)$$

from which the relationship between the peak currents of PMSM and BLDC is obtained as:

$$I_p = \frac{\sqrt{3}}{2} I_{ps} \quad (5.10)$$

The ratio of their power outputs is obtained from these relationships as follows:

$$\text{Power Output Ratio} = \frac{\text{PMDC Brushless Power}}{\text{PMSM Power}} = \frac{2 \times E_p \times I_p}{3 \times \frac{E_p}{\sqrt{2}} \times \frac{I_{ps}}{\sqrt{2}}} = 1.1547 \quad \blacksquare \quad (5.11)$$

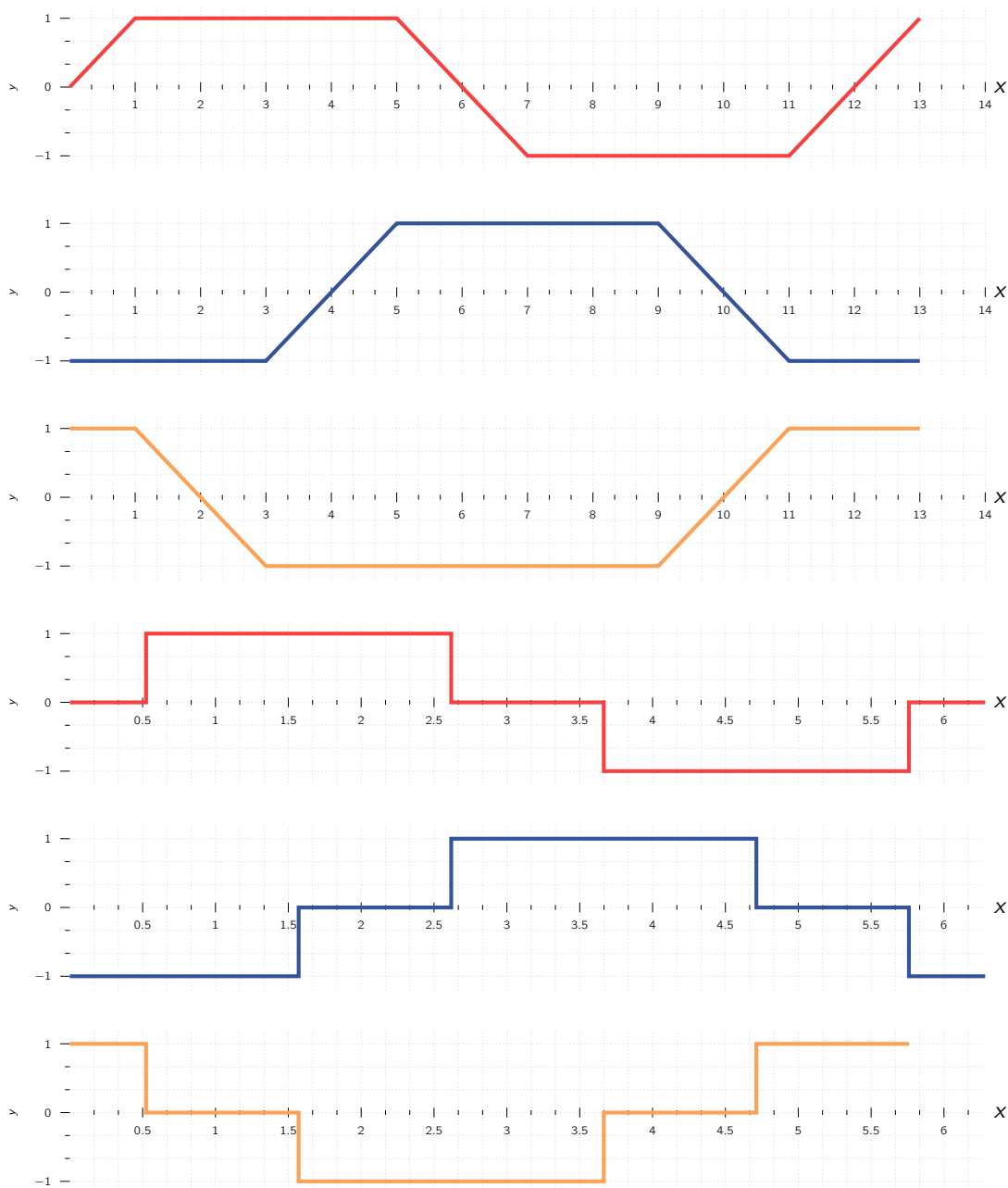


Figure 5.9.: The waveforms of a BLDC motor during operation.

Power output ratio has been derived under the assumption that the power factor of the PM synchronous motor is unity¹².

¹²Just as a small reminder, **unity** in this context means the motor is not producing or requiring any reactive power from the perspective of the grid.

As we can see from the waveform, the control is simple if the absolute position of the rotor is known. Knowing the rotor position amounts to certain knowledge of the rotor field and the induced EMF and, following this logic, instances of applying the appropriate stator currents for control.

5.4. Vector Control

For us to implement a usable vector control, we need to derive the dynamic model of the PMSM. Luckily for us, the derivation of the dynamic model relatively similar to that of an IM and therefore we can use it as a base¹³.

¹³For a quick refreshment please look at Chapter 3

5.4.1. Mathematical Model

The two-axes (**dq**) PMSM stator windings can be considered to have **equal turns per phase**. The rotor flux can be assumed to be concentrated along the **d** axis while there is zero flux along the **q** axis.

This is an assumption similarly made in the derivation of indirect vector-controlled IM drives.

In addition, for simplicity, it is assumed that the machine core losses are negligible¹⁴. Following our previous assumption, we will also assume the rotor flux (λ_r) to be **constant** at a given operating point.

While the variations in rotor temperature alter the magnet flux, its variation with time is considered to be negligible.

¹⁴This simplicity is a semi necessity as core losses of materials exhibit non-linear properties which add significant complexity to the modelling of the drive.

An advantage over IM is the lack of need to include the rotor voltage equations as there is no external source connected to the rotor magnets, and variation in the rotor flux with respect to time is negligible.

The stator equations of the IM in the rotor reference frames using flux linkages are taken to derive the model of the PMSM. The rotor frame of reference is chosen because the position of the rotor magnets determines, independently of the stator voltages and currents, the instantaneous induced emfs and subsequently the stator currents and torque of the machine.

This is not the case in the IM: there, the rotor fluxes are not independent variables, they are influenced by the stator voltages and currents, and that is why any frame of reference is suitable for the dynamic modelling of the induction machine.

When rotor reference frames are considered, it means the equivalent **qd** axis stator windings are transformed to the reference frames that are revolving at rotor speed. The consequence is that there is zero speed differential between the rotor and stator magnetic fields and the stator **qd** axis windings have a fixed phase relationship with the rotor magnet axis, which is the **d** axis in the modelling.

The stator flux-linkage equations are:

$$\begin{aligned} v_{qr}^r &= R_q i_{qs}^r + p_t \lambda_{qs}^r + \omega_r \lambda_{ds}^r \\ v_{ds}^r &= R_d i_{ds}^r + p_t \lambda_{ds}^r - \omega_r \lambda_{qs}^r \end{aligned}$$

where R_q , R_d are the quadrature and direct axis winding resistances which are equal and from here will be defined as R_s for simplicity, and the q and d axes stator flux linkages in the rotor reference frames are

$$\lambda_{qs}^r = L_s i_{qs}^r + L_m i_{qr}^r \quad (5.12)$$

$$\lambda_{ds}^r = L_s i_{ds}^r + L_m i_{dr}^r \quad (5.13)$$

The self-inductances of the stator **qd** axes windings are equal to L_m only when the rotor magnets have an arc of electrical 180°. That hardly ever is the case in practice.

This has the implication that the reluctance along the magnet axis and the inter-polar axis are different. When a stator winding¹⁵ is in alignment with the rotor magnet axis, the reluctance of the path is maximum. The magnet reluctance is almost the same as the air gap reluctance, and hence its inductance is the lowest at this time.

The inductance then is referred to as the direct-axis inductance L_d . At this time, the q axis winding faces the inter-polar path in the rotor, where the flux path encounters no magnet but only the air gaps and iron in the rotor, resulting in lower reluctance and higher inductance. The inductance of the q axis winding is L_q at this time. As the rotor magnets and the stator q and d axis windings are fixed in the rotor, the rotor is L_q at the rotor. The rotation is the rotor of the robot and the rotor is L_q and d axis, the cut-passed. In other vision, the torque is the rotor flux linkage in the q and d axes, the currents in the rotor and stator are required. The permanent-magnet excitation can be modeled as a constant current source, i.e., The rotor flux is along the d axis, so the d axis rotor current is i.e., the q axis current in the rotor is zero, because there's no flux along this axis in the rotor, by assumption. Then the flux linkages are written as

$$\lambda_{qs}^r = L_q i_{qs}^r \quad (5.14)$$

$$\lambda_{ds}^r = L_d i_{ds}^r + L_m i_{fr} \quad (5.15)$$

where L_m is the mutual inductance between the stator winding and rotor magnets. Substituting these flux linkages into the stator voltage equations gives the stator equations:

$$\begin{bmatrix} v_{qs}^r \\ v_{ds}^r \end{bmatrix} = \begin{bmatrix} R_q + L_q p_t & \omega_r L_d \\ -\omega_r L_q & R_d + L_d p_t \end{bmatrix} \begin{bmatrix} i_{qs}^r \\ i_{ds}^r \end{bmatrix} + \begin{bmatrix} \omega_r L_m i_{fr} \\ 0 \end{bmatrix} \quad (5.16)$$

The electromagnetic torque is given by

$$T_e = \frac{3}{2} \frac{P}{2} \left(\lambda_{ds}^r i_{qs}^r - \lambda_{qs}^r i_{ds}^r \right) \quad (5.17)$$

which, upon substitution of the flux linkages in terms of the inductances and currents, gives us:

$$T_e = \frac{3}{2} \frac{P}{2} \left(\lambda_{af} i_{qs}^r - (L_d - L_q) i_{qs}^r i_{ds}^r \right) \quad (5.18)$$

where the rotor flux linkages that link the stator are

$$\lambda_{af} = L_m i_{fr} \quad (5.19)$$

We consider rotor flux linkages as **constant except for temperature effects**. The temperature sensitivity of the magnets reduces the residual flux density and, as a consequence, the flux linkages with increasing temperature.

The samarium-cobalt magnets have the least amount of temperature sensitivity - 2 to -3 % per 100°C rise in temperature. Neodymium magnets have -12 to -13% per 100°C rise in temperature sensitivity; the ceramic magnets have -19% per 100°C rise in temperature sensitivity. Therefore, the temperature sensitivity of the magnets has to be included in the dynamic simulation by appropriately correcting for the rotor flux linkages from their nominal values.

5.4.2. Vector Control

The poly-phase PMSM control is rendered equivalent to that of the DC machine by a decoupling control known as vector control. The vector control separates the torque and flux channels in the machine through its stator-excitation inputs. The vector control for PMSM is very similar to vector-controlled IM drives. Many variations of vector control similar to that of the IM are possible.

Here, the vector control of the PMSM is derived from its dynamic model. Considering the currents as inputs, the three (3)phase currents are:

$$i_{as} = i_s \sin(\omega_r t + \delta) \quad i_{bs} = i_s \sin\left(\omega_r t + \delta - \frac{2\pi}{3}\right) \quad i_{cs} = i_s \sin\left(\omega_r t + \delta + \frac{2\pi}{3}\right) \quad (5.20)$$

where ω_r is the electrical rotor speed and δ is the angle between the rotor field and stator current phasor, known as the torque angle¹⁶. The rotor field is travelling at a speed of ω_r rad s⁻¹. Therefore, **qd** axes stator currents in the rotor reference frame for a **balanced** three-phase operation are given by

$$\begin{bmatrix} i_{qs}^r \\ i_{ds}^r \end{bmatrix} = \frac{2}{3} \begin{bmatrix} \cos \omega_r t & \cos\left(\omega_r t - \frac{2\pi}{3}\right) & \cos\left(\omega_r t + \frac{2\pi}{3}\right) \\ \sin \omega_r t & \sin\left(\omega_r t - \frac{2\pi}{3}\right) & \sin\left(\omega_r t + \frac{2\pi}{3}\right) \end{bmatrix} \begin{bmatrix} i_{as} \\ i_{bs} \\ i_{cs} \end{bmatrix} \quad (5.21)$$

Substituting Eq. (5.20) to Eq. (5.21) gives the stator currents in the rotor reference frames:

$$\begin{bmatrix} i_{qs}^r \\ i_{ds}^r \end{bmatrix} = i_s \begin{bmatrix} \sin \delta \\ \cos \delta \end{bmatrix} \quad (5.22)$$

The above equation shows the **qd** axes currents are constants in rotor reference frame¹⁷. As these are constants, they are very similar to a armature and field currents in the separately-excited DC machine. The *q* axis current is distinctly equivalent to the armature current of the DC machine; the *d* axis current is field current, but not in its entirety. It is only a partial field current; the other part is contributed by the equivalent current source representing the permanent magnet field¹⁸. Substituting this equation into the electromagnetic torque expression gives the torque:

$$T_e = \frac{3P}{2} \left[\frac{1}{2} \left(L_d - L_q \right) i_s^2 \sin 2\delta + \lambda_{af} i_s \sin \delta \right] \quad (5.23)$$

¹⁶Depending on the context or the textbook this term is also known as the load-angle.

¹⁷As δ is a constant for a given load torque.

¹⁸We will look at this in detail in the section on flux-weakening operation.

For $\delta = \pi/2$,

$$T_e = \frac{3}{2} \frac{P}{2} \lambda_{af} i_s = K_I \lambda_{af} i_s \quad \text{Nm} \quad \text{where} \quad K_I = \frac{3}{2} \frac{P}{2} \quad (5.24)$$

Eq. (5.18) is similar to torque generated in the DC motor and vector-controlled IM.

If the torque angle is maintained at 90° and flux is kept **constant**, then the torque is controlled **solely** by the stator-current magnitude, giving an operation very similar to that of the armature-controlled separately-excited DC motor.

The electromagnetic torque is positive for the motoring action, if δ is positive. Note that the rotor flux linkages λ_{af} are positive. Then the phasor diagram for an arbitrary torque is shown in Figure 9.9. Note that

$$i_{qs}^r = \text{Torque-producing component of stator current} = i_T \quad (5.25)$$

$$i_{ds}^r = \text{Flux-producing component of stator current} = i_f \quad (5.26)$$

and the torque angle is given by.

$$\theta_T = \delta \quad (5.27)$$

Eq. (5.25) and Eq. (5.27) complete the similarity of the vector-controlled PMSM and IMs. Note that the mutual flux linkage is the resultant of the rotor flux linkages and stator flux linkages. It is then given as

$$\lambda_m = \sqrt{(\lambda_{af} + L_d i_{ds}^r)^2 + (L_q i_{qs}^r)^2} \quad \text{Wb Turn} \quad (5.28)$$

If δ is greater than $\pi/2$, i_{ds}^r becomes negative. Hence, the resultant mutual flux linkages decrease. This is the key to flux-weakening in the PMSM drives. If δ is negative with respect to the rotor or mutual flux linkages, the machine becomes a generator.

5.4.3. Drive System Schematic

From the previous derivations and the understanding gained from them, the vector-controlled PMSM drive schematic is obtained and is known in **Fig. 5.10**.

5.5. Control Strategies

The torque-angle control provides a wide variety of control choices in the PMSM drive system. Some key control strategies are the following:

- constant torque-angle control or zero-direct-axis-current control;
- unity power-factor control;

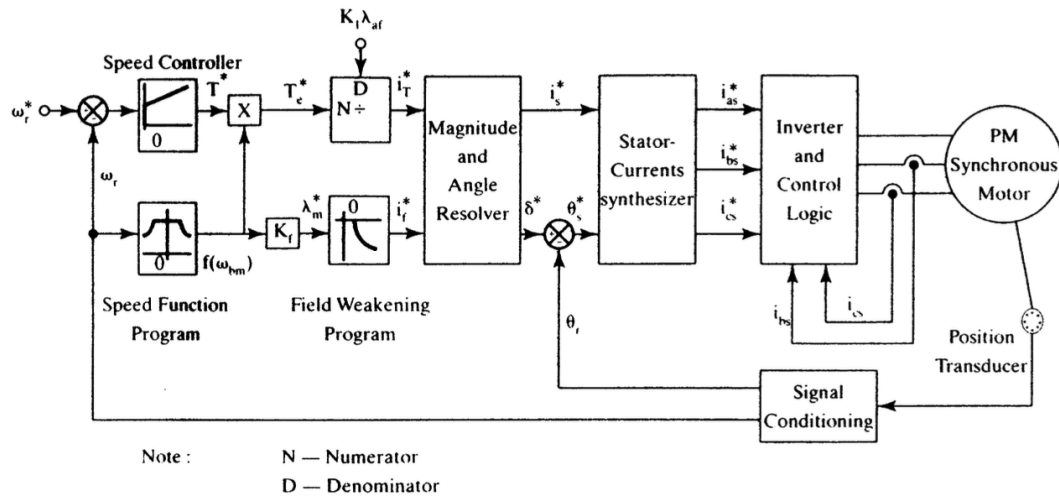


Figure 5.10.: Vector controlled PMSM drive.

- constant mutual air gap flux-linkages control;
- optimum-torque-per-ampere control;
- flux-weakening control.

These control strategies are derived systematically and analysed in the following, but illustrated for steady-state operation only.

Constant Torque-Angle Control In this control, the torque angle δ is maintained at 90 degree. Therefore, the field or direct-axis current is made to be zero, leaving only the torque or quadrature-axis current in place. This is the mode of operation for speeds lower than the base speed. Such a strategy is commonly used in many of the drive systems.

Unity Power Factor Control Unity-power-factor (UPF) control implies that the VA rating of the inverter is fully utilised for real power input to the PMSM. Upper control is enforced by controlling the torque angle as a function of motor variables.

Constant Mutual Flux Linkages Control In this control strategy, the resultant flux linkage of the stator q and d axes and rotor, known as the mutual flux linkage, is maintained constant, most usually at a value equal to the rotor flux linkages, λ_{af} . Its main advantage is that, by the limiting of the mutual flux linkage, the stator-voltage requirement is kept comparably low. In addition, varying the mutual flux linkages provides a simple and straightforward flux-weakening for operation at speeds higher than the base speed. Hence, mutual flux-linkages control is one of the powerful techniques useful in the entire speed range, as against other schemes that are limited to operation lower than the base speed only.

Optimum Torque-per-Ampere Control A control strategy to maximise electromagnetic torque for unit stator current is valuable from the optimum-machine and inverter-utilisation points of view. As in other control strategies, this control strategy is enforced with torque-angle control.

5.6. Flux Weakening Operation

The upper limits placed on the available DC-link voltage and current rating of a given inverter cause the maximum motor-input voltage and current to be **limited**. The voltage and current limits affect the maximum-speed-with-rated-torque capability and the maximum torque-producing capability of the motor drive system.

It is required and desirable to produce the rated power with the highest attainable speed such as:

electric cars, machine-tool-spindle drives, people-carriers in airport lobbies.

Corresponding to the maximum input machine voltage and rated torque, the machine attains a speed called **rated speed**.

Above this speed, the induced EMF will exceed the maximum input voltage, making the flow of current into machine-phases impractical.

To overcome this situation, the induced EMF is constrained to be less than the applied voltage by **weakening the air gap flux linkages**. The flux-weakening is made to be **inversely proportional** to the stator frequency, so that the induced EMF is a constant and will **NOT** increase with the increasing speed.

This section considers the operation of the PMSM drives when they are constrained to go within the permissible envelope of the maximum inverter voltage and current to produce the rated power and to provide this at the highest attainable rotor speed. The rated power is intended for steady-state operation whereas higher power is preferred for fast accelerations and deceleration during transient operation. Effective current control during the flux-weakening operation, with high transient capability, is preferable to a saturation of the current loop, resulting in significant harmonic content in the stator currents, resulting in higher torque ripples and higher losses.

There are two (2) approaches considered in this section:

Direct The demagnetising current is predetermined only by rotor speed

Indirect The demagnetising stator current is derived as a function of not only rotor speed but also the electromagnetic torque.

5.6.1. Maximum Speed

To understand the scope of the flux-weakening of the PMSM drive, it is essential to find the maximum speed for a given set of stator voltages and currents. The maximum operating speed with zero torque is calculated from the steady-state stator voltage equations as follows.

The normalised stator equations in the rotor reference frames are given as

$$v_{qsn}^r = (R_{sn} + L_{qn} p_t) i_{qsn}^r + \omega_{rn} (L_{dn} i_{dsn}^r + 1) \quad (5.29)$$

$$v_{dsn}^r = -\omega_{rn} L_{qn} i_{qsn}^r + (R_{sn} + L_{dn} p_t) i_{dsn}^r \quad (5.30)$$

where the **abc-to-qd0** transformation valid for voltages, currents, and flux linkages is:

$$\begin{bmatrix} v_{qsn}^r \\ v_{dsn}^r \end{bmatrix} = \frac{2}{3} \begin{bmatrix} \cos \theta_r & \cos \left(\theta_r - \frac{2\pi}{3} \right) & \cos \left(\theta_r + \frac{2\pi}{3} \right) \\ \sin \theta_r & \sin \left(\theta_r - \frac{2\pi}{3} \right) & \sin \left(\theta_r + \frac{2\pi}{3} \right) \end{bmatrix} \begin{bmatrix} v_{asn} \\ v_{bsn} \\ v_{csn} \end{bmatrix}$$

The steady-state stator-voltage equations are obtained by setting the derivative of the current variables to zero in Eq. (5.29):

$$\begin{aligned} v_{qsn}^r &= R_{sn} i_{qsn}^r + \omega_{rn} (L_{dn} i_{dsn}^r + 1) \\ v_{dsn}^r &= -\omega_{rn} L_{qn} i_{qsn}^r + R_{sn} i_{dsn}^r \end{aligned}$$

when $i_{qsn}^r = 0$, and the stator-voltage phasor is given as:

$$v_{sn}^2 = (v_{dsn}^r)^2 + (v_{qsn}^r)^2 = \omega_{rn}^2 (1 + L_{dn} i_{dsn}^r)^2 + R_{sn}^2 (i_{dsn}^r)^2$$

from which the maximum speed for a given stator-current magnitude of i_{dsn}^r is

$$\omega_{rn}(\max) = \frac{\sqrt{v_{sn}^2 - R_{sn}^2 (i_{dsn}^r)^2}}{(1 + L_{dn} i_{dsn}^r)} \quad (5.31)$$

Note that the denominator of Eq. (5.31) has to be positive, giving the condition that the maximum stator current to be applied to counter the magnet flux linkages is:

$$i_{dsn}^r(\max) < -\frac{1}{L_{dn}} \quad (5.32)$$

5.6.2. Direct Flux Weakening

The direct-flux-weakening algorithm finds the demagnetising component of stator current satisfying the maximum current and voltage limits only. It is very similar to the field control of a separately-excited DC machine, where the field current is determined usually by the speed alone. Such a method has the advantage of simplicity, but it has the disadvantage of not optimising the stator current by considering the operating torque in the machine.

Such an optimisation is possible with a torque-request feed forward. The PMSM drive-system control with both constant-torque and constant-power operation is presented in this section. Flux-weakening algorithm, control scheme, controller realisation, simulation, and performance are described in this section.

¹⁹neglecting the resistive terms

By considering the steady state, the voltage phasor is written¹⁹ as:

$$v_{sn}^2 = \omega_{rn}^2 \left((1 + L_{dn} i_{dsn}^r)^2 + (L_{qn} i_{qsn}^r)^2 \right) \text{ p.u.}$$

where the voltage phasor (v_{sn}) is defined as

$$v_{sn} = \sqrt{(v_{qsn}^r)^2 + (v_{dsn}^r)^2} \text{ p.u.}$$

The quadrature current i_{qsn}^r can be written in terms of the stator-current phasor and the direct-axis current as:

$$i_{qsn}^r = \sqrt{(i_{qsn}^r)^2 - (i_{dsn}^r)^2} \text{ p.u.}$$

Substituting Eq. (5.6.2) into Eq. (5.32) gives the following equation relating the voltage phasor, current phasor, and rotor speed.

$$v_{sn}^2 = \omega_{rn}^2 \left(L_{qn}^2 \left(i_{sn}^2 - (i_{dsn}^r)^2 \right) + (1 + L_{dn} i_{dsn}^r) \right) \text{ p.u.} \quad (5.33)$$

Note that the voltage phasor and current phasor (v_{sn} , i_{sn}) are the **maximum values** that could be obtained from the inverter operation.

Therefore, for the flux-weakening operation, these are considered to be **constant**. That leads to the appreciation that the equation contains only two (2) variables,

$$\omega_{rn} \text{ and } i_{dsn}^r.$$

Therefore, from one of these two variables the other could be computed analytically. This is the key to the control and operation of the PMSM drive in the flux-weakening region.

Further, Eq. (5.33) is written in terms of i_{dsn}^r and ω_{rn} as:

$$v_{sn} = \omega_{rn} \sqrt{a(i_{dsn}^r)^2 + bi_{dsn}^r + c} \text{ p.u.}$$

where the constants are:

$$a = L_{dn}^2 - L_{qn}^2 \quad b = 2L_{dn} \quad c = 1 + L_{qn}^2 i_{sn}^2$$

Assuming the rotor speed is available for feedback control and using equations (9.93) to (9.97) gives the d axis stator current, which would automatically satisfy the constraints of maximum stator current, i_a , and stator voltage, v_{sn} . From the stator-current magnitude and the d axis stator current, by using equation (9.92), the maximum permitted q axis stator current could be calculated.

The d and q axes currents then determine the stator-phase currents obtained by using the inverse transformation from equation (9.85):

$$\begin{bmatrix} i_{asn} \\ i_{bsn} \\ i_{csn} \end{bmatrix} = \begin{bmatrix} \cos \theta_r & \sin \theta_r \\ \cos \left(\theta_r - \frac{2\pi}{3} \right) & \sin \left(\theta_r - \frac{2\pi}{3} \right) \\ \cos \left(\theta_r + \frac{2\pi}{3} \right) & \sin \left(\theta_r + \frac{2\pi}{3} \right) \end{bmatrix} \begin{bmatrix} i_{qsn}^r \\ i_{dsn}^r \end{bmatrix}$$

Combining equations $i_{qsn}^r = i_{sn} \sin \delta$ and $i_{dsn}^r = i_{sn} \cos \delta$ with (9.98) gives the normalised stator phase currents via the following relationship:

$$\begin{bmatrix} i_{asn} \\ i_{bsn} \\ i_{csn} \end{bmatrix} = \begin{bmatrix} \sin(\theta_r + \delta) \\ \cos(\theta_r + \delta - \frac{2\pi}{3}) \\ \cos(\theta_r + \delta + \frac{2\pi}{3}) \end{bmatrix}$$

The torque angle is obtained as:

$$\delta = \tan^{-1} \left(\frac{i_{qsn}^r}{i_{dsn}^r} \right)$$

The calculated q axis stator current, together with d axis stator current, determines the torque, T_{et} , that could be produced, and it is then used to modify the torque command, T_{ec} , generated from the speed error in a drive system.

If the torque request, T_{ec} , is more than T_{ef} , the torque calculated by the flux-weakening module, then the final torque request is made **equal** to the calculated one. If T_{ce} is less than T_{ef} , then the final torque command is maintained at T_{ce} . This final torque request is denoted as T_e^* . From this T_e^* , the required q axis current in the machine could be calculated from the torque equation, since i_{dsn}^r request is known:

$$i_{qsn}^r = \frac{T_e^*}{\left(1 + (L_{dn} - L_{qn}) i_{dsn}^r \right)} \text{ p.u.}$$

Although the above relationships were derived for steady-state performance, it is to be noted that some voltage reserve is to be available for dynamic control of currents. With a smaller voltage reserve, the current loops will become sluggish; beyond their limit points, they will no longer control the current, thus making the applied voltages six-step. This results in currents rich in harmonics and hence in higher air gap-torque pulsations in the machine.

An example of PMSM control schematic is shown in **Fig. 5.11**.

Control Scheme

The control scheme for the PMSM drive both in the region of constant torque and in that of flux-weakening could be formulated from the derivations and understanding provided discussed previously. Schematically, the control scheme is shown in **Fig. 5.11**. Assuming a speed-controlled drive system, the torque command T_{ec} is generated by the **speed error**. Depending on the mode of operation, this torque command is processed by Block 1 or Block 2.

1. Block 1 corresponds to the constant-torque-mode controller.
2. Block 2 corresponds to the flux-weakening-mode controller.

The outputs of these controllers are the stator-current-magnitude command and the torque-angle command. They, together with the electrical rotor position, provide the phase-current commands through the transformation block. The current commands are enforced with an inverter by current feedback control, with any one of the current control schemes available. For illustration, pulse-width modulation for the current control is chosen. The rotor position and rotor speed are obtained with an encoder and a signal conditioner, respectively.

5.7. Speed-Controller Design

The design of the speed-controller is important from the point of view of implementing desired transient and steady-state characteristics to the speed-controlled PMSM drive system. A proportional-integral (PI) controller is sufficient for many initial applications²⁰. Selection of the gain and time constants of such a controller by using the symmetric-optimum principle is straightforward if the **d** axis stator current is assumed to be zero (**0**).

²⁰Therefore that is the only method we will consider

In the presence of a **d** axis stator current, the **d** and **q** current channels are cross-coupled, and the model is non-linear, as a result of the torque term.

Under the assumption of $i_{ds}^r = 0$, the system becomes linear and resembles that a separately-excited DC with constant excitation. From then on, the block-diagram derivation, current-loop approximation, speed-loop approximation, and derivation of the speed-controller by using symmetric optimum are identical to those for a DC or vector-controlled IM speed-controller design.

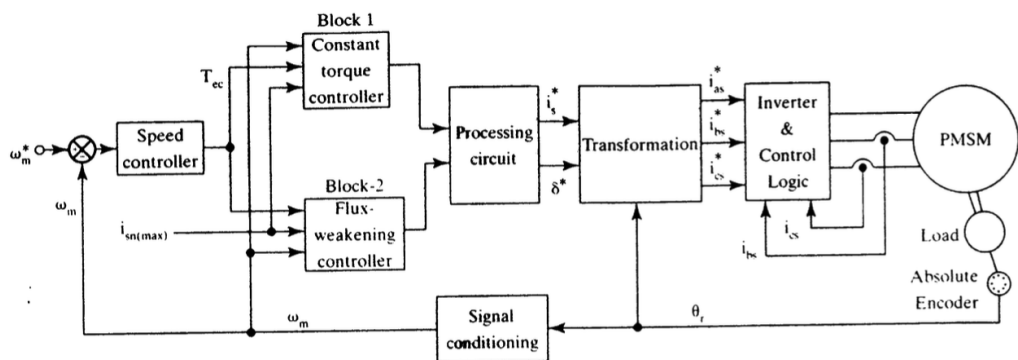


Figure 5.11.: A Schematic Example of a PMSM-drive control strategy.

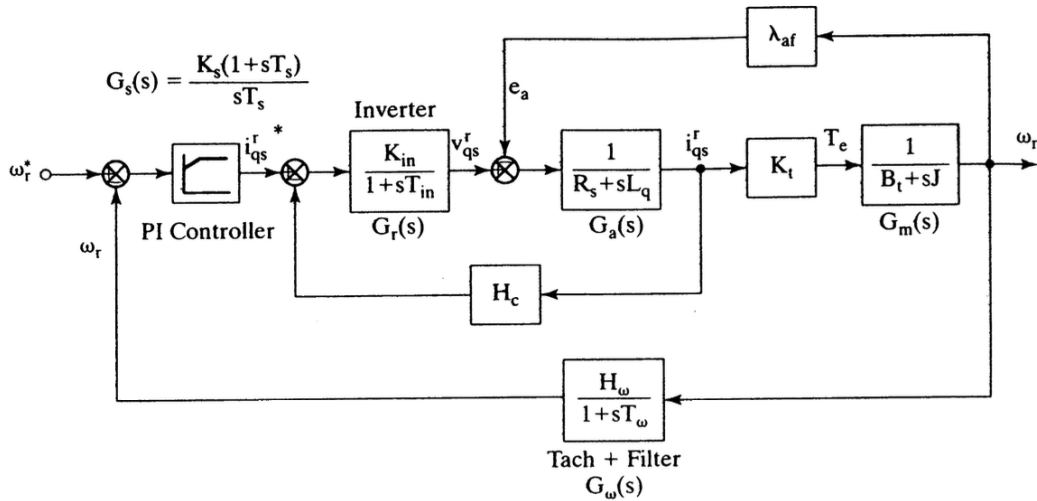


Figure 5.12.: Block diagram of the speed-controlled PMSM drive.

5.7.1. Deriving the Block Diagram

The motor **q** axis voltage equation with the **d** axis current being zero becomes

$$v_{qs}^r = (R_s + L_q p_t) i_{qs}^r + \omega_r \lambda_{af} \quad (5.34)$$

and the electro-mechanical equation is:

$$\frac{P}{2} (T_e - T_l) = J p_t \omega_r + B_1 \omega_r \quad \text{where} \quad T_e = \frac{3}{2} \frac{P}{2} \lambda_{af} i_{qs}^r \quad (5.35)$$

To simplify further, let us assume to be the load as pure **frictional**, which makes:

$$T_l = B_1 \omega_m \quad (5.36)$$

Doing the necessary substitutions, we derive the electro-mechanical equation as:

$$(J p_t + B_1) \omega_r = \left[\frac{3}{2} \left(\frac{P}{2} \right)^2 \lambda_{af} \right] i_{qs}^r = K_t i_{qs}^r \quad (5.37)$$

where,

$$B_t = \frac{P}{2} B_1 + B_1 \quad K_t = \frac{3}{2} \left(\frac{P}{2} \right)^2 \lambda_{af} \quad (5.38)$$

Eq. (5.34) and Eq. (5.37), when combined into a block diagram with the current- and speed-feedback loops added, are shown in **Fig. 5.12**.

We can model the entire inverter as a simple gain with a **time lag** as follows: The inverter is modelled as a gain with a time lag by

$$G_r(s) = \frac{K_{in}}{1 + sT_{in}} \quad \text{where} \quad K_{in} = 0.65 \frac{V_{dc}}{V_{cm}} \quad \text{and} \quad T_{in} = \frac{1}{f_c} \quad (5.39)$$

where V_{dc} is the dc-link voltage input to the inverter, V_{cm} is the maximum control voltage, and f_c is the switching (carrier) frequency of the inverter. The induced EMF due to rotor flux linkages e_a , is

$$e_a = \lambda_{af} \omega_r \quad V \quad (5.40)$$

5.8. Sensorless Control

²¹For i_q and i_d axes respectively.

All previous methods used in controlling PMSM, requires two (2) current sensors²¹ and an absolute-rotor-position sensor. The rotor position generally is sensed with an optical encoder or a resolver for high-performance applications. The position sensors cost is similar to the cost of the low-power motor, therefore making the total system cost **non-competitive** compared to other types of motor drives. As for the current sensors, they are not as expensive as the rotor-position sensor.

Other types of drives (i.e., DC and IM) also require current sensors use in feedback control.

With these in mind, the control and operation of PMSM drive without a rotor-position sensor would enhance its applicability to many control sensors and provide a back-up control sensor-based diversity as sensor features.

The basis for this control strategy is that the error between measured and calculated currents from the machine model gives the difference between the current error speed and the actual rotor speed of the motor drive. Minimising this result is the synchronous operation of the motor drive by estimating its rotor position accurately.

The following assumptions are made to develop this control algorithm.

- Motor parameters and rotor PM flux are **constant**.
- Induced EMFs in the machine are **sinusoidal**²².
- It operates in the constant-torque region, and flux-weakening operation is **NOT** considered.

²²This is just saying the drive is a PMSM

The two (2) phase currents constitute the inputs to the electrical rotor position and speed estimator. The error between the reference speed ω_r^* , and the estimated rotor speed ω_{rm} , is **amplified and limited** to provide the torque-producing component of the stator current, i_T^* , which is the **q** axis stator current in the rotor reference frames.

The estimated rotor position, together with i_T^* , provides the stator current commands, which are enforced by a three-phase inverter feeding the PMSM. The position and speed estimator is derived from the machine equations, shown previously.

Let us consider the machine is running at a speed ω_r , whereas the model starts with an assumed rotor speed ω_m . The assumed rotor position, naturally, θ_{rm} lags behind the actual rotor position θ_r by $\delta\theta$ radians. They are related to the actual and assumed or model speed as follows:

$$\theta_r = \int \omega_r dt \quad (5.41)$$

$$\theta_{rm} = \int \omega_{rm} dt \quad (5.42)$$

$$\delta\theta = \theta_r - \theta_{rm} = \int (\omega_r - \omega_{rm}) dt \quad (5.43)$$

²³These calculation are carried out in a reference frame at an assumed rotor speed.

We will use the machine model we developed earlier, to compute the stator currents²³. That implies

the reference frames are α and β axes and **NOT** d and q axes, which are the usual rotor reference frames.

Therefore, the machine equations in the assumed rotor-speed reference frames are:

$$\begin{bmatrix} p_t i_{\alpha m} \\ p_t i_{\beta m} \end{bmatrix} = \begin{bmatrix} -\frac{R_s}{L_q} & -\omega_{rm} \frac{L_d}{L_q} \\ \omega_{rm} \frac{L_q}{L_d} & -\frac{R_s}{L_q} \end{bmatrix} \begin{bmatrix} p_t i_{\alpha m} \\ p_t i_{\beta m} \end{bmatrix} + \begin{bmatrix} -\frac{\omega_{rm} \lambda_{af}}{L_q} \\ 0 \end{bmatrix} + \begin{bmatrix} \frac{V_\alpha}{L_q} \\ \frac{V_\beta}{L_d} \end{bmatrix} \quad (5.44)$$

In the model α and β reference frames, the actual machine equations are written from the d and q axes as:

$$\begin{bmatrix} p_t i_\alpha \\ p_t i_\beta \end{bmatrix} = \begin{bmatrix} -\frac{R_s}{L_q} & -\omega_{rm} \frac{L_d}{L_q} \\ \omega_{rm} \frac{L_q}{L_d} & -\frac{R_s}{L_q} \end{bmatrix} \begin{bmatrix} p_t i_\alpha \\ p_t i_\beta \end{bmatrix} + \begin{bmatrix} -\frac{\omega_{rm} \lambda_{af}}{L_q} \cos \delta\theta \\ \frac{\omega_{rm} \lambda_{af}}{L_d} \sin \delta\theta \end{bmatrix} + \begin{bmatrix} \frac{V_\alpha}{L_q} \\ \frac{V_\beta}{L_d} \end{bmatrix} \quad (5.45)$$

The variables without the second subscript indicate that they are **actual machine variables**. The machine model²⁴ variables end with subscript m . The actual machine equations are derived on the understanding that α - β axes are the considered reference axes and hence the rotor flux linkages have components on them from the d axis given as a function of the error in rotor position, $\delta\theta$. It is assumed that the entire rotor field is aligned on the d axis.

²⁴or estimated.

5.9. Brushless DC Motor

PMSMs having **trapezoidal** induced EMF are known as BLDC machines. The advantage of such a machine in comparison to the PMSM was discussed in the early part of this chapter. The major reason for the popularity of these machines over their counterparts is **control simplicity**. To initiate the onset and computation of current in the phase of a machine, the beginning and end of the constant portion of the induced EMF have to be tracked. That amounts to only six (6) discrete positions for a three-phase machine in each electrical cycle. These signals could easily be generated with three Hall sensors displaced from each other by 120° electrical.

The Hall sensors are mounted facing a small magnet wheel fixed to the rotor and having the same

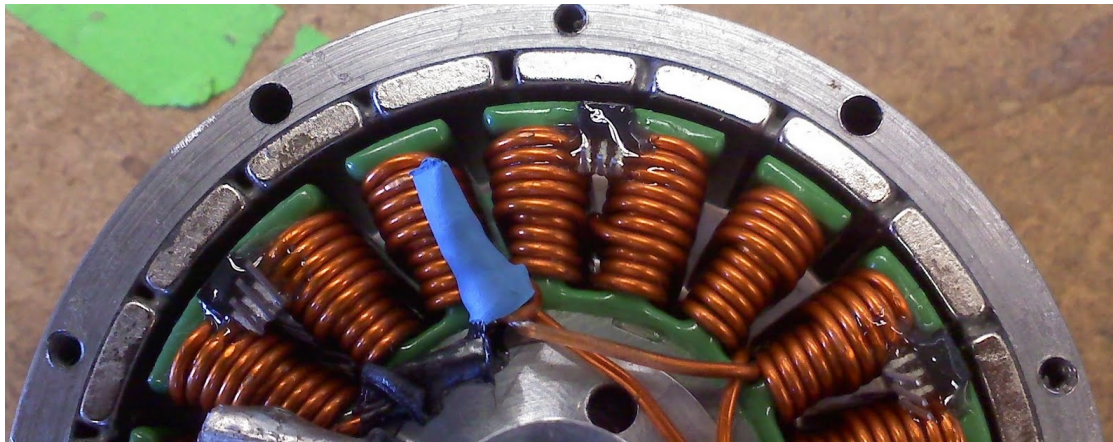


Figure 5.13.: Placement of the hall sensors on the stator [61].

number of poles as the rotor of the PMSM, or the extra magnet wheel may be dispensed with by extending the rotor beyond the stack length of the stator and using the rotor magnets to provide the position information. Such an arrangement tracks the absolute position of the rotor magnets and hence the shape and position of the induced EMFs in all the machine phases. In contrast to the PMSM, which requires continuous and instantaneous absolute rotor position, the BLDC position-feedback requirement is much simpler: it requires only six (6) discrete absolute positions for a three-phase machine, resulting in a major cost saving in the feedback sensor. Further, the control involves significant vector operations in the PMSM drive, whereas such operations are not required for operation of the BLDC drive.

5.9.1. Mathematical Model

The flux distribution in a BLDC is **trapezoidal**. Therefore, the **dq** rotor reference frames model developed for the PMSM is **NOT** applicable. Given the non-sinusoidal flux distribution, it is prudent to derive a model of the BLDC in phase variables. The derivation of this model is based on the assumptions that:

1. Induced currents in the rotor due to stator harmonic fields are neglected
2. Iron and stray losses are negligible.
3. Damper windings are not usually a part of the BLDC, which are assumed to provided by the inverted.

The motor is considered to have three phases, even though the derivation procedure is valid for any number of phases.

The coupled circuit equations of the stator windings in terms of motor electrical constants are

$$\begin{bmatrix} V_{as} \\ V_{bs} \\ V_{cs} \end{bmatrix} = \begin{bmatrix} R_s & 0 & 0 \\ 0 & R_s & 0 \\ 0 & 0 & R_s \end{bmatrix} \begin{bmatrix} i_{as} \\ i_{bs} \\ i_{cs} \end{bmatrix} + \begin{bmatrix} L_{aa} & L_{ab} & L_{ac} \\ L_{ba} & L_{bb} & L_{bc} \\ L_{ca} & L_{cb} & L_{cc} \end{bmatrix} P_t \begin{bmatrix} i_a \\ i_b \\ i_c \end{bmatrix} + \begin{bmatrix} e_{as} \\ e_{bs} \\ e_{cs} \end{bmatrix} \quad (5.46)$$

where R_s is the stator resistance per phase, **assumed to be equal for all three phases**. The induced EMFs e_{as} , e_{bs} , and e_{cs} are all assumed to be trapezoidal, where E_p is the peak value, derived as:

$$E_p = (B/v) N = N (B l r \omega_m) = N \Phi_a \omega_m = \lambda_p \omega_m$$

where N is the number of conductors in series per phase, v is the velocity, l is the length of the conductor, r is the radius of the rotor bore, ω_m is the angular velocity, and B is the flux density of the field in which the conductors are placed.

This flux density is solely due to the rotor magnets.

The product BIr , denoted as Φ_a , has the dimensions of flux and is directly proportional to the air-gap flux (Φ_g):

$$\Phi_a = Bir = \frac{1}{\pi} B\pi/r = \frac{1}{\pi} \Phi_g$$

Note that the product of flux and number of conductors in series has the dimension of flux linkages and is denoted by λ_p . Since this is proportional to phase a flux linkages by a factor of $1/\pi$, it is hereafter referred to as **modified flux linkages**.

If there is no change in the rotor reluctance with angle because of a non-salient rotor, and assuming three (3) symmetric phases, the following are obtained:

$$L_{aa} = L_{bb} = L_{cc} = L \quad \text{and} \quad L_{ab} = L_{ba} = L_{ca} = L_{ac} = L_{bc} = L_{cb} = M \quad \text{H}$$

Substituting equations (9.182) and (9.183) in Eq. (5.46) gives the BLDC model as:

$$\begin{bmatrix} v_{as} \\ v_{bs} \\ v_{cs} \end{bmatrix} = R_s \begin{bmatrix} 1 & 0 & 0 \\ 0 & 1 & 0 \\ 0 & 0 & 1 \end{bmatrix} \begin{bmatrix} i_{as} \\ i_{bs} \\ i_{cs} \end{bmatrix} + \begin{bmatrix} L & M & M \\ M & L & M \\ M & M & L \end{bmatrix} \begin{bmatrix} i_a \\ i_b \\ i_c \end{bmatrix} + \begin{bmatrix} e_{as} \\ e_{bs} \\ e_{cs} \end{bmatrix} \quad (5.47)$$

and the electromagnetic torque is given by:

$$T_e = (e_{as}i_{as} + e_{bs}i_{bs} + e_{cs}i_{cs}) \frac{1}{\omega_m} \quad \text{N m} \quad (5.48)$$

5.9.2. Commutation-Torque Ripple

The desired current waveform is **rectangular** and 120° wide in each half-cycle for a three-phase BLDC drive. The leakage inductance, L_l , causes the stator currents to take a **finite time** to rise and fall, therefore distorting the decay rate of current into a trapezoidal shape. The effect of this is the torque ripple generated at the current transitions.

For a three-phase machine, there will be six (6) torque ripple for every 360° electrical as the six current transitions occur.

They will also reduce the average torque if the current transmitted at 120° electrical, whereby the constant-voltage source is reduced below 120° electrical. The consequences of a set of practical currents on the performance of the BLDC drive can be analysed by using a Fourier-series approach as follows. The torque expressions are given considering only a two (2) pole machine²⁵.

The phase a current can be resolved into Fourier series as:

$$i_{as}(\theta_r) = \frac{4I_p}{\pi(\theta_2 - \theta_1)} \left[(\sin \theta_2 - \sin \theta_1) \sin \theta_r + \frac{1}{3^2} (\sin 3\theta_2 - \sin 3\theta_1) \sin 3\theta_r + \dots \right] \quad (5.49)$$

²⁵for a P-pole machine, the expressions have to be multiplied by the number of pole pairs.

Similarly, the Fourier series of the flux linkages of phase a , assuming a trapezoidal waveform and constancy for $(\pi - 2h)$ electrical degrees in each half-cycle, is

$$\lambda_{af}(\theta_r) = \frac{4\lambda_p}{\pi h} \left[\sin h \sin \theta_r + \frac{1}{3^2} (\sin 3h \sin 3\theta_r) + \frac{1}{5^2} (\sin 5h \sin 5\theta_r) + \dots \right] \quad (5.50)$$

where λ_p is the peak value of the modified flux linkages.

The b and c phase currents and their modified flux linkages can be derived with the only difference being the phase shift relative to the phase a .

The fundamental electromagnetic torque is computed by considering the product of fundamental terms in the air gap flux linkages and respective stator currents for a 2-pole machine:

$$T_{e1} = \lambda_{af1}(\theta_r) i_{as1}(\theta_r) + \lambda_{bf1}(\theta_r) i_{bs1}(\theta_r) + \lambda_{cf1}(\theta_r) i_{cs1}(\theta_r) \quad \text{N m} \quad (5.51)$$

Substituting the fundamental terms and expanding the expressions gives us the monolithic expression:

$$T_{e1} = \frac{16I_p\lambda_p}{\pi^2 h(\theta_2 - \theta_1)} \left[\sin h (\sin \theta_2 - \sin \theta_1) \sin^2 \theta_r \right. \quad (5.52)$$

$$\left. + \sin h (\sin \theta_2 - \sin \theta_1) \sin^2 (\theta_r - 2\pi/3) \right. \quad (5.53)$$

$$\left. + \sin h (\sin \theta_2 - \sin \theta_1) \sin^2 (\theta_r + 2\pi/3) \right] \quad (5.54)$$

For $h = \pi/6$, the electromagnetic torque for three phases is evaluated as

$$T_{e1} = (I_p \lambda_p) \left[\frac{48}{\pi^3 (\theta_2 - \theta_1)} (\sin \theta_2 - \sin \theta_1) \right] \frac{3}{2} \quad (5.55)$$

$$= 2.3193 (I_p \lambda_p) \frac{(\sin \theta_2 - \sin \theta_1)}{\theta_2 - \theta_1} \quad \text{N m} \quad (5.56)$$

The normalised fundamental torque in p.u. as a function of θ_2 for θ_1 and h equal to 30° . This shows that increasing the rise time of the current decreases the fundamental torque. At higher speeds, for the same rise time of the current, note that θ_2 increases; hence, there will be a greater reduction in the fundamental torque of the motor drive.

For 120° electrical rectangular current, the fundamental torque is

$$T_{e1} = 2.011 (I_p \lambda_p) \quad (5.57)$$

The commutation torque is at six (6) times the fundamental frequency. It can be seen as the result of the sum of the fundamental rotor flux linkages interacting with the fifth- and seventh-current harmonics and the fundamental of the current interacting with the fifth- and seventh-harmonic rotor flux linkages. It is derived as follows.

$$T_{e6} = \frac{4}{\pi h} \frac{4\lambda_p I_p}{\pi(\theta_2 - \theta_1)} \left[(\sin \theta_2 - \sin \theta_1) \left(-\frac{1}{5^2} (\sin 5h) + \frac{1}{7^2} (\sin 7h) \right) \right]$$

$$+ \frac{4}{\pi h} \frac{4}{\pi(\theta_2 - \theta_1)} \left[\sin h \left(-\frac{1}{5^2} (\sin 5\theta_2 - \sin 5\theta_1) + \frac{1}{7^2} (\sin 7\theta_2 - \sin 7\theta_1) \right) \right]$$

5.9.3. Sensorless Control

The drive system is **dependent** on the position and current sensors for control. Elimination of both types of sensors is desirable in many applications, particularly in low-cost but high-volume applications, for cost and packaging considerations. Between the two (2) sensors, the current sensor is easier to accommodate in the electronic part of the system as the position sensor requires a considerable labour and volume in the motor for its mounting. That makes it all the more important to do without the position sensor for the control of the BLDC drive system.

Current Sensing As least two (2) phase currents are required for the current control of a three-phase machine. The phase currents can be sensed from the DC-link current. Therefore, one (1) sensor is sufficient for current control of the machine.

The current sensors are relatively expensive if galvanic isolation is required.

If isolation is **NOT** necessary, then the currents can be sensed inexpensively with precision resistors by measuring the voltage drop across them. The latter option is used widely in low-cost motor drives. Another approach is to use Metal-Oxide Semiconductor Field-Effect Transistor (MOSFET) devices, we'd expect to distinguish current-strong capability, to measure the currents. Alternatively, the MOSFET device itself serves as a sensing resistor during its conduction. The use of the drain-source voltage drop to estimate currents is plagued with inaccuracies due to temperature effect, and, for precise current control, the feedback from this voltage drop is **NOT** a viable method. Hall-effect current sensors are ideal for sensing the currents with **galvanic isolation**. At this stage, it is very nearly impossible to do away with current feedback for the control of the BLDC machine to deliver high performance.

If precise torque and speed controls are **NOT** required, current feedback control and hence current sensing can be dispensed with. Then, a simple duty cycle using an open-loop Pulse Width Modulation (PWM) voltage controller is sufficient. However, the steering of the current to the appropriate machine phases requires the rotor-position information. A number of methods have come into practice to estimate rotor position without an externally mounted sensor.

Position Estimation Position can be sensed by Hall sensors overlooking a magnet wheel mounted on the shaft of the rotor extension with the magnets. This will provide just sufficient commutation signals,

i.e., six (6) per electrical cycle for a three-phase machine.

Such a low discrete pulse count is not suitable for high-performance applications. Optical encoders and resolver provide the rotor position with high resolution, but they are expensive. Further, the position sensors require extensive mounting arrangements. High-volume applications demand that they be designed with, on account of the cost and manufacturing burdens.

Many methods are possible to estimate the commutation signals, which are briefly described here.

Estimation by using machine model The induced EMF can be sensed from the machine model by using the applied currents and voltages and machine parameters of resistance, self-inductance, and mutual inductance. The advantage of this method is that an isolated signal can be extracted, because the input currents and voltages are themselves isolated signals. The voltages can be extracted from the base or gate drive signals and the DC-link voltage. The variations in the DC-link voltage can be estimated from the DC-link filter parameters and the DC-link current. Parameter sensitivity, particularly that of the stator resistance, will introduce an error in the induced EMF estimation, resulting in inaccurate commutation signals to the inverter.

Induced emf from sensing coils Sensing coils in the machine can be installed inexpensively to obtain induced-EMF signals. The advantages of this method are that the signals are fairly clean, parameter-insensitive, and **galvanically isolated**. The disadvantages are in the additional manufacturing process and additional wire harness from the machine. The latter is **NOT** acceptable in refrigerator compressor motor drives, because of hermetic sealing requirements.

Sensing EMFs from inactive phases One of the most commonly used methods for acquiring position information is to monitor the induced EMF of the machine phases when they are **NOT** being energised. Note that a machine phase is inactive for 33.33% of the time and that only two (2) phases conduct at any given time. During the inactive time, an induced EMF appears across the machine winding, which can be sensed. The induced EMF of the phase gives the information on zero crossing and on when the EMF reaches the constant region, indicating when that phase has to be energised. The polarity of the induced EMF determines the appropriate polarity of the current to be injected into that machine phase. Instead of waiting for the constant region of the induced EMF for energising a machine phase, the induced EMF on integration from its zero crossing will attain a particular value corresponding to thirty degrees from the zero crossing instant. The integrator output corresponding to thirty degrees from the positive zero crossing could be termed the threshold value used in energizing a phase.

Third-harmonic induced EMF An alternative method is to detect the third-harmonic induced EMF in the machine windings and use them to generate the control signals. A three-phase, star-connected, four-wire system will allow the collection of the third-harmonic induced EMF, and this can be inexpensively instrumented with four (4) resistors.

All the methods that rely on the induced EMF have the disadvantage that, at standstill, the position information is **not available**, as there is no induced EMF at zero speed. Even at very low speeds, the induced EMF might not be easily detectable. Therefore, a method to generate the control signals at and around zero speed has to be incorporated for successful starting of the machine and up to a speed at which the induced-emf methods can come in to generate the position information reliably. Therefore, a starting procedure at standstill is required. This procedure can consist of two (2) steps:

- i. Exciting one or two phases, the rotor can be aligned to a predetermined rotor position. This way, the starting position is known: hence, correct starting control signals are generated.

When the rotor starts moving at slow speed, the induced emf is so small that it cannot be used for generating the commutation pulses until the rotor speed reaches a certain level. This fact necessitates a second step to complete the starting process.

- ii. Once the rotor starts moving, the stator phases are energized at a slowly varying frequency, keeping the stator currents constant. The rate of frequency variation is kept low so that synchronism is maintained and can be controlled modestly if the load is known beforehand. If not, the stator frequency is altered by trial and error until it reaches the minimum speed at which the induced emfs are of sufficient magnitude to render them useful for control. This constitutes the second step in the starting process. The problem with this approach is that this is not precise; some jitter and vibrations can be felt during the starting, which may not be significantly adverse in many applications.

In many cases, step (i) is skipped, and only step (ii) is used for starting of the machine.

A method based on the salient of the rotor is another alternative, but caution must be used here: the saliency in the BLDCs is not very significant. This requires a detection of the machine inductance and its profile, from which the rotor position can be extracted.

Torque Smoothing

It is not possible to generate ideal rectangular currents, caused by the time delay introduced by the machine inductance (L_d , L_q).

Therefore, the currents become more or less trapezoidal and produce a large commutation-torque ripple, as much as 10 to 15% of the rated torque. Further, the induced EMFs are **NOT** exact trapezoids, because of significant slot harmonics²⁶. They, in turn, will generate harmonic ripple torques, resulting in low torque performance [62]. The quality of the induced EMFs is further affected by the type of armature winding. Windings are chosen for low-cost manufacturing, high-volume applications, and they invariably cause a greater deviation from the ideal measurements. The cumulative effect of all these imperfections leads to a drive with **uneven torque over an electrical cycle** of its operation. That makes the drive highly unsuitable for high-performance applications. To overcome these disadvantages, methods based on current-shaping to counter the ill effects of the flux distribution are successful [63].

²⁶Harmonics generated by motor slots due to the regular variation of reluctance and flux over the stator surface. The stator windings have to go somewhere.

To overcome the unevenness in the flux-density distribution, it is measured or computed, and the current is continuously adjusted accordingly, to generate a constant torque. To counter the commutation-torque pulsation, the incoming-phase and outgoing-phase currents are coordinated in such a manner that the sum of the torque produced by the two phases is kept **constant**. All of the algorithms require a set of fast-acting current-control loops to shape the current, with no deviation either in magnitude or phase from their references.

Design of Current and Speed Controllers

As BLDC is similar to the separately-excited armature-controlled DC machine, as can be seen from its mathematical model, the methods which are appropriate to the design of the current and speed controllers for separately-excited armature-controlled DC can be easily employed here without the need of higher complexity. The design of current and speed controllers directly relevant to this motor drive can be obtained from Chapter 2.

Parameter Sensitivity of the BLDC Drive

The motor parameters which are sensitive to variations in temperature are **stator resistances** and **rotor magnets**. The use of inner current loops overcomes the effect of stator-resistance variations. The use of speed-control loop counters the rotor flux-linkages variation. In that process, the linearity of the torque with its reference might be lost. In order to preserve the torque linearity in the drive system, methods similar to the air gap-power feedback control have to be resorted to.

The inductance variation is a function of saturation and hence of the exciting current. Therefore, it is easy to counter the inductance variations if the excitation current is measured and known.

Glossary

AC Alternating Current. 5, 9, 16–18, 22, 28–30, 36, 45, 49, 50, 80, 86, 90, 100

ANSI American National Standards Institution. 57

API American Petroleum Institute. 58

BLDC Brushless DC. vii, viii, 16, 109, 110, 123–125, 127, 129, 130

DC Direct Current. vii, 1, 5–7, 9–19, 21–29, 31–39, 41–43, 45, 50, 68, 69, 74, 80, 86, 88–90, 95, 99, 100, 113, 114, 116, 117, 120, 122, 127, 128, 130

EMF Electro-motive Force. iv, vii, 7, 10, 13, 14, 16, 17, 21, 22, 24–26, 28, 31, 33, 37, 40, 54, 55, 69, 90, 91, 93–95, 108–110, 116, 121–124, 128, 129

IEC International Electrotechnical Commission. 57

IM Induction Machine. viii, 1, 5, 49–60, 65–67, 70, 72, 73, 75, 76, 78, 79, 82, 83, 85, 89, 90, 92, 111, 113, 114, 120, 122

MMF Magneto-motive Force. 8, 60, 62, 65, 93, 104

MOSFET Metal-Oxide Semiconductor Field-Effect Transistor. 127

NEMA National Electrical Manufacturers Association. 57, 58

PM Permanent Magnet. vii, viii, 1, 5, 16, 99–101, 105, 106, 108, 109, 122

PMSM Permanent Magnet Synchronous Motor. viii, 69, 100, 106–109, 111, 113–120, 122–124

PWM Pulse Width Modulation. 127

RHS Right Hand Side. 40, 68

RMS Root-Mean Square. 109

SCR Silicon Controlled Rectifier. 5, 28, 29, 33, 99

SynM Synchronous Machine. 99, 106, 107

Bibliography

- [1] Ned Mohan, Tore M Undeland, and William P Robbins. *Power electronics: converters, applications, and design*. John wiley & sons, 2003.
- [2] M Nedeljković and Z Stojiljković. "Fast current control for thyristor rectifiers". In: *IEEE Proceedings-Electric Power Applications* 150.6 (2003), pp. 636–638.
- [3] Galina Mirzaeva, Robert E Betz, and Terrence J Summers. "Evaluation of current density in DC motor brushes for mining machines based on air-gap field measurement". In: *IEEE Transactions on Industry Applications* 46.4 (2010), pp. 1255–1263.
- [4] Dimitris A Barkas et al. "Brushed DC motor drives for industrial and automobile applications with emphasis on control techniques: A comprehensive review". In: *Electronics* 9.6 (2020), p. 887.
- [5] Nuca Ilie et al. "Rehabilitation of the tram DC traction with modern power converters". In: *2014 International Conference and Exposition on Electrical and Power Engineering (EPE)*. IEEE. 2014, pp. 704–709.
- [6] David J Griffiths. *Introduction to electrodynamics*. Cambridge University Press, 2023.
- [7] Zurek. *Carbon brushes of small universal electric motor (circular saw)*. 2006. URL: https://commons.wikimedia.org/wiki/File:Carbon_brushes.jpg.
- [8] Electrical Academia. *DC Motor Assembly*. 2018. URL: <https://electricalacademia.com/wp-content/uploads/2018/03/DC-motor-field-structure-and-armature-assembly.jpg>.
- [9] H Wayne Beaty and Donald G Fink. *Standard handbook for electrical engineers*. McGraw-Hill New York, 2013.
- [10] Ernesto Soressi. "New life for old compound DC motors in industrial applications?" In: *2012 IEEE international conference on power electronics, drives and energy systems (PEDES)*. IEEE. 2012, pp. 1–6.
- [11] Dieter Gerling and Dieter Gerling. "DC-machines". In: *Electrical Machines: Mathematical Fundamentals of Machine Topologies* (2015), pp. 37–88.
- [12] Robert Stein et al. "Dc Motors". In: *Electric Power System Components: Transformers and Rotating Machines* (1979), pp. 398–442.
- [13] Greensky Power. *What are the disadvantages of brushless DC motor?* 2023. URL: <https://greensky-power.com/disadvantages-of-brushless-dc-motor/>.

- [14] Yan Yin et al. "Braking performance of a novel frictional-magnetic compound disc brake for automobiles". In: *Proceedings of the Institution of Mechanical Engineers, Part D: Journal of Automobile Engineering* 233.10 (2019), pp. 2443–2454.
- [15] AEMT. *DC Motor Maintenance*. 2025. URL: https://www.theaemt.com/static/70457409-aa48-42b4-a9a1b3990d868988/opengraphimage_83f4e8796336604b59d7216d0ecd81a5_f719d893132e/Page-24.jpg.
- [16] Hong Cheng, Daokuan Yang, and Cong Wang. "Research on the nonlinear control strategy of three-phase bridgeless rectifier under unbalanced grids". In: *Electronics* 10.24 (2021), p. 3090.
- [17] Polaris. *Motor Lamination*. 2025. URL: <https://www.polarislaserlaminations.com/motor-laminations.html>.
- [18] Arfat Siddique, GS Yadava, and Bhim Singh. "Applications of artificial intelligence techniques for induction machine stator fault diagnostics". In: *4th IEEE International Symposium on Diagnostics for Electric Machines, Power Electronics and Drives, 2003. SDEMPED 2003*. IEEE. 2003, pp. 29–34.
- [19] SI Malafeev and VI Konyashin. "Induction motor drives for electric mining shovels: synthesis, design and research". In: *2018 International conference on industrial engineering, applications and manufacturing (ICIEAM)*. IEEE. 2018, pp. 1–6.
- [20] Aveek Mangal. "Optimal control of induction machines under minimum energy in opencast mining machinery." In: *Journal of Mines, Metals & Fuels* 68.7 (2020).
- [21] Rajib Datta and VT Ranganathan. "Variable-speed wind power generation using doubly fed wound rotor induction machine-a comparison with alternative schemes". In: *IEEE transactions on Energy conversion* 17.3 (2002), pp. 414–421.
- [22] José Manuel Terras et al. "Estimation of the induction motor parameters of an electric vehicle". In: *2010 IEEE Vehicle Power and Propulsion Conference*. IEEE. 2010, pp. 1–6.
- [23] Derya Ahmet Kocabas, Emrah Salman, and Ahmet Kubilay Atalay. "Analysis using DQ transformation of a drive system including load and two identical induction motors". In: *2011 IEEE International Electric Machines & Drives Conference (IEMDC)*. IEEE. 2011, pp. 1575–1578.
- [24] indiamart. *Wound rotor induction motor*. 2025. URL: <https://www.indiamart.com/proddetail/wound-rotor-induction-motor-2851549755030.html>.
- [25] Hannu Karkkainen et al. "Converter-fed induction motor efficiency: Practical applicability of IEC methods". In: *IEEE Industrial Electronics Magazine* 11.2 (2017), pp. 45–57.
- [26] Juha Pyrhönen. "The high-speed induction motor: Calculating the effects of solid-rotor material on machine characteristics". In: *Acta Polytechnica Scandinavica, Electrical Engineering Series;(Finland)* 68 (1991).
- [27] Ion Boldea. *Induction Machines Handbook: Transients, Control Principles, Design and Testing*. CRC press, 2020.
- [28] Laurence HA Carr. "Recent progress in induction-motor construction". In: *Journal of the Institution of Electrical Engineers* 78.472 (1936), pp. 383–391.

- [29] Ali Challoop, Ahmed Sultan, and Mehdi Bonneya. "Improvement performance of squirrel cage induction motor using rotor bar skew". In: *AIP Conference Proceedings*. Vol. 2591. 1. AIP Publishing. 2023.
- [30] Chunyu Wang et al. "Analysis of vibration and noise for different skewed slot-type squirrel-cage induction motors". In: *IEEE Transactions on Magnetics* 53.11 (2017), pp. 1–6.
- [31] H Hafezi and A Jalilian. "Design and construction of induction motor thermal monitoring system". In: *Proceedings of the 41st International Universities Power Engineering Conference*. Vol. 2. IEEE. 2006, pp. 674–678.
- [32] Surajit Chattopadhyay, Aveek Chattopadhyaya, and Samarjit Sengupta. "Measurement of harmonic distortion and Skewness of stator current of induction motor at crawling in Clarke plane". In: *IET Science, Measurement & Technology* 8.6 (2014), pp. 528–536.
- [33] Subhasis Nandi, Shehab Ahmed, and Hamid A Toliyat. "Detection of rotor slot and other eccentricity related harmonics in a three phase induction motor with different rotor cages". In: *IEEE Transactions on Energy Conversion* 16.3 (2001), pp. 253–260.
- [34] Gene Collin Mechler. "Manufacturing and cost analysis for aluminum and copper die cast induction motors for GM's powertrain and R&D divisions". In: *Massachusetts Institute of Technology, Massachusetts* (2010).
- [35] *Rotating electrical machines - Part 1: Rating and performance*. Standard. Geneva, CH: International Electrotechnical Commission, 2007.
- [36] *Rotating electrical machines - Dimensions and output series - Part 1: Frame numbers 56 to 400 and flange numbers 55 to 1080*. Standard. Geneva, CH: International Electrotechnical Commission, 2007.
- [37] Jorma Luomi. "Transient phenomena in electrical machines". In: *Chalmers University, Sweden* (1998).
- [38] Akim Murakami and Sergey Edward Lyshevski. *Electromechanical systems, electric machines, and applied mechatronics*. CRC press, 2018.
- [39] Surajit Chattopadhyay et al. "Clarke and park transform". In: *Electric Power Quality* (2011), pp. 89–96.
- [40] He C Stanley. "An analysis of the induction machine". In: *Electrical Engineering* 57.12 (1938), pp. 751–757.
- [41] AM Wahl and LA Kilgore. "Transient starting torques in induction motors". In: *Transactions of the American Institute of Electrical Engineers* 59.11 (1940), pp. 603–607.
- [42] R Krishnan and Frank C Doran. "Study of parameter sensitivity in high performance inverter-fed induction motor drive systems". In: *1984 Annual Meeting Industry Applications Society*. IEEE. 1984, pp. 510–524.
- [43] Gábor Kohlrusz and Dénes Fodor. "Comparison of scalar and vector control strategies of induction motors". In: *Hungarian Journal of Industry and Chemistry* (2011), pp. 265–270.
- [44] F Blaschke. *Method for controlling asynchronous machines*. US3824437A.

- [45] Hioki. *Working Principle and Characteristics of Zero flux Current Sensors*. 2025. URL: <https://www.hioki.com/global/learning/test-tools/zeroflux-current-sensing.html>.
- [46] Md Azizur Rahman. "History of interior permanent magnet motors [History]". In: *IEEE Industry Applications Magazine* 19.1 (2012), pp. 10–15.
- [47] Advanced Magnets. *Typical Physical and Chemical Properties of Some Magnetic Materials*. 2025. URL: <https://www.advancedmagnets.com/custom-magnets/>.
- [48] Omegatron. *A stack of Tong Ka Cin ferrite magnets shown attracting several iron objects*. 2006. URL: https://commons.wikimedia.org/wiki/File:Ceramic_magnets.jpg.
- [49] Stanford Magnets. *What you need to know about ceramic magnets*. 2025. URL: <https://www.stanfordmagnets.com/what-you-need-to-know-about-ceramic-magnets.html>.
- [50] National Magnetic Group. *Ceramic 1 (Hard Ferrite)*. 2025. URL: <https://www.magneticsgroup.com/material/c1-2/>.
- [51] All Magnets. *Ceramic Magnets*. 2025. URL: <https://allmagnetics.com/ceramic.htm>.
- [52] AlnicoDauermagnet. *Direct Industry*. 2025. URL: <https://www.directindustry.de/prod/thyssenkrupp-magnettechnik/product-102383-951937.html>.
- [53] Bernard Dennis Cullity and Chad D Graham. *Introduction to magnetic materials*. John Wiley & Sons, 2011.
- [54] Alnico Magnets. *ALNICO Magnets*. 2025. URL: <https://www.arnoldmagnetics.com/products/alnico-magnets/>.
- [55] Stanford Magnets. *How Does Temperature Affect Samarium Cobalt Magnets?* 2025. URL: <https://www.stanfordmagnets.com/how-does-temperature-affect-samarium-cobalt-magnets.html>.
- [56] K Strnat et al. "A family of new cobalt-base permanent magnet materials". In: *Journal of Applied Physics* 38.3 (1967), pp. 1001–1002.
- [57] Stanford Magnets. *Coatings for Sintered NdFeB Magnets*. 2025. URL: <https://www.stanfordmagnets.com/coatings-for-sintered-ndfeb-magnets.html>.
- [58] M Drak and LA Dobrzański. "Corrosion of Nd-Fe-B permanent magnets". In: *Journal of Achievements in Materials and Manufacturing Engineering* 20.1-2 (2007), pp. 239–242.
- [59] GW Warren, G Gao, and Q Li. "Corrosion of NdFeB permanent magnet materials". In: *Journal of applied physics* 70.10 (1991), pp. 6609–6611.
- [60] Qiangqiang Lin et al. "Comparison of PMSM and BLDC applications in servo system". In: *International Conference of Fluid Power and Mechatronic Control Engineering (ICFPME 2022)*. Atlantis Press. 2022, pp. 67–74.
- [61] Michal Podmanick (https://electronics.stackexchange.com/users/341316/michal.podmanick%bd). *How do Hall-effect sensors work in multi-pole BLDC motors?* Electrical Engineering Stack Exchange. URL: <https://electronics.stackexchange.com/q/706091> (version: 2024-03-15). eprint: <https://electronics.stackexchange.com/q/706091>. URL: <https://electronics.stackexchange.com/q/706091>.

- [62] Mostafa Valavi et al. "Slot harmonic effect on magnetic forces and vibration in low-speed permanent-magnet machine with concentrated windings". In: *IEEE Transactions on Industry Applications* 50.5 (2014), pp. 3304–3313.
- [63] Balamurali Surakasi et al. "A novel methodology to enhance the smooth running of the pm bldc motor drive using pwm-pwm logic and advance angle method". In: *Machines* 11.1 (2022), p. 41.

